

**Electrochemically Directed Self-Assembly and Conjugated Polymer  
Semiconductors for Organic Electronic Applications**

by

Rajesh Gopalakrishna Pillai

A Thesis submitted to the Faculty of Graduate Studies of  
The University of Manitoba  
in partial fulfilment of the requirements of the degree of

**Doctor of Philosophy**

Department of Chemistry, University of Manitoba

Winnipeg, MB, Canada R3T 2N2

Copyright © 2010 by Rajesh Gopalakrishna Pillai

## **Abstract**

The research work presented in this thesis investigates the mechanistic details of conventional as well as electrochemically directed self-assembly of alkylthiosulfates and explores the use of conjugated semiconducting polymers for organic electronic applications. Here, the significance of the use of conjugated polymers is twofold; first, to explore their applications in nanoelectronics and second, the possibility of using them as a top contact on the self-assembled monolayers (SAMs) for molecular electronic applications. Throughout this work, deposition of the organic materials was performed on prefabricated device structures that required no further lithographic or metal deposition steps after modification of the electrodes with the organic molecules.

Self-assembly of alkylthiosulfates on gold are reported to form monolayers identical to those formed from the corresponding alkanethiols. However, these self-assembly processes follow more complex mechanisms of monolayer formation than originally recognized. Studies on the mechanism of alkylthiosulfate chemisorption on gold shows that the self-assembly process is influenced by electrolyte and solvent. Plausible mechanisms have been proposed for the role of trace water in the solvent on conventional as well as electrochemically assisted self-assembly of alkylthiosulfates on gold. Electroanalytical and spectroscopic techniques have been used to explore the mechanistic details of electrochemically directed self-assembly of alkylthiosulfates on gold. It has been found that the self-assembly process is dynamic under electrochemical conditions and the heterogeneous electron transfer process between the organosulfur

compound and gold is mediated through gold surface oxide and accompanied by corrosion.

Conducting polymers are serious candidates for organic electronic applications since their properties can be controlled by the manipulation of molecular architecture. Unique electronic properties of conjugated polypyrrole hybrid materials (PPy<sup>0</sup>DBS<sup>-</sup>Li<sup>+</sup>) with immobile dopant anions and mobile cations have been observed and explained on the basis of movement of the cations in an applied electric field. Based on this principle, functioning polymer resistive memory devices have been demonstrated which can be scalable to lower dimensions for nanoelectronics applications. Finally, proof of concept for using a conducting polymer as a top contact in molecular electronic devices created using electrochemically directed self-assembly is demonstrated.

*Dedicated to My Loving Parents*

*"Try not to become a man of success, but rather try to become a man of value."*

-Albert Einstein

## Acknowledgements

I would like to thank the following people for their guidance and help at various stages of my research work at the University of Manitoba.

I express my sincere thanks to my supervisor, Dr. Michael S. Freund, for giving me the opportunity to research in my area of interest and for introducing me to a whole new world of conducting polymers. I am very grateful for his encouragement, patience, guidance and support.

Past and present members of my advisory committee: Dr. Douglas J. Thomson, Dr. Torsten Hegmann, Dr. Mario Bieringer and Dr. Mahesh C. Chaturvedi.

Members of the defense committee: Dr. Heinz-Bernhard Kraatz, Dr. Douglas J. Thomson and Dr. Torsten Hegmann.

Dr. Cyrus Shafai and Dwayne Chrusch at the Nano-Systems Fabrication Laboratory (NSFL, U of M) in the department of Electrical and Computer Engineering for helping with various microfabrication processes.

Past and present members of Freund, Thomson and Hegmann research groups: Dr. Jun Hui Zhao, Dr. Kevin McEleney, Dr. Bhavana Deore, Dr. Sergei Rudenja, Dr. Shaune McFarlane, Dr. Elda Bravo-Grimaldo, Dr. Aminuir Rahman, Vineeth Yathindranath, Denise McInnes, Monica Braun, Matt Pilapil, Joseph English, Insun Yu, Graeme Suppes, Eftekhar Hossain and Mike McDonald.

Last but not least, I would like to thank my parents and my wife Chithra, for their unconditional love and support.

## List of Abbreviations

AFM	Atomic Force Microscopy
CMOS	Complimentary Metal-Oxide Semiconductor
DBS	Dodecylbenzene Sulfonate
DMF	N,N-Dimethyl Formamide
DRAM	Dynamic Random Access Memory
EQCM	Electrochemical Quartz Crystal Microbalance
FGCC	Field Generated Carrier Current
ICPs	Intrinsically Conducting Polymers
IDA	Interdigitated Array Electrode
LEDs	Light Emitting Diodes
MPCs	Monolayer protected Clusters
OCP	Open-Circuit Potential
OLEDs	Organic Light Emitting Diodes
PEDOT	Poly(3,4-ethylenedioxythiophene)
PPy	Polypyrrole
PSS	Poly(styrenesulfonate)
SAMs	Self Assembled Monolayers
SCLC	Space Charge Limited Current
SDS	Sodium Dodecylsulfate
SEM	Scanning Electron Microscopy
STM	Scanning Tunneling Microscopy
TBAP	Tetrabutylammonium Perchlorate
TBATFB	Tetrabutylammonium Tetrafluoroborate
THF	Tetrahydrofurane
TMTU	Tetramethylthiourea
UME	Ultramicroelectrode
XPS	X-ray Photoelectron Spectroscopy

# Electrochemically Directed Self-Assembly and Conjugated Polymer Semiconductors for Organic Electronic Applications

Abstract	ii
Acknowledgements	vi
Table of Contents	vii
List of Abbreviations	x
List of Figures	xi
List of Tables	xvi
List of Schemes	xvii

## Chapter 1. General Introduction

1.1 Self-Assembled Monolayers	2
1.1.1 Introduction to Self-Assembly	2
1.1.2 Preparation of Self Assembled Monolayers (SAMs)	4
1.1.2.1 Conventional Self-Assembly	6
1.1.2.2 Electrochemically Directed Self-Assembly	7
1.1.3 Characterization of Self-Assembled Monolayers (SAMs)	10
1.1.3.1 Contact Angle Goniometry	10
1.1.3.2 Open-Circuit Potential (OCP) Measurements	12
1.1.3.3 Redox Blocking Behavior	13
1.1.3.4 Electrochemical Quartz Crystal Microbalance (EQCM) Analysis	14
1.1.3.5 X-ray Photoelectron Spectroscopy (XPS)	15
1.1.4 Applications of Self-Assembled Monolayers	18
1.2 Conjugated Polymers	20
1.2.1 Introduction to Conjugated Polymers	17
1.2.2 Polypyrroles	24
1.2.2.1 Chemical and Electrochemical Synthesis of Polypyrrole	24
1.2.2.2 Structure and Properties of Polypyrrole	25
1.2.3 Polythiophenes	29
1.2.3.1 Functionalized Polythiophenes	29
1.2.3.2 Poly(3,4-ethylenedioxythiophene): Poly(styrenesulfonate) (PEDOT:PSS) composite	30
1.3 Organic Electronics	31
1.3.1 SAMs for Molecular Electronics	31
1.3.2 Large-Area Molecular Junctions with Conjugated Polymer Soft Contacts	35
1.4 Thesis Overview	36
References	40

## **Chapter 2. Self-Assembly of Alkylthiosulfates on Gold: Role of Electrolyte and Trace Water in the Solvent**

2.1 Introduction	56
2.2 Experimental	58
2.2.1 Synthesis of Alkylthiosulfates	58
2.2.2 Electrochemistry	59
2.2.3 Contact Angle Measurements	60
2.3 Results and Discussion	60
2.3.1 Mechanism of Alkylthiosulfate Self-Assembly on Gold	60
2.3.2 Role of Electrolyte	63
2.3.3 Role of Trace Water in the Solvent	67
2.4 Conclusions	71
References	73

## **Chapter 3. Electrochemically Assisted Self-Assembly of alkylthiosulfates and Alkanethiols on Gold: Role of Gold Oxide Formation and Corrosion**

3.1 Introduction	79
3.2 Experimental	83
3.2.1 Materials	83
3.2.2 Synthesis	83
3.2.3 Electrochemistry	83
3.2.4 Electrochemical Quartz Crystal Microbalance (EQCM) Measurements	84
3.2.5 X-ray Photoelectron Spectroscopy (XPS) Analysis	84
3.3 Results and Discussion	84
3.3.1 Gold Oxide Formation and Corrosion	99
3.3.2 Electrochemical Stability and Exchange of Monolayers	105
3.4 Conclusions	107
Acknowledgements	108
References	108

## **Chapter 4. Field-Induced Carrier Generation in Conjugated Polymer Semiconductors for Dynamic, Asymmetric Junctions**

4.1 Introduction	116
4.2 Experimental	119
4.2.1 Preparation of IDA/Polymer Structures	119
4.2.2 Scanning Electron Microscopy (SEM) Analysis	120
4.2.3 X-ray Photoelectron Spectroscopy (XPS) Analysis	120
4.2.4 Construction and Testing of Memory Device	121

4.3 Results and Discussion	121
4.3.1 Electrical Characterization of PPy Devices	125
4.3.2 Application as Memory Device	127
4.3.3 Fabrication of Smaller Polypyrrole Composite Device	132
4.4 Conclusions	135
Acknowledgements	136
References	136

## **Chapter 5. Dynamic Resistive Crossbar Memories Based on Conjugated Polymer Composites**

5.1 Introduction	143
5.2 Experimental	144
5.3 Results and Discussion	146
5.3.1 Electrical Characterization of PPy Crossbar Devices	146
5.3.2 Application as Memory Device	151
5.3.3 Scalability and Reproducibility of 10x10 Crossbar Junctions	152
5.4 Conclusions	156
Acknowledgements	156
References	156

## **Chapter 6. Preparation of Molecular Electronic Junctions on Gold Crossbar Arrays by Electrochemically Directed Self-Assembly**

6.1 Introduction	163
6.2 Experimental	166
6.2.1 Preparation of Alkylthiosulfates	166
6.2.2 Fabrication of Au crossbars	166
6.2.3 Electrodeposition of Polypyrrole	166
6.2.4 Preparation of Au/PEDOT:PSS/SAMs/Au Molecular Junctions	167
6.2.5 Scanning Electron Microscopy (SEM)	168
6.2.6 Electrical Characterization	168
6.3 Results and Discussion	168
6.3.1 Characterization of Au/PEDOT:PSS/SAMs/Au Junctions	169
6.3.2 I-V Behavior of Au/PEDOT:PSS/SAMs/Au Junctions	171
6.4 Conclusions	173
Acknowledgements	174
References	175

## **Chapter 7. Summary and Future Outlook**

7.1 Thesis Summary	179
7.2 Future Outlook	182

## List of Figures

<b>Figure 1.1</b> Schematic of an ideal alkanethiolate SAM formed on Au (111) surface	5
<b>Figure 1.2.</b> Schematic representation of various surface tensions acting on a liquid drop on solid surface at equilibrium.	10
<b>Figure 1.3.</b> Cyclic voltammograms of a gold electrode in 3 mM $K_4Fe(CN)_6$ before and after modification with a dodecanethiol SAM.	13
<b>Figure 1.4.</b> Chemical structures of some of the conjugated conducting polymers.	21
<b>Figure 1.5.</b> Comparison of electrical conductivities of some metals and doped conjugated conducting polymers.	22
<b>Figure 1.6.</b> Mechanism of pyrrole polymerization.	26
<b>Figure 1.7.</b> Redox behavior of polypyrrole containing immobile dopant anion (DBS <sup>-</sup> ) and mobile cation.	28
<b>Figure 1.8.</b> Cyclic voltammogram of gold IDA electrodes with electrodeposited polypyrrole containing immobile dopant anion (DBS) in aqueous 0.1 M $LiClO_4$ .	28
<b>Figure 1.9.</b> Chemical structure of PEDOT:PSS polymer	31
<b>Figure 1.10.</b> Schematic representation of some molecular junction test-beds.	34
<b>Figure 1.11.</b> Fabrication of large area molecular Junctions.	36
<b>Figure 2.1.</b> OCP vs. time response of a gold electrode in THF (no electrolyte) upon the addition of a) dodecylthiosulfate b) dodecanethiol.	62
<b>Figure 2.2.</b> OCP vs. time response of a gold electrode in THF containing 0.1 M a) TBATFB b) TBAP after the addition of dodecylthiosulfate.	64
<b>Figure 2.3.</b> Cyclic voltammograms (1.0 mM $K_3Fe(CN)_6$ ) of gold electrode before and after modification (30 min ) with 10 mM a) sodium dodecylthiosulfate b) dodecanethiol in THF in the absence	66

and presence of electrolytes.

**Figure 2.4.** OCP vs. time response of a gold electrode in THF upon the addition of a) TBAP b) TBATFB electrolytes 68

**Figure 2.5.** Variation of Ferrocyanide/Ferricyanide oxidation peak current for gold electrodes kept in THF solution (30 minutes) containing 10mM dodecylthiosulfate and 0.1 M TBATFB with varying water content. 69

**Figure 2.6.** OCP vs. time response of a gold electrode after the addition of dodecylthiosulfate to a solution of 0.1 M TBATFB and a) THF b) THF with 0.3 M water. 70

**Figure 3.1.** Cyclic voltammograms for dodecylthiosulfate in various on gold disc electrodes. 86

**Figure 3.2.** Cyclic voltammograms for dodecylthiosulfate in THF on different electrode on substrates. 87

**Figure 3.3.** Cyclic voltammograms (0.1 M TBATFB, 100 mV/s) for dodecylthiosulfate and dodecanethiol in a) THF and b) methanol using gold disc electrodes. 89

**Figure 3.4.** Cyclic voltammograms for a) dodecanethiol and b) dodecylthiosulfate in THF on a gold UME at different concentrations. 90

**Figure 3.5.** The peak currents in the cyclic voltammograms for 10 mM dodecanethiol in THF (with 0.1 M TBATFB) on gold EQCM electrode are plotted as a function of scan rate. 91

**Figure 3.6.** Cyclic voltammograms for a blank THF solution (0.1 M TBATFB, 100 mV/s) containing approximately 1.5 mM of water on a polycrystalline gold electrode before and after addition of 5 mM dodecanethiol. 93

**Figure 3.7.** Cyclic voltammogram (a) and the corresponding frequency change (b) for a 10 mM solution of dodecanethiol in THF using a gold EQCM electrode. 94

**Figure 3.8.** Cyclic voltammogram and the corresponding frequency change for a 10 mM solution of dodecanethiol in THF on a platinum coated gold EQCM electrode. 96

<b>Figure 3.9.</b> Cyclic voltammogram and the corresponding frequency change for a 10 mM solution of dodecanethiol in methanol using a gold EQCM electrode.	98
<b>Figure 3.10.</b> Cyclic voltammograms on a gold UME electrode in blank THF (0.1 M TBATFB, 10mV/s) solution with ~0.005 mM and ~1.5mM water.	100
<b>Figure 3.11.</b> Amperometric current-time data for gold disc electrodes held at a) 0.3 V and b) 1.2 V after addition of 10 mM dodecanethiol and 10 mM dodecylthiosulfate.	104
<b>Figure 4.1.</b> Optical micrographs of the IDA electrodes (top) and SEM micrograph of the cross-section of an IDA (bottom) showing two gold electrodes covered by a ca. 6 $\mu\text{m}$ thick polypyrrole film.	122
Figure 4.2. XPS spectra and the corresponding integrated peak intensity data calculated for electrochemically prepared PPy composite films on gold.	123
<b>Figure 4.3.</b> Schematic electron energy level diagram for a reduced PPy polymer that contains immobile anions compensated by mobile cations.	124
<b>Figure 4.4.</b> $I$ - $V$ behavior of a PPy composite device in the oxidized state as grown prior to reduction ( $\text{PPy}^+\text{DBS}^-$ ) and in the reduced state with $\text{Li}^+$ incorporated into the film ( $\text{PPy}^0\text{DBS}^-\text{Li}^+$ ).	126
<b>Figure 4.5.</b> Current as a function of time following the application of voltages that span the SCLC and FGCC regions and normalized to the initial current.	127
<b>Figure 4.6.</b> Current-time plot of $\text{PPy}^0\text{Li}^+\text{DBS}^-$ device at different forward potentials.	129
<b>Figure 4.7.</b> Current-time plot for $\text{PPy}^0\text{DBS}^-\text{Li}^+$ device at different delay time ( $T_0$ ) values.	129
<b>Figure 4.8.</b> The schematic of a memory circuit, designed to capture two distinct current transit behaviors that correspond to the cation distribution in the device.	130
<b>Figure 4.9.</b> The wave forms for the read-write clock (CLK), the current passing through the PPy composite, and the output of the	131

memory circuit during the storing and reading back the bit sequence 10011011.

**Figure 4.10.** Optical micrograph of gold electrodes with an approximately 1  $\mu\text{m}$  gap before (a) and after (b) the deposition of a PPy composite. 132

**Figure 4.11.** a) Current - voltage and b) Current – time behaviors of polypyrrole composite device, with smaller electrode spacing. 133

**Figure 4.12.** Current versus time behaviour of polypyrrole composite device with smaller electrode spacing. 134

**Figure 5.1.** The schematic diagram of the Au/SiO<sub>2</sub>/Au crossbar polymer junction (top) and the 10x10 crossbar junctions (bottom). 145

**Figure 5.2.** The polymer junction (AFM image in inset) shows three types of *I-V* characteristics under an applied voltage. 146

**Figure 5.3.** Schematic configuration of charge carriers in the polymer junction (bottom) and the corresponding internal electric field distribution (top). 148

**Figure 5.4.** Normalized time dependent currents under the steady state for different delay times ( $T_0$ ) introduced between forward and reversed fields. 149

**Figure 5.5.** The temporal behavior of currents normalized to their initial values under applied step voltages. 149

**Figure 5.6.** Two opposite transient states representing when reading potential (2 V) was applied, 1 was written high at 2.5 V and 0 was written low at 1.0 V. 151

**Figure 5.7.** Schematic electronic memory circuit used to capture two transient conductance behaviors and their digitized states. 152

**Figure 5.8.** The waveforms of W/R clock (CLK1), current signal and memory data of 11100011100 bits were captured using an electrical memory circuit for W/R process. 153

**Figure 5.9.** The current of electrochemical deposition indicates three stages of polymer's growth that can be utilized for controlling the 155

thickness of the polymer.

**Figure 5.10.** The histogram of the currents measured at 100 mV for the 100 crossbar polymer junctions shows the relative narrow distribution. 154

**Figure 5.11.** The histograms of the normalized differential currents measured at zero and 2 s for reading the signals 1 and 0, respectively, on the 10x10 polymer crossbar junctions show two highly polarized conducting states with fairly narrow distributions of the transient signals. 155

**Figure 6.1.** Schematic representation of the cross-sectional view of an ideal molecular junction (Au/PEDOT: PSS/SAM/Au) on gold crossbar arrays. 170

**Figure 6.2.** Optical photographs and SEM images of gold crossbar junctions before and after monolayer deposition and spin coating of PEDOT. 170

**Figure 6.3.** Cyclic voltammograms of a top electrode in gold crossbar array, before and after modification with 10 mM sodium hexadecylthiosulfate. 171

**Figure 6.4.** Auger spectra collected at different locations of the gold crossbar array electrode. 173

## List of Tables

**Table 2.1.** Advancing hexadecane contact angle ( $\theta_a$ )\* on a gold electrode treated with 10 mM hexadecylthiosulfate in THF for 30 minute under different conditions. 67

**Table 3.1.** XPS peak area ratios of C 1s and Au 4f<sub>7/2</sub> peak of dodecylthiosulfate (C12-TS) and hexadecylthiosulfate (C16-TS) monolayers on gold electrode. 106

## List of Schemes

<b>Scheme 2.1.</b> Proposed mechanism for alkanethiol adsorption on gold surface	61
<b>Scheme 2.2.</b> Proposed mechanism for alkylthiosulfate adsorption on gold surface	61
<b>Scheme 2.3.</b> Proposed mechanism for alkylthiosulfate adsorption on gold surface in presence of trace water in the solvent.	71
<b>Scheme 3.1.</b> Mechanism of alkanethiol and alkylthiosulfate monolayer formation on gold at anodic potentials through the reduction of gold surface oxide	99
<b>Scheme 3.2.</b> Gold corrosion induced by electrochemically directed self-assembly of alkanethiol and alkylthiosulfate on gold.	101

Chapter 1:  
General Introduction

## 1.1 Self-Assembled Monolayers

### 1.1.1 Introduction to Self-Assembly

The term 'self-assembly' refers to the spontaneous association of components into patterns or structures without external intervention.<sup>1, 2</sup> It has been specifically used to represent a reversible process that involves pre-existing components and can be controlled by specific design of the components.<sup>2, 3</sup> Depending on the nature of the structures formed in a self-assembly process, these systems can be broadly divided in to two major classes; static and dynamic. In static self-assembly, the system is at equilibrium and does not dissipate energy.<sup>2</sup> For example, surfactant micelles formed by the aggregation of self-assembled surfactant molecules are in equilibrium with the surfactant molecules in solution.<sup>1</sup> In dynamic self-assembly, the system is at non-equilibrium conditions and characteristic orders are formed only with the consumption of energy.<sup>4</sup> Therefore, unlike static systems, the structures or patterned formed by dynamic self-assembly can be readjusted or reconfigured after their formation in response to the changes in the surroundings.<sup>5</sup> For example, in magnetohydrodynamic self-assembly, millimetre-sized magnetic disks subjected to a magnetic field rotating at varying speed are reported to form dynamic patterns at the liquid-air interface.<sup>6</sup> Typically, the structures formed in the dynamic self-assembly need constant supply of energy for their existence.<sup>5</sup> Most of the self-assembly processes in living cells including mitosis are dynamic in nature as they need constant supply of energy to prevent the death of the living cell.<sup>4, 5</sup>

Self-assembly processes have been observed at scales ranging from molecular to the macroscopic level.<sup>2, 7-9</sup> They involve both natural and artificial components at different dimensions such as molecules, cells, polymers, organisms and planetary systems.<sup>2, 9, 10</sup> Examples for self-assembly in the molecular scale involve Langmuir Blodgett films, amphiphilic peptide fibres and self assembled monolayers.<sup>3, 8, 11</sup> In nano and meso-scale self-assembling systems, higher-order architectures are built from the corresponding building blocks including nanoparticles, nanorods, nanotubes and dendrimers.<sup>7, 8</sup> Significant advances have been made in understanding these self-assembling systems and exploiting their potentials for a wide range of scientific and technological applications. For example, self-assembly of peptide-amphiphiles yield structures range from micelles or nanofibers to patterned membranes that can be used as model bioactive systems for bioadhesion studies and scaffolds for tissue engineering as well as targeted drug delivery.<sup>12</sup> Self-assembling liquid crystalline materials that combine nano-scale mobility and order are excellent candidates for many applications including information displays, sensors and drug delivery vehicles.<sup>13</sup> Lyotropic liquid crystals have been widely used as templates for the synthesis of nanostructures with well-defined size and shape.<sup>13</sup> Self assembly of nanoparticles at liquid-liquid interface can be controlled by tuning their size and chemical characteristics of the ligands. By controlling the type and chemical characteristics of the ligand, crosslinked sheets of nanoparticles can be generated at the liquid-liquid interface find applications as novel encapsulants, filtration devices with distinct porosities, and controlled release materials.<sup>14</sup> A variety of artificial self-assembling systems has been developed based on the self-assembly of components

in the macroscopic scale.<sup>9</sup> These centimetre-sized components can be self-propelled or externally propelled and find various applications ranging from passive mechanical parts to mobile robots.<sup>9</sup>

Molecular self-assembly processes involve a delicate balance between the attractive and repulsive forces between the component molecules. The attractive force (driving force) helps to bring molecules together and the repulsive force acts against their association.<sup>1, 3</sup> The major driving forces for molecular self-assembly are Van der Waals, hydrophobic, solvation,  $\pi$ - $\pi$  stacking and hydrogen bonding.<sup>1, 15</sup> The repulsive forces include steric, hydration and solvation.<sup>1</sup> Examples of molecular self-assembly include molecular crystals, Langmuir monolayers, micelles and self assembled monolayers (SAMs).<sup>2, 3, 15</sup> Among these systems, SAMs have received wide attention since they can be used as prototypes for fundamentals studies and for possible applications in nanoscience and technology.<sup>2, 3</sup>

### **1.1.2 Preparation and Properties of Self Assembled Monolayers (SAMs)**

SAMs are well-ordered ensembles formed by the adsorption of organic molecules, from solution or gas phase, onto the surface of a solid or liquid (e.g. mercury).<sup>1, 3, 11</sup> A schematic diagram of an ideal alkanethiolate SAM on gold surface is shown in Figure 1.1.<sup>3</sup> The organic molecules that constitute SAMs have a characteristic 'head group' and 'tail group' usually separated by a hydrocarbon spacer chain.<sup>11</sup> The head group has a high affinity for the substrate and forms relatively strong chemical bonds with the substrate. The surface properties of the SAMs mainly depend on the nature of the terminal functional group (tail group).<sup>15</sup> Unlike other adventitious organic

materials adsorbed on metal or metal oxide surfaces, SAMs form well-defined, homogenous films with reproducible physical properties including conductivity, wettability and corrosion resistance.<sup>3</sup>

Well-known examples for SAMs include organosulfur compounds on various metal (Au, Ag, Pt, Cu, Hg) and semiconductor (GaAs, InP) surfaces, organosilicon derivatives on hydroxylated surfaces (quartz, glass, mica), alkylmonolayers on silicon, and fatty acids on metal oxides (Al<sub>2</sub>O<sub>3</sub>, AgO).<sup>3, 15, 16</sup> Several sulfur containing head groups have been used for the preparation of SAMs on gold and other transition metal substrates. These compounds include aliphatic and aromatic thiols and disulfides, sulfides, thiophene, xanthates, thiocarbamates, thioureas, thiocarboxylic acids and alkylthiosulfates.<sup>3, 15, 17</sup> In these groups, alkanethiolate monolayers on gold are probably the most extensively studied to date.

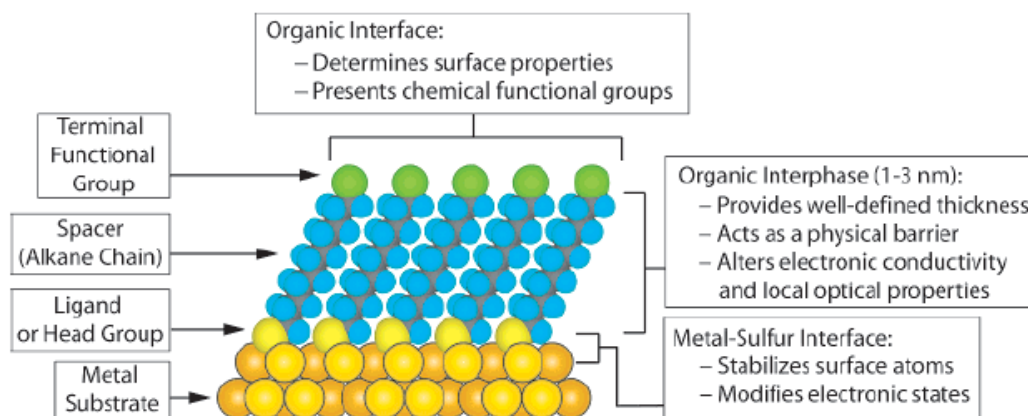


**Figure 1.1** Schematic of an ideal alkanethiolate SAM formed on Au (111) surface<sup>3</sup>

The precursor molecules used for the preparation of alkanethiolate SAMs on gold include alkanethiols<sup>18</sup> (X(CH<sub>2</sub>)<sub>n</sub>SH), dialkyl sulfides<sup>19</sup> (X(CH<sub>2</sub>)<sub>m</sub>S(CH<sub>2</sub>)<sub>n</sub>X), dialkyl

disulfides<sup>20</sup> ( $X(CH_2)_mS-S(CH_2)_nX$ ) and alkylthiosulfates<sup>17, 21</sup> ( $X(CH_2)_nSSO_3^-$ ), where n and m are the number of methylene units and X represents the tail group (-CH<sub>3</sub>, -COOH, -OH) of the hydrocarbon chain. A relatively strong gold-sulfur bond (~45 kcal/mol) and van der Waals interactions between the hydrocarbon chains allow the formation of densely packed, crystalline or semi-crystalline monolayers on gold surface. The monolayers formed from aromatic as well as short chain thiols are relatively less well-ordered and more permeable and electron transfer redox probes than those formed from thiols with long aliphatic hydrocarbon chains.<sup>18</sup> Kinetic studies show that the presence of electron donating substituents facilitates the adsorption process while the electron withdrawing group retards the chemisorption process suggesting that electronic environment of the sulfur atom affect the adsorption of organosulfur species on gold.<sup>22</sup>

There are two different self-assembly techniques available for the formation of alkanethiolate monolayers on gold surfaces; conventional self-assembly and electrochemically directed self-assembly.

#### **1.1.2.1 Conventional Self-Assembly**

Conventional self-assembly techniques rely on the spontaneous organization of molecules on the substrate surface.<sup>3, 15</sup> In this case, adsorption of precursor molecules from their dilute solutions occurs on substrates under open-circuit conditions without any external intervention. Nuzzo and Allara published the first report on the spontaneous self-assembly of dialkyl disulfides on gold from their dilute solutions in non-aqueous solvents.<sup>20</sup> Dialkyl disulfides presumably undergo dissociative chemisorption involving S-S bond scission and form monolayers indistinguishable with

that formed from the corresponding alkanethiols.<sup>15</sup> Although dialkyl sulfides adsorb on gold surfaces, the resulting monolayers are poorly ordered and less densely packed monolayers than the corresponding alkanethiol SAMs.<sup>19</sup> Lukkari and co-workers first reported the adsorption of alkylthiosulfates on gold surface, under anaerobic conditions, to form monolayers similar to that formed from the corresponding alkanethiols.<sup>17</sup>

Conventional self-assembly techniques suffer from some inherent limitations. For example, conventional self-assembly process is very slow and usually takes 24 hours or more for the formation of a well ordered alkanethiol monolayer on gold.<sup>23</sup> Moreover, it requires a clean gold surface and has limited control over monolayer formation.<sup>21, 24</sup> Most of these limitations have been eliminated in the electrochemically directed self-assembly technique.<sup>21</sup>

#### **1.1.2.2 Electrochemically Directed Self-Assembly**

Self-assembly of alkanethiols under electrochemical conditions has been found to increase the kinetics of monolayer formation.<sup>23, 25-31</sup> Electrochemical deposition of alkanethiols on different metal surfaces including gold<sup>25-27</sup> silver<sup>28</sup> and mercury<sup>29</sup> has been reported. Different terminologies have been used in the literature to represent alkanethiol self-assembly performed under electrochemical control. For example, Lennox and Ma reported the potential assisted deposition of alkanethiols on gold where potentials lower than the oxidation potential of gold are applied.<sup>23</sup> Here, monolayer formation is 'assisted' by increasing the adsorption rate under applied potential that enable the formation of a good monolayer in ~15 min compared to ~24hrs needed in

conventional self-assembly methods.<sup>23</sup> Paik and co-workers studied the electrochemical processes associated with the potential dependent adsorption of organosulfur molecules on gold and silver surfaces using QCM gravimetry and electrochemical techniques.<sup>30</sup> They proposed that, at fixed electrode potentials, the adsorption mechanism of alkanethiols involves heterogeneous electron transfer steps and proceeds through an anodic reaction for thiol adsorption whereas the adsorption of disulfides associated with a cathodic reaction. Brett and co-workers studied the effect of applied potential on SAM formation from dilute ethanolic solutions of alkanethiols.<sup>31</sup> Electron transfer blocking experiments with ferro/ferricyanide redox probe and EQCM data show that a well-packed monolayer can be formed in shorter time periods, as low as 100s.<sup>31</sup> Weisshaar and co-workers reported the oxidative deposition of alkanethiolate monolayers on gold using converse reductive desorption reaction of alkanethiolate SAMs.<sup>32</sup> Here densely packed alkanethiolate monolayers were electrochemically deposited from solutions of alkanethiols in ethanolic KOH. Cheng and co-workers published a comparative study of electrochemically directed assembly and conventional self-assembly of acetyl-protected conjugated thiols on gold.<sup>26</sup> After basic deprotection of the thiols, monolayers were deposited selectively on electrodes kept under anodic potentials (+0.4 V vs. Ag/AgNO<sub>3</sub>) since the electrochemically directed assembly found approximately 800 times faster than the conventional method.<sup>26</sup> Kraatz and co-workers reported the electro-assisted deposition of ferrocenoyl peptide (Fc-peptides) disulfides on gold surface. The electrodeposition was performed from ethanolic solutions of Fc-peptide disulfides at cathodic potentials. The surface concentration of the

electrodeposited films were consistently superior to those formed from conventional self-assembly techniques.

Electrochemically directed self-assembly enables the selective formation of alkanethiolate monolayers on specific substrates exposed to the same solution containing organosulfur species. For example, selective formation of alkanethiolate monolayers on closely spaced electrodes from a solution of alkylthiosulfate and the electrolyte, tetrabutylammonium tetrafluoroborate (TBATFB), in THF were reported.<sup>21</sup> Here, TBATFB was found to inhibit the spontaneous self-assembly of alkylthiosulfate and thereby enabling electrochemically directed self-assembly where monolayer formation occurs only on those electrodes kept under a certain anodic potentials ( $\sim 1.2$  V vs. Ag/AgNO<sub>3</sub>).<sup>21, 33</sup> The electrodes kept under open-circuit conditions experienced little or no deposition of monolayers.

Electrochemically directed self-assembly technique offers some significant advantages over conventional self-assembly.<sup>21, 33</sup> This technique is sufficiently fast that a good monolayer can be formed in less than five minutes compared to 24 hours normally required in conventional self-assembly methods.<sup>21</sup> For practical applications, electrochemically directed self-assembly method offers some considerable advantage over the conventional self-assembly techniques. For example, electrochemical deposition is suitable for fabrication processes that require speed and reproducibility. The fact that this is fast and is less sensitive to surface conditions for gold will make this approach much more compatible with a range of technologies that can use SAMS for surface treatment. Furthermore, the monolayer coverage can be electrochemically

controlled. More significantly, electrochemically directed self-assembly enables the selective formation of monolayers.<sup>21</sup> For example, alkanethiolate monolayers can be selectively formed on desired electrode areas in an array of gold electrodes kept under electrochemically directed self-assembly conditions. This is very important for the application of self assembled monolayers in molecular electronics and sensors where electrode arrays can be selectively modified with the desired organic molecules.

### 1.1.3 Characterization of Self-Assembled Monolayers

Numerous characterization methods including electroanalytical and spectroscopic techniques have been used to study SAM modified material surfaces.<sup>11, 15</sup> An outline of some of the characterization techniques used for this thesis work is given below.

**1.1.3.1 Contact Angle Goniometry:** The wetting properties of monolayers are explored through contact angle goniometry. For a liquid drop on a solid substrate, the contact angle is the angle between the liquid-vapour interface and the solid surface.<sup>34, 35</sup>

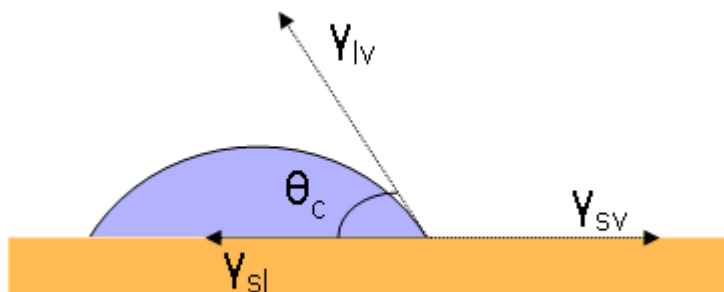


**Figure 1.2.** Schematic representation of various surface tensions acting on a liquid drop on solid surface at equilibrium.

The fundamental relation between the surface tensions and contact angle is given by Young's equation. For a liquid drop on solid surface (Figure 1.2) , the mechanical equilibrium between the three interfacial tensions, represented as solid-liquid ( $\gamma_{sl}$ ), solid vapour ( $\gamma_{sv}$ ), and liquid vapour ( $\gamma_{lv}$ ), is given by Young's equation as

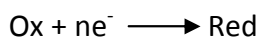
$$\gamma_{lv} \cos \theta_c = \gamma_{sv} - \gamma_{sl} \quad (1)$$

where  $\theta_c$  is the Young contact angle.<sup>36-38</sup> The experimentally observed contact angles often deviate from Young's equation due to roughness and chemical heterogeneity of the surface.<sup>36</sup> The contact angle made by an advancing liquid ( $\theta_a$ ) and that made by the receding liquid ( $\theta_r$ ) may not be identical and results in contact angle hysteresis (H).

$$H = \theta_a - \theta_r \quad (2)$$

For a smooth heterogeneous surface (e.g. partially formed SAMs), the advancing contact angle is a good approximation of Young's contact angle.<sup>37</sup> Typically, pure liquids that do not react (e.g. adsorption) with the material surfaces are used for contact angle measurements. The common liquids used for the characterization of SAMs are water ( $H_2O$ ,  $\gamma_{lv} = 72.7$ ) and hexadecane (HD,  $\gamma_{lv} = 27.6$ ).<sup>39</sup> The wetting properties of SAMs depend on the hydrophobic or hydrophilic nature of their terminal functional group. For example, the water contact angles,  $\theta_a$  ( $H_2O$ ), range from zero to  $118^\circ$  have been reported for SAMs with polar functional groups including alcohols and fluorinated ( $-CF_3$ ) alkanes, respectively.<sup>18</sup> The hexadecane contact angles,  $\theta_a$  (HD), ranging from zero to  $71^\circ$  are expected under similar conditions.<sup>18</sup> Well ordered and densely packed monolayers of alkanethiols and alkylthiosulfates on gold give  $\theta_a$  (HD) values close to  $44-46^\circ$ .<sup>17, 33, 18</sup>

**1.1.3.2 Open-Circuit Potential (OCP) Measurements:** These are potentiometric measurements monitoring changes in the electrochemical potential of a working electrode related to a reference electrode while no net current flow through the external circuit of the electrochemical cell. OCP measurements are based on Nernst equation, which relates the concentration (C) of electroactive species in solution in contact with the working electrode surface to the electrode potential (E); i.e. for the reaction



$$E = E^{0'} + 0.059/n \log [C_{\text{Ox}}/C_{\text{Red}}]$$

where  $E^{0'}$  is the formal redox potential for the electron transfer process.<sup>40</sup> This relation shows that the potential of the working electrode can also be altered by the oxidation or reduction reaction taking place at the electrode surface.

OCP-time measurements provide valuable information regarding the nature of electrochemical process (oxidation or reduction) going on the electrode surface. For example, OCP shifts can be related to the change in charge accumulated on the electrode surface.<sup>41</sup> Here the shift in OCP to more positive values may indicate an electrochemical process that either removes excess negative charge or increases the excess positive charge on the electrode, depending on the potential of the electrode with respect to its potential of zero charge.<sup>41</sup> Small changes in the OCP values are expected in presence of reactions at the interface involving dissolved oxygen and hydronium ions.<sup>42</sup> OCP measurements have been used for *in-situ* analysis of charge

transfer processes at the electrode-electrolyte interface during self-assembly of alkanethiols on gold.<sup>30, 42, 43</sup>

**1.1.3.3 Redox Blocking Behavior:** Electron transfer blocking experiments involving redox couples in solution are used as an indirect means for monitoring adsorption and surface passivation.<sup>11, 44, 45</sup> The presence of a densely packed monolayer prevents redox molecules in solution from approaching the electrode surface.<sup>11</sup> In cases where adsorption results in a passivating layer, electron transfer between the electrode surface and the redox species in solution will be attenuated (Figure 1.3). The degree of

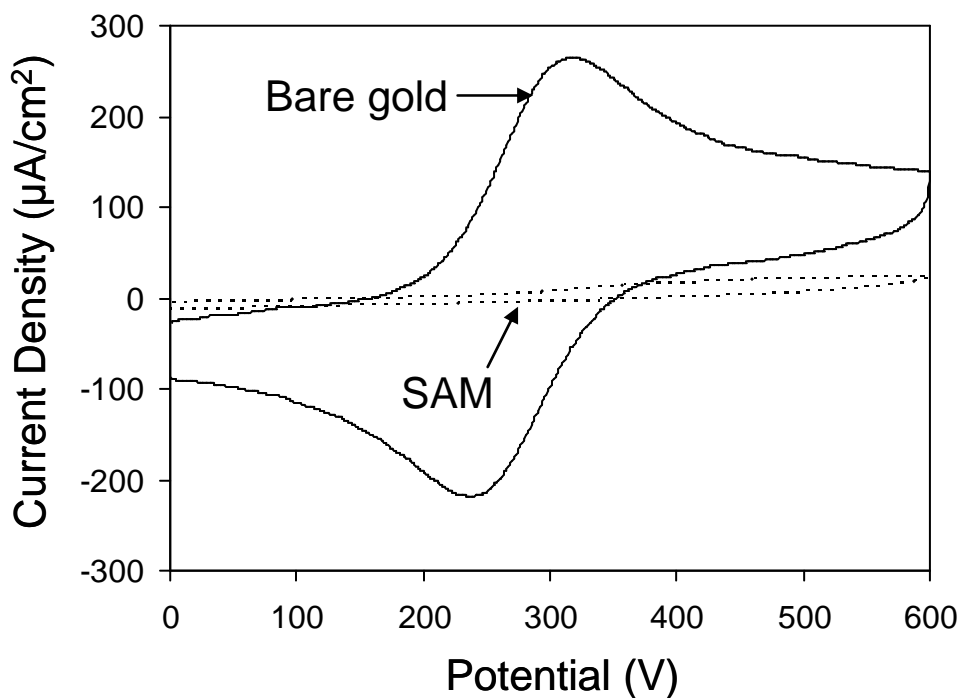


**Figure 1.3** Cyclic voltammograms of a gold electrode in 3 mM  $\text{K}_4\text{Fe}(\text{CN})_6$  (0.1 M KCl, scan rate  $100 \text{ mV s}^{-1}$ ; saturated Ag/AgCl reference electrode) before and after modification with a dodecanethiol SAM.

attenuation of the faradaic current relative to the current at the bare electrode is often used to assess the monolayer quality, since the presence of disorder or pinholes (bare metal sites) will result in a measurable redox current from solution species.<sup>11, 44</sup>

Generally, the blocking behavior depends on the nature of solvent and redox species involved. The electron transfer blocking ability of SAMs decreases in non-aqueous solvents due to possible 'solvation' of the hydrocarbon chains that may increase in the permeability of SAMs.<sup>11</sup> There are a wide range of redox probes reported, differing in their hydrophobicity and molecular size. For example, hydroxymethylferrocene (FcOH) and methylviologen didiodide ((MV)I<sub>2</sub>) are relatively hydrophobic compared with potassium hexacyanoferrate(II) (K<sub>4</sub>[Fe(CN)<sub>6</sub>]) and hexaammineruthenium(III) chloride ([Ru(NH<sub>3</sub>)<sub>6</sub>]Cl<sub>3</sub>).<sup>46</sup> Hydrophilic/hydrophobic interactions between the redox probe and the monolayer determines the heterogeneous electron transfer distance between the redox probe and the electrode.<sup>46</sup> Therefore, even pinhole-free SAMs are not blocked in non-aqueous solvents (e.g. acetonitrile) containing hydrophobic redox probes.<sup>11</sup>

**1.1.3.4 Electrochemical Quartz Crystal Microbalance (EQCM):** The working principle of quartz crystal microbalances (QCM) is based on the *converse piezoelectric effect* in which application of an electric field across the crystal afforded a mechanical strain.<sup>34</sup> The QCM is comprised of a thin AT-cut quartz crystal sandwiched between two metal electrodes.<sup>34, 35</sup> The crystal oscillates at its resonance frequency when an alternating electric field is applied between the electrodes. The resonance frequency is sensitive to any mass change associated with the quartz crystal and electrodes. The quantitative

relationship that correlates a change in frequency with a change in mass is given by the Sauerbrey relationship as

$$\Delta f = -2f_o^2 \Delta m / A(\mu_q \rho_q)^{1/2}$$

where  $\Delta f$  is the frequency change measured,  $f_o$  the resonant frequency of the quartz crystal prior to mass change,  $\Delta m$  the mass change,  $A$  the piezoelectrically active area,  $\mu_q$  the shear modulus of quartz, and  $\rho_q$  is the density of quartz.<sup>34, 35</sup>

QCMs are extensively used for mass measurements either in the gas phase, including thin film deposition and sensing, as well as under electrochemical conditions (EQCM).<sup>34</sup> The versatility to use one side of the EQCM electrode as working electrode in an electrochemical cell while simultaneously recording the charge flux, interfacial capacitance and mass change makes EQCM technique an excellent tool for various scientific and technological applications.<sup>35</sup> EQCM has been used to study the kinetics of monolayer formation of n-alkanethiols and their electrochemically induced desorption.<sup>31, 47</sup> For example, kinetics of octanethiol and hexadecanethiol SAM formation on microcrystalline gold surface show Langmuir type adsorption in a limited concentration range.<sup>47</sup> During the adsorption process, the alkanethiol-gold system is reported to be in dynamic equilibrium with free gold sites and alkanethiolate species.<sup>47</sup>

**1.1.3.5 X-ray Photoelectron Spectroscopy (XPS):** XPS is a very sensitive spectroscopic technique that provides valuable information related to the chemical composition and electronic structure of surface and near surface regions in the materials.<sup>48-50</sup> During analysis, samples are kept at ultra high vacuum (UHV) conditions and are irradiated with

a monochromatic x-ray source. The kinetic energies of the ejected photoelectrons are then analyzed according to the energy conservation in the photoemission process,

$$E_{h\nu} = E_{B(i)} + E_k + E_\phi$$

where  $E_{h\nu}$  is the energy of the monochromatic x-ray,  $E_{B(i)}$  is the binding energy of the electron in the  $i$ 'th level relative to the Fermi level ( $E_F$ ) of the sample (defined as  $E_F=0$ ),  $E_k$  is the kinetic energy of the emitted photoelectrons and  $E_\phi$  is the spectrometer work function (typically  $\sim 4.5$  eV).<sup>48, 51</sup> This energy conservation relation can be used to calculate the binding energy ( $E_{B(i)}$ ) of the electrons, provided the spectrometer work function is known and the kinetic energy of the respective photoelectrons is determined using an electron energy analyzer.<sup>51</sup> Typical XPS spectra have photoelectron binding energies plotted in the abscissa (x-axis) against their abundance (represented as photoelectron counts or counts per second). The binding energy ( $E_{B(i)}$ ) values provide useful information including oxidation state and chemical environment of the elements present in the material. Usually, a survey spectrum is initially collected to identify the elements present in the film which can be used to estimate the chemical composition. Furthermore, high resolution XPS analysis enable to resolve small shift in peak positions associated with a change in chemical environment of elements. For example, high resolution XPS analysis has been used to distinguish the chemical state of sulfur in various organosulfur compounds on gold surface.<sup>52, 53</sup> Generally, the S(2p) spectra of thiolate adsorbed on gold give two strong peaks around 162 eV (S(2p<sub>3/2</sub>)) and 163.2 eV (S(2p<sub>1/2</sub>)) with 2:1 intensity ratio, consistent with spin-orbit splitting effect.<sup>52</sup> On the contrary, atomic sulfur and physisorbed organosulfur compounds give S(2p) peaks at

161 eV and 163-164 eV, respectively.<sup>53, 54</sup> Hence, the thiolate species on gold surface can be distinguished from atomic sulfur and physisorbed organosulfur molecules.

XPS has been extensively used for the characterization of self-assembled monolayers. For example, SAMs of alkanethiols, dialkyl disulfides and alkylthiosulfates on gold surface have been found to be nearly indistinguishable by XPS and confirmed the presence of a gold-sulfur bond.<sup>17, 18, 27, 33, 53</sup> Angle resolved XPS has been used to estimate the thickness of dodecanethiol SAMs on Au (111) and the values are in good agreement with the Ellipsometry results.<sup>50</sup> Huang and Hemminger studied the UV photooxidation products of alkanethiol or thiophenol SAMs on evaporated gold using XPS.<sup>55</sup> They found that the XPS S2p spectra for the monolayers photolyzed in air constitute two types of sulfur; the one at 162.8 eV corresponds to thiolate species and other at 167.5 eV for sulfonates.<sup>55</sup> Caster and co-workers used XPS to detect unbound organosulfur compounds left on SAM surface due to improper rinsing or the use of poor solvents.<sup>53</sup> The 2Sp<sub>3/2</sub> binding energy values (~164 eV) for unbound alkanethiols and disulfides shift to 162 eV in SAMs due to gold-thiolate bond formation.<sup>53</sup> Ishita and co-workers used high resolution XPS to study the correlation between S(2p) peak signals and organosulfur SAMs on Au(111) surface.<sup>52</sup> Lee and co-workers used XPS to study the air oxidation of SAMs in the absence of light.<sup>56</sup> High resolution XPS S(2p) spectra showed that alkanethiol SAMs formed on thermally evaporated gold (glass or silicon as substrate) with smaller surface grain-size undergo extensive oxidation in air to form less adsorbing species including sulfinates and sulfonates.<sup>56</sup>

### 1.1.4 Applications of Self Assembled Monolayers

Compared to other self assembling systems, SAMs have some major advantages for their application in nanoscience and technology.<sup>3, 15, 57</sup> For example, SAMs are easy to prepare and do not require any special equipments or conditions (e.g. Langmuir Blodgett (LB) troughs, ultrahigh vacuum).<sup>3</sup> However, no reliable procedures have been developed to yield high quality, pinhole (defect)-free SAMs.<sup>11</sup> The chances of pinholes formation in SAMs can be reduced by appropriate treatment of the bulk electrode material including surface annealing, cleaning of organic contaminants and etching to expose the fresh metal surface for removing inorganic oxides.<sup>11</sup> For typical alkanethiolate SAMs, the maximum pinhole radius is reported as 8- $\mu\text{m}$  and the maximum uncovered area of one percent or less.<sup>58, 59</sup> The presence of pinholes and other surface defects in SAMs will reduce the surface passivation and may limit their usage in applications where the barrier properties of the surface films are critical. For example, presence of pinholes or surface defects in SAMs will limit their ability to act as a passivating surface film as these defects may expose the underlying metal to the adverse environment and enhance corrosion. Similarly, SAMs with fewer surface defects are desirable for their use in molecular electronics where these defects can possibly 'short-circuit' the molecular junctions. However, for applications of SAMs involving control of surface wettability or lubrication may not require as good monolayer as compared to the above mentioned applications where barrier properties are critical. SAMs offer good stability relative to other thermodynamically unstable and kinetically stable systems including LB films.<sup>60</sup> They can be prepared on objects of all sizes, ranging

from nanoscale to macroscale.<sup>2, 3</sup> The macroscopic surface properties (e.g. wetting, adhesion) of SAMs can be related to their molecular level structure.<sup>3, 15</sup> Furthermore, SAMs are relatively insensitive to impurities and stable in a wide range of solvents including water.<sup>61</sup> Therefore, SAMs are considered as the best candidates for many fundamental studies and applications.

The presence of well-ordered and densely packed hydrocarbon chains in SAMs find various applications in tribology and surface coatings.<sup>62</sup> For example, monolayers of functionalized organic molecules have been used as molecular lubricants for micro and nano devices.<sup>62, 63</sup> Monolayers of alkanethiols on various metal surfaces including copper and gold are reported to form passivating barrier layers that prevent corrosion.<sup>64-66</sup> SAMs find applications in soft lithography as 'inks' to construct surface features in the micrometer to nanometer scale.<sup>67</sup> These patterned surfaces has been used for numerous applications particularly in biological systems.<sup>67</sup>

Functionalized self-assembled monolayers offer many opportunities to tune the surface properties of SAMs.<sup>19, 60, 68, 69</sup> For example, dynamic control of surface wettability has been reported for (16-mercapto)hexadecanoic acid monolayers undergoing conformational transition under an applied electric field.<sup>68</sup> SAMs have been used as a 'molecular glue' for the immobilization of biomaterials and artificial receptors including proteins, nucleotides and antibodies.<sup>69</sup> Chemical and biosensors based on SAMs usually employ an electrochemical, optical or piezoelectric transducer for sensing the analyte.<sup>69</sup> Mixed self assembled monolayers are used for microarray applications<sup>70</sup> and for making surface gradients with varying wettability.<sup>71</sup> SAMs are very promising

candidates for molecular scale electronics where they can act as active molecular components to perform basic functions of an electronic circuit including conduction, rectification and storage.<sup>72-74</sup>

## **1.2 Conjugated Conducting Polymers**

### **1.2.1 Introduction to Conducting Polymers**

For the past three decades, the significance of conjugated conducting polymers have continued to increase due to their potential applications ranging from conductors to batteries to display devices.<sup>75-78</sup> These polymers are very versatile materials that combine the chemical as well as mechanical properties of conventional polymers and electronic properties of metals or semiconductors.<sup>78, 79</sup> In contrast to silicon based systems, conjugated polymeric materials are flexible, processible, lightweight and can be transparent. Depending on the conduction mechanism, conjugated polymers can be further classified as a) ionically conducting polymers and b) intrinsically conducting polymers (ICPs).<sup>75, 80</sup> The major charge carriers in an ionically conducting polymer are ions and those in ICPs are electrons or holes. ICPs show reversible redox behaviour usually accompanied by a large change in the electronic, mechanical and optical properties of the material.<sup>80</sup> The pioneers who laid the foundation for ICP research, Hideki Shirakawa, Alan J. Heeger and Alan J. MacDiarmid, were awarded the Nobel Prize in Chemistry in 2000 'for the discovery and development of electronically conducting polymers'.<sup>81-83</sup> Some of the extensively studied conducting polymers (Figure 1.4) include polyacetylene, polyaniline, polypyrrole, polythiophene and poly(p-phenylene).<sup>75, 77, 79</sup>

Similar to conventional silicon based semiconductors, conjugated polymers can be 'doped' to change their conductivity. Unlike the inorganic semiconductors, doping in conducting polymers does not represent the replacement of atoms in the material framework.<sup>84</sup> These polymers can be chemically or electrochemically doped *via* oxidation (p-doping) or reduction (n-doping) of the conjugated electronic system.<sup>84, 85</sup> The doping level in the conducting polymers determines their conductivity. Unlike silicon, the conjugated polymers can be reversibly doped to high doping levels (typically 25%) which can be manipulated using chemical or electrochemical methods.<sup>85</sup>

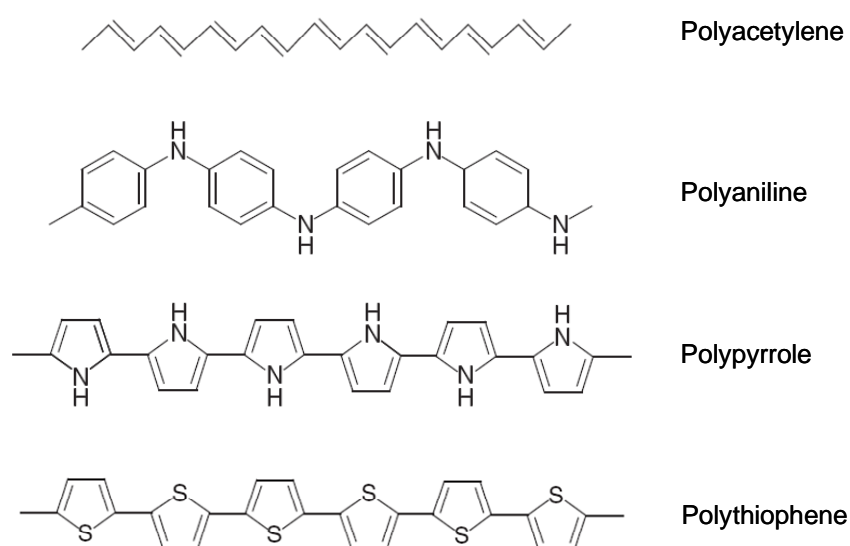


**Figure 1.4.** Chemical structures of some of the conjugated conducting polymers.

The electrical conductivity of these polymers between their doped (oxidized) and undoped (reduced) state is reported to change by 12 to 15 orders of magnitude.<sup>76, 85</sup> Typical conductivities of the conjugated polymers in their doped state are shown in Figure 1.5.<sup>80</sup> Of the various ICPs studied, Iodine doped polyacetylene has been reported the highest conductivity ( $>10^5$  S/cm) to date.<sup>86</sup>

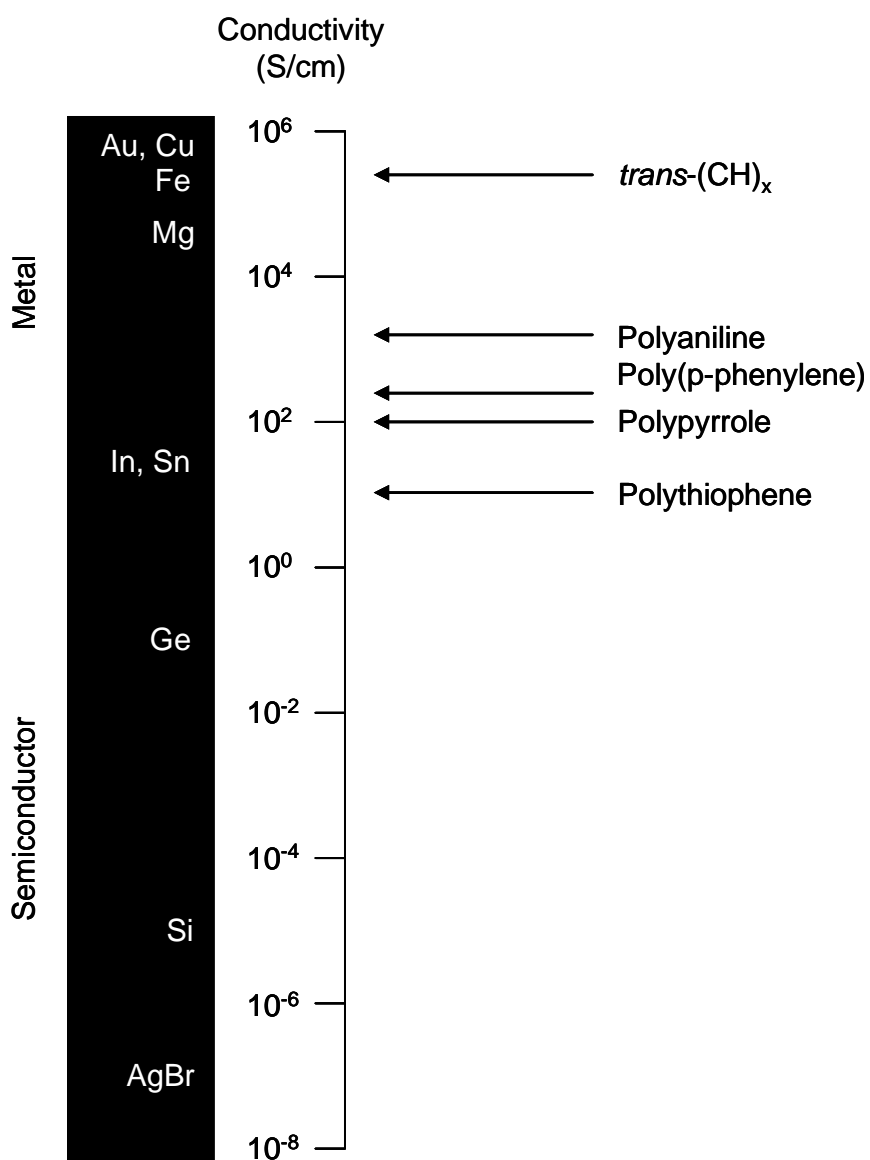


**Figure 1.5** Comparison of electrical conductivities of some metals and doped conjugated conducting polymers.<sup>80</sup>

The ability to vary the doping level of conjugated polymers offers interesting optical, electrical and mechanical properties which can be used for various applications. For example, their ability to change the color or emit visible light has been exploited in

the fabrication of electrochromic devices<sup>87</sup> and light emitting diodes (LEDs) respectively.<sup>88</sup> Conjugated polymer based microactuators make use of the volume change associated with the change in doping level.<sup>89</sup> Electrical conductivity of these polymers has been exploited in the development of conjugated polymer based electronic devices including Schottky diodes,<sup>90</sup> thin film transistors<sup>91</sup> and rechargeable batteries<sup>92</sup>. Furthermore, these polymers find potential applications in microelectronics<sup>93</sup> and chemical as well as bio sensing.<sup>84</sup>

ICPs can be prepared using chemical or electrochemical methods. Usually, chemical and electrochemical syntheses proceed by simultaneous polymerization and doping of the conjugated polymer.<sup>75</sup> Chemical synthesis is considered as the desirable method for the bulk production of conducting polymers than more commonly practiced electrochemical methods.<sup>78, 94</sup> Some advantages of chemical synthesis of conjugated conducting polymers include the following: a) the polymer can be prepared or coated on non-conducting substrates; b) ultrathin films can be prepared by spin coating on even non-conducting substrates of relatively large area; and c) polymer dispersions can be used to coat on large areas. During chemical synthesis, the monomers are treated with ionizing agents to create charge carriers by oxidation or reduction.<sup>79</sup> Some of the oxidizing dopants used for chemical synthesis of conducting polymers including  $\text{AsF}_5$ ,  $\text{SbF}_5$ ,  $\text{FeCl}_3$ ,  $\text{AlCl}_3$  and  $\text{I}_2$ .<sup>79</sup>

Compared to chemical routes, electrochemical synthesis of conducting polymers also has some unique advantages.<sup>94, 95</sup> For example, anodic electropolymerization enables direct attachment of polymer film on inert metal surfaces (e.g Au, Pt) in the

absence of a catalyst. The thickness of the polymer film can be controlled by monitoring the charge passed during polymer deposition, which is then related to the amount of polymer deposited using Faraday's law.<sup>95</sup> Furthermore, electropolymerization is a convenient method for *in situ* monitoring of polymer film growth by various spectroscopic and electrochemical techniques.<sup>95</sup> The limitations of electrochemical synthesis include low yield and absence of well defined structure of the polymer.<sup>76</sup>

### **1.2.2 Polypyrroles**

Polypyrroles are one of the most extensively studied conducting polymers to date because of the considerable interest in its use for fundamental research as well as for commercial applications.<sup>76, 96, 97</sup> Compared to other conducting polymers including polyacetylene, polypyrrole possess the ability to make derivatives with wide conductivity ranges and offers excellent chemical as well as thermal stability.<sup>97</sup> For the past few years significant progress has been made to improve the physical properties of polypyrroles including conductivity, processability and stability.

#### **1.2.2.1 Chemical and Electrochemical Synthesis of Polypyrrole**

Polypyrrole can be synthesized from pyrrole monomer by oxidative electrochemical polymerization or chemical oxidation using oxidizing agents.<sup>76, 96, 98</sup> An important advantage is the relatively low oxidation potential of the pyrrole monomer, which enables the use of mild or moderate oxidizing agents, including  $\text{FeCl}_3$ ,  $\text{Fe}_2(\text{SO}_4)_3$ ,  $\text{K}_3[\text{Fe}(\text{CN})_6]$ ,  $\text{I}_2$  and  $\text{CuCl}_2$ , for the chemical synthesis of polypyrrole.<sup>76</sup> Ferric salts are often used for the synthesis of highly conducting polypyrroles with conductivities greater than 100 S/cm.<sup>76, 99, 100</sup> The parameters that affect the

conductivity of chemically synthesized polymer include monomer to oxidant ratio, nature of the solvent, time of reaction and temperature.<sup>76</sup>

Electrochemical synthesis of polypyrrole involves anodic deposition of pyrrole monomer, dissolved in a suitable solvent, in presence of dopant anions (usually present as electrolyte).<sup>76, 96</sup> Inert electrode materials such as gold, platinum, glassy carbon are used as anodes to avoid possible oxidation of the substrate under oxidative electrochemical conditions. Polypyrrole electrochemical deposition can be performed under galvanostatic, potentiostatic or potentiodynamic conditions.<sup>76</sup> The applied electrochemical conditions influences the polymer growth which in turn influences the structure and properties of the resulting polymer film.<sup>76, 96</sup> At lower potentials, the polymer deposition rate will be slower and yield relatively homogenous films.<sup>85</sup> However, higher potentials give rapid film growth rate, non-uniform films and possible over-oxidation.<sup>101</sup> In galvanostatic deposition, the electrode is kept at constant current conditions that the potentials can move to values where unwanted side reactions such as over-oxidation may occur. Therefore, potentiostatic depositions are preferred over galvanostatic conditions to avoid any over-oxidation of the polymer.<sup>85</sup>

#### **1.2.2.2 Structure and Properties of Polypyrrole**

The mechanism of pyrrole electropolymerization is often represented as  $E(CE)_n$  as it involves successive chemical (C) and electron transfer reaction (E) steps.<sup>76, 98</sup> Among the various mechanisms proposed for pyrrole polymerization, the mechanism suggested by Diaz et al. is considered the most widely accepted one.<sup>96, 98, 102</sup> The

polymerization is initiated by oxidation of the pyrrole monomer at the electrode surface to yield a resonance stabilized radical cation, as shown in Figure 1.6.<sup>98</sup>

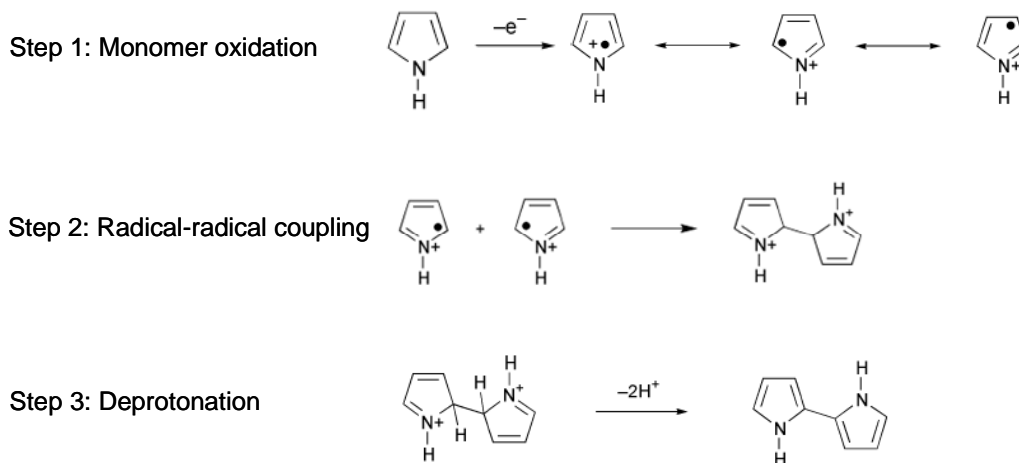


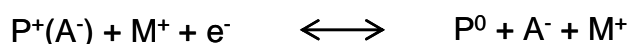
**Figure 1.6.** Mechanism of pyrrole polymerization<sup>98, 102</sup>

In the propagation step, these radical cations couple together through a bond between their  $\alpha$ -positions to form a dihydromer dication which can undergo deprotonation to form an aromatic dimer.<sup>102</sup> This dimer molecule of pyrrole can undergo further oxidation reactions similar to that of the monomer and propagate to oligomers and large polymer chains.<sup>103, 104</sup> The polymerization reaction can undergo termination when the radical cations are inactivated by the nucleophilic attack of water or other impurities present in the system<sup>102</sup> or upon precipitation of the polymer. Pyrrole polymerization is accompanied by a decrease in the pH of the solution which is consistent with the proposed polymerization mechanism involving elimination of  $\alpha$ -protons.<sup>97</sup>

During oxidative electropolymerization of polypyrrole, two electrons are removed from each  $\alpha$  positions and approximately one electron for every four monomer

units to form the doped (oxidized) form.<sup>85</sup> Therefore, approximately 2.25 electrons are removed from each monomer during pyrrole polymerization.<sup>85, 96, 98</sup>

Similar to other conducting polymers, polypyrrole can be electrochemically cycled between its oxidized (conducting) and reduced (insulating) forms. This reversible electrochemical process occurs between the polymer (P), dopant anion (A<sup>-</sup>) and cation (M<sup>+</sup>) in solution can be represented as<sup>89</sup>



i.e. the anions are inserted and de-inserted into the polypyrrole film during redox process and the film shows volume expansion in the oxidized state. However, when the polypyrrole is doped with a large, bulky dopant anion (e.g. dodecylbenzene sulfonate, DBS<sup>-</sup>), only the cations are exchanged during redox process to compensate the charge on the anions trapped inside the polymer (Figure 1.7).<sup>85, 89</sup> Here, the polymer film shows expansion of volume in the reduced state.<sup>105, 106</sup>



The ability of the polypyrrole film to undergo potential induced volume changes has been successfully exploited in the development of microactuators which can be used for analytical as well as biomedical applications.<sup>89, 107</sup>

Polypyrrole with amphiphilic bulky dopants such as dodecylbenzene sulfonates (DBS<sup>-</sup>) has been reported to yield good electrical conductivity and mechanical properties.<sup>89, 107-</sup>

<sup>109</sup> The PPyDBS films can be electrodeposited from the aqueous solution of the

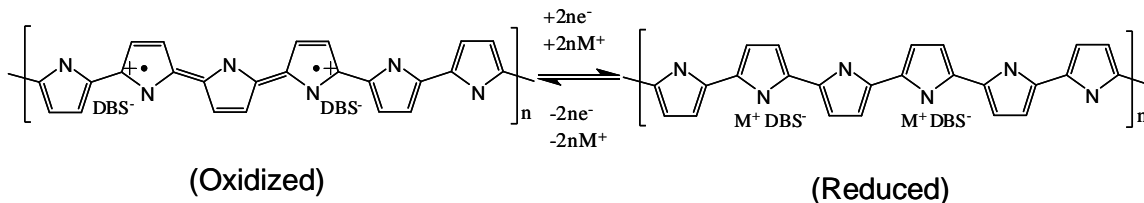


**Figure 1.7** Redox behavior of polypyrrole containing immobile dopant anion (DBS<sup>-</sup>) and mobile cation (M = Li<sup>+</sup>, Na<sup>+</sup> etc.).

monomer and electrolyte by potentiostatic or potentiodynamic methods.<sup>85</sup> The thickness of the resulting PPyDBS films can be estimated from the amount of charge passed during the electrodeposition of the polymer (200 mC/cm<sup>2</sup> for a 1 μm film).<sup>85</sup> As discussed earlier, the redox process of PPyDBS film is accompanied by insertion and deinsertion of the cation present in the solution (Figure 1.8). Therefore, in the reduced state the polymer film contains immobile dopant anions and mobile cations. This composite system is reported to exhibit some interesting electronic properties in the dry state.<sup>110, 111</sup>

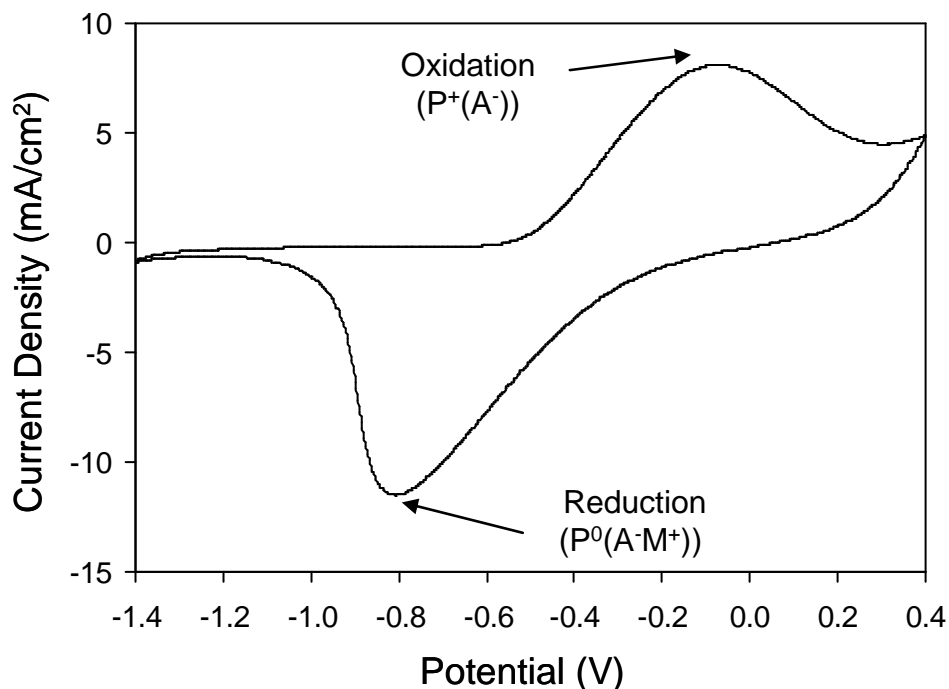


**Figure 1.8.** Cyclic voltammogram of gold IDA electrodes with electrodeposited polypyrrole containing immobile dopant anion (DBS) in aqueous 0.1 M LiClO<sub>4</sub>.

### 1.2.3 Polythiophenes

The properties of some of the conducting polymers, polyacetylene and polypyrrole for example, are highly impeded by their reactivity towards atmospheric oxygen and moisture.<sup>112</sup> Polythiophenes constitute an important class of environmentally stable conducting polymers with the least sensitivity towards oxygen and moisture in their doped and undoped state.<sup>76</sup> The substantial stability of polythiophene and its derivatives towards oxygen and moisture find large area of application including energy conversion and storage, catalysis, sensors and organic electronics.<sup>95, 112-114</sup>

Polythiophenes can be synthesized using chemical or electrochemical methods. Chemical synthesis of polythiophenes involves the treatment of thiophene monomer with a catalytic initiator (e.g.  $\text{FeCl}_3$ , sulphuric acid). The limitations in the processability of polythiophenes are partially compensated in functionalized polythiophenes.

#### 1.2.3.1 Functionalized Polythiophenes

Usually, 3,4 disubstituted polythiophenes are less conducting due to poor conjugation of the polymer backbone by steric effects.<sup>115</sup> For example, doped poly(3,4 dimethylthiophene) exhibit lower conductivity than unsubstituted polythiophenes due to sterically induced twist in the polymer backbone.<sup>115</sup> Oxygen directly attached to the thiophene ring reduces the band gap of the conducting polymer. Furthermore, it avoids any steric twist of the polymer chain which can disrupt the conjugation and lower the conductivity.<sup>115</sup> However, reports of  $\text{FeCl}_3$  doped poly(3-butoxy-4-methylthiophene) exhibiting high conductivity (2 S/cm) indicates that preparation of highly conducting 3,

4-disubstituted polythiophenes could be possible.<sup>94, 116</sup> These results led to the development of one of the most stable conducting polymer, poly(3, 4-ethylenedioxythiophene) or PEDOT.<sup>114, 117</sup> Oxidatively doped PEDOT is almost optically transparent due to a shift in absorbance to the NIR and exhibits excellent conductivity and stability in the doped state.<sup>115, 118</sup> The poor processability of PEDOT has been partially circumvented in PEDOT:PSS composite as described below.<sup>113, 114</sup>

### **1.2.3.2 Poly(3,4-ethylenedioxythiophene):poly(styrenesulfonate) (PEDOT:PSS) composite**

Lefebvre and co-workers reported the first chemical synthesis of PEDOT:PSS from aqueous acetonitrile solutions of EDOT and PSS by oxidation using ferric salts.<sup>94</sup> Commercial aqueous dispersions of PEDOT: PSS have been prepared by Bayer AG from the chemical polymerization of EDOT in a solution of PSS using  $\text{Na}_2\text{S}_2\text{O}_8$  as the oxidizing agent.<sup>113</sup>

PEDOT: PSS has been used in the development of field effect transistors, electronic displays, light emitting diodes and photovoltaic cells.<sup>118</sup> PEDOT:PSS composite can also act as a cation exchanger since cations are trapped inside the composite during the reduction of PEDOT to compensate the negative charge on the immobilized bulky dopant anion (PSS).<sup>94</sup> Since PEDOT:PSS exhibit good ionic (cation) and electronic conductivities, they are used as catalyst supporters in fuel cells, cathode materials in supercapacitors and high power Li ion batteries.<sup>94</sup>

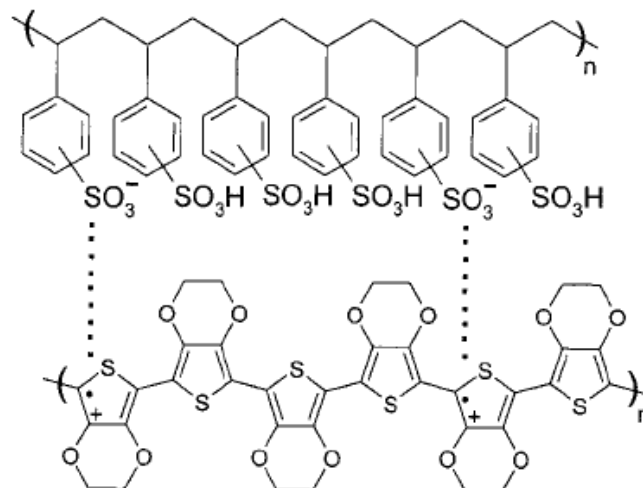


**Figure 1.9.** Chemical structure of PEDOT:PSS polymer<sup>113</sup>

In PEDOT: PSS, the sulfonate anions of insulating PSS act as the counter ions to balance the charge on positively doped, highly conducting PEDOT (Figure 1.9).<sup>118</sup> SEM analysis of the PEDOT: PSS films show an inhomogeneous three dimensional net work of PEDOT islands dispersed in PSS matrix.<sup>119</sup>

## 1.3 Organic Electronics

### 1.3.1 SAMs for Molecular Electronics

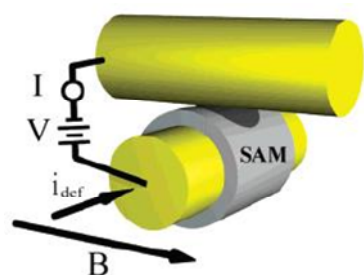
Molecular electronics involve the use of materials of molecular dimensions as active electronic components.<sup>120-122</sup> Here the key idea is have molecules embedded between a pair of electrodes that can perform the basic electronic functions including conduction, rectification and storage to further reduce the size of electronic devices.<sup>121</sup> SAMs can be used as the active molecular components in these junctions due to their ability to form densely packed, well-ordered molecular layers with a wide range of chemical and electronic properties. For the identification of such systems, interpretation

of their electrical measurements relating to the molecular structure, current-voltage response and the mechanism of electron transport is required.<sup>3</sup>

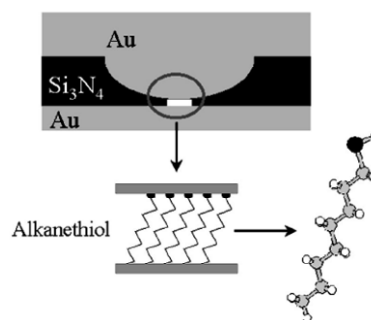
The basic components of a typical molecular junction are one or more molecules sandwiched between a set of two electrodes. For the electrical characterization of these junctions, reliable and reproducible contacts between the molecules and the two probing electrodes are necessary.<sup>3, 123</sup> Except for the break junctions, the second or top electrodes are fabricated after patterning the first or bottom electrode with SAMs. The fabrication of a reliable top electrode is the most challenging part of molecular junction construction.<sup>3, 74, 123, 124</sup> For example, vapour deposition of metals on SAMs possibly cause filamentary growth of the metal atoms through SAMs and results in a very low yield of working devices.<sup>123</sup> Therefore, an ideal top electrode needs to be well defined and reproducible to avoid any short circuits between the electrodes.

A wide range of experimental test-beds, mainly differing in the nature of the top electrode, has been reported for making SAMs based molecular junctions.<sup>122, 123, 125</sup> For example, crossed-wire molecular junctions (Figure 1.10a) are fabricated using two cylindrical metal fibers, of a few micrometers diameter, mounted on a test stage in a crossed geometry.<sup>126</sup> One of the wires is covered with the SAM and the gap between the wires is tuned using magnetic force. Nanopore molecular junctions (Figure 1.10b) have been fabricated on silicon nitride coated silicon wafers.<sup>127, 128</sup> The 'nanopores' were fabricated on suspended silicon nitride membrane using e-beam lithography and plasma etching followed by gold deposition to fill the pores.<sup>127 128</sup> After modifying the gold surface with SAMs, the top electrode contacts are made by low temperature deposition

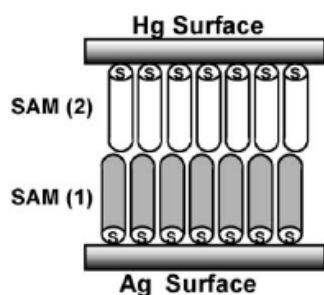
of titanium ( $\sim 0.3$  nm) and gold ( $\sim 80$  nm).<sup>127</sup> Usually the pore size is between 30-60 nm, smaller than the average domain size of SAM.<sup>127</sup> Liquid metal junctions (Figure 1.10c) employ metallic species in their liquid state (e.g. mercury) as the contact electrodes for the molecular junctions. In mercury drop liquid metal junctions, hanging mercury drop electrode (HMDE) is typically used as one of the contact electrode for making molecular junction.<sup>129, 130</sup> However, short-circuiting the junctions by amalgam formation with the bottom electrode (e.g. gold) through the defects in SAMs is possible. Furthermore, the molecules present on opposite electrodes of the liquid metal junction can interdigitate with each other due to hydrophobic interaction between the tail groups.<sup>131, 132</sup> Molecular electronic junctions using crossbar electrode configuration (Figure 1.10d) have been reported for the measurement of electrical properties of covalently attached aromatic molecules on carbon substrate with copper top contacts.<sup>133</sup> These junctions constitute large ensemble of molecules ( $10^6$ - $10^{12}$ ) sandwiched between two conducting contacts placed perpendicular to each other. Crossbar electrodes configured molecular junctions have the potential for making scalable, high density nanoelectronic devices.<sup>134</sup> Break junctions (Figure 1.10e) of a few nanometer sizes are typically formed by passing high electrical current through lithographically defined metal nanowires.<sup>135, 136</sup> The high current density in the nanowire causes electromigration (motion of atoms in materials subjected to high electron current density) and eventual break down of the material to form junctions with  $\sim 1$ -2 nm gap.<sup>135</sup> Similar nano gap junctions, formed by mechanical breakdown of the gold wires, have been used to study the electrical properties of aromatic dithiol molecules.<sup>137</sup>



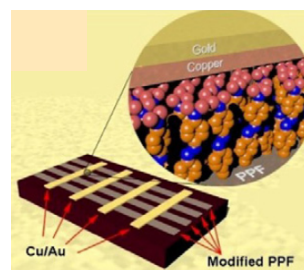
a) Crossed-wire junction



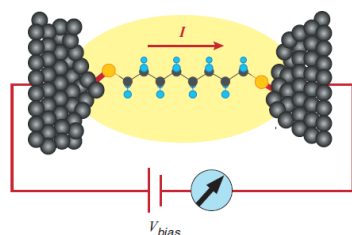
b) Nanopore junction



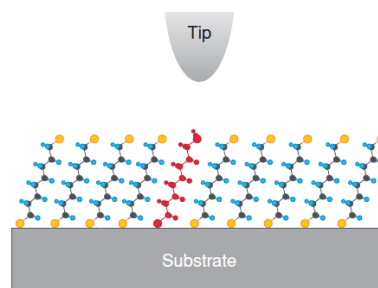
c) Liquid metal junction



d) Crossbar junction



e) Break junction



f) STM/cp AFM junction

**Figure 1.10.** Schematic representation of some molecular junction test-beds: a) Au/SAM/Au crossed-wire junction<sup>126</sup> b) Au/SAM/Au nanopore junction<sup>127, 128</sup> c) Hg/SAM/Ag liquid metal junction<sup>138</sup> d) carbon/organic molecules/copper crossbar junction<sup>133</sup> e) Metal/Single molecule/Metal break junction<sup>74</sup> f) Metal/SAM/Metal STM/cpAFM junction<sup>74</sup>.

Scanning probe techniques including scanning tunneling microscopy (STM) and conducting probe atomic force microscopy (cpAFM) (Figure 1.10f) have been used for studying electronic transport through a monolayer of molecules.<sup>74, 139-141</sup> In these

techniques, conducting metal tips have been used as the top electrode for making metal-SAM-metal junctions. For example, in cpAFM, a metal coated AFM tip under controlled load can form mechanically stable electrical contacts with the monolayer surface.<sup>141</sup> The current-voltage characteristics of metal-SAM-metal junctions prepared using scanning probe techniques show that the junction resistance increases with the monolayer thickness (hydrocarbon chain length), as expected for a dielectric electron tunneling junction.<sup>74</sup>

However, most of these molecular junction test-beds require complex fabrication process that may not be useful in making real devices. Furthermore, the uncertainties associated with the experimental setup (e.g. actual contact area of the junction) affect the reproducibility and reliability of the test results. Therefore single molecule and large area junction measurements often show different conductance value.<sup>123</sup>

### **1.3.2 Large Area Molecular Junctions with Conjugated Polymer Soft Contacts**

There are recent reports about the formation of large area molecular junctions with SAMs where a conjugated conducting polymer composite, PEDOT:PSS, is used as the top electrode contact.<sup>124</sup> The current-voltage characteristics of these molecular junctions involving alkanethiol or alkanedithiol SAMs show that the predominant electron transfer mechanism is tunneling.<sup>123, 142</sup>

The fabrication of large area molecular junctions is schematically described in Figure 1.11.<sup>124</sup> The gold bottom contacts are evaporated on a Si/SiO<sub>2</sub> wafer. An insulating photoresist is spin coated on the wafer and the holes of diameter ranging

from 10 to 100 $\mu$ m are patterned using standard photolithography methods. The SAMs of alkanethiols or dithiols are deposited on the exposed gold surface which can act as the bottom electrode in the molecular junctions. After SAM formation, a water based suspension of PEDOT:PSS is spin coated to form a highly conducting ( $\sim 30$  S/cm) top contact over the SAMs. The use of water based suspension may reduce the chances of penetration through the hydrophobic monolayer and shorting of the junctions. A gold top electrode is vapour deposited over the polymer layer using a shadow mask and the exposed PEDOT:PSS is removed by reactive ion etching. These junctions show good long term stability at the room temperature.<sup>143</sup>

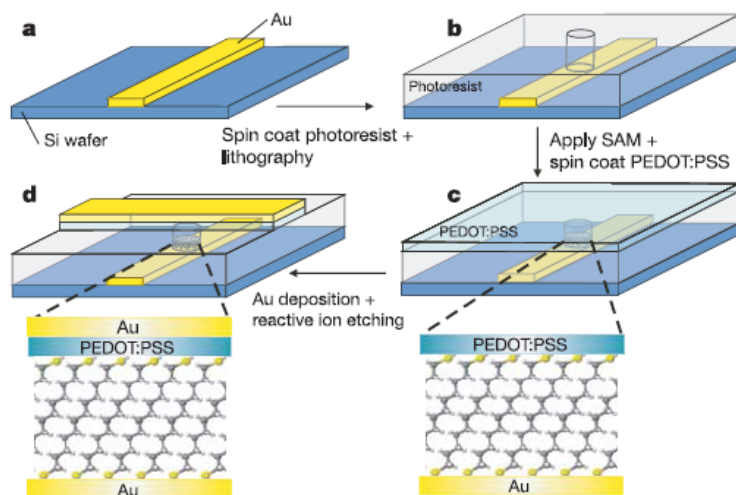


**Figure 1.11.** Fabrication of large area molecular Junctions.<sup>124</sup> a) Fabrication of bottom gold electrode b) formation of vertical interconnects by photolithography c) SAM sandwiched between bottom gold electrode and PEDOT:PSS top layer d) Completion of the junction by deposition of top gold electrode

## 1.4 Thesis Overview

The research work discussed in this thesis is related to an investigation of the mechanistic aspects of electrochemically directed self-assembly of alkylthiosulfates and its potential for use in molecular electronic applications. In this work, depositions of the organic materials were performed on prefabricated device structures that no further lithographic or metal deposition steps required after modification of the electrodes with the organic molecules.

The initial chapters of this thesis focus on exploring the mechanistic aspects of alkylthiosulfate chemisorption by conventional and electrochemically directed self-assembly. The following chapters discuss the unique electronic properties observed with a conducting polymer composite material. The idea of using conducting polymers in this work is for two specific reasons. First, to explore their applications in nanoelectronics and second, the possibility of using them in contact on SAMs for molecular electronics applications. Finally, proof of concept for using a conducting polymer as a top contact in molecular electronic devices created using electrochemically directed self-assembly is demonstrated.

In Chapter 2, the mechanism of alkylthiosulfate chemisorption, particularly the role of solvent and electrolyte, on gold is discussed. The results are compared with the corresponding alkanethiols since they form monolayers similar to that of alkylthiosulfates. It has been found that the electrolyte controls alkylthiosulfate self-assembly by sequestering trace water, otherwise available for alkylthiosulfate

chemisorption on gold. Finally, a mechanism for alkylthiosulfate self-assembly on gold surface has been proposed.

Electrochemically directed self-assembly of alkylthiosulfate enables fast and selective monolayer formation on gold surfaces. However, to date the mechanism of monolayer formation in electrochemically directed self-assembly has not been investigated in detail. For example, existing literature assumes that the mechanism of self-assembly involves direct electron transfer from alkylthiosulfate molecules to gold. Chapter 3 portrays an in-depth analysis of the mechanism of electrochemically directed self-assembly and shows that the mechanism involves mediation by gold oxide and the direct electron transfer do not occur. Furthermore, the results presented demonstrate that a similar mechanism occurs with alkanethiols.

Recently, stable molecular electronic junctions are reported with SAMs and conducting polymers that act as soft top contacts. Conducting polymers are considered as excellent candidates for organic electronic applications since their properties can be controlled by the manipulation of molecular architecture. In Chapter 4, a new approach that exploits the field-induced drift of dopants in a semiconducting polymer composite (PPy<sup>+</sup>DBS<sup>-</sup>Li<sup>+</sup>) containing immobile dopant anions and mobile cations is discussed. The composite shows a unique conducting mechanism involving ion drift driven by an electric field within the solid bulk polymer, which is consistent with our experimental studies. In the solid state, the composite show a field dependent resistance with a time dependence as a function of the mobility of the cation. Using this method, a functioning dynamic memory device has been demonstrated. This approach has more favourable

scaling of properties in comparison to interfacial phenomena observed with Si-based devices.

Chapter 5 explores the scalability of the dynamic polymer memory device, discussed in the previous chapter, to smaller dimensions for nanoelectronics applications. The deposition of semiconducting polymer composite ( $\text{PPy}^+\text{DBS}^-\text{Li}^+$ ) is performed on gold crossbar architecture and demonstrated resistive memory in a  $10 \times 10$  crossbar array junctions. The ability to electrochemically control the deposition of the polymer shows that these junctions can be made with good reproducibility. Analysis of the working junctions shows good repeatability and reliability of this approach.

In Chapter 6, discuss about the challenges that identified in making a proof-of-concept molecular junction device using electrochemically directed self-assembly of alkylthiosulfates on gold crossbar arrays. Alkylthiosulfates with varying hydrocarbon chain lengths are electrochemically deposited on discrete top electrodes in a  $10 \times 10$  gold crossbar array. Solution-casted PEDOT: PSS polymer with high conductivity was used as a top contact for the SAMs. The molecular junctions were characterized using electrochemical methods and electron microscopy. Electrical measurements were performed across the top and bottom electrodes in the junction. Important design rules have been suggested for the creation of SAMs based molecular junctions in the future.

Chapter 7 presents an overall summary of the thesis and suggests possible directions for future work.

## References

1. Lee, Y. S., *Self-Assembly and Nanotechnology : A Force Balance Approach*. John Wiley & Sons: Hoboken, N.J., 2008.
2. Whitesides, G. M.; Grzybowski, B., Self-Assembly at All Scales. *Science* **2002**, 295, (5564), 2418-2421.
3. Love, J. C.; Estroff, L. A.; Kriebel, J. K.; Nuzzo, R. G.; Whitesides, G. M., Self-assembled Monolayers of Thiolates on Metals as a Form of Nanotechnology. *Chemical Reviews* **2005**, 105, (4), 1103-1169.
4. Whitesides, G. M.; Boncheva, M., Beyond molecules: Self-assembly of mesoscopic and macroscopic components. *Proceedings of the National Academy of Sciences of the United States of America* **2002**, 99, (8), 4769-4774.
5. Fialkowski, M.; Bishop, K. J. M.; Klajn, R.; Smoukov, S. K.; Campbell, C. J.; Grzybowski, B. A., Principles and Implementations of Dissipative (Dynamic) Self-Assembly. *Journal of Physical Chemistry B* **2006**, 110, (6), 2482-2496.
6. Grzybowski, B. A.; Stone, H. A.; Whitesides, G. M., Dynamic Self-Assembly of Magnetized, Millimetre-Sized Objects Rotating at a Liquid-Air Interface. *Nature* **2000**, 405, (6790), 1033-1036.
7. Colfen, H.; Mann, S., Higher-order organization by mesoscale self-assembly and transformation of hybrid nanostructures. *Angewandte Chemie-International Edition* **2003**, 42, (21), 2350-2365.
8. Grzybowski, B. A.; Wilmer, C. E.; Kim, J.; Browne, K. P.; Bishop, K. J. M., Self-assembly: from crystals to cells. *Soft Matter* **2009**, 5, (6), 1110-1128.
9. Gross, R.; Dorigo, M., Self-Assembly at the Macroscopic Scale. *Proceedings of the IEEE* **2008**, 96, (9), 1490-1508.
10. Salgado, E. N.; Radford, R. J.; Tezcan, F. A., Metal-Directed Protein Self-Assembly. *Accounts of Chemical Research* **2010**, 43, (5), 661-672.
11. Finklea, H. O., Self-Assembled Monolayers on Electrodes. In *Encyclopedia of Analytical Chemistry : Applications, Theory, and Instrumentation*, Meyers, R. A., Ed. Wiley: New York, **2000**.
12. Kokkoli, E.; Mardilovich, A.; Wedekind, A.; Rexeisen, E. L.; Garg, A.; Craig, J. A., Self-Assembly and Applications of Biomimetic and Bioactive Peptide-Amphiphiles. *Soft Matter* **2006**, 2, (12), 1015-1024.

13. Hegmann, T.; Qi, H.; Marx, V. M., Nanoparticles in Liquid Crystals: Synthesis, Self-Assembly, Defect Formation and Potential Applications. *Journal of Inorganic and Organometallic Polymers and Materials* **2007**, 17, (3), 483-508.
14. Boker, A.; He, J.; Emrick, T.; Russell, T. P., Self-assembly of nanoparticles at interfaces. *Soft Matter* **2007**, 3, 1231-1248.
15. Ulman, A., Formation and structure of self-assembled monolayers. *Chemical Reviews* **1996**, 96, (4), 1533-1554.
16. Gooding, J. J.; Mearns, F.; Yang, W. R.; Liu, J. Q., Self-Assembled Monolayers into the 21(st) Century: Recent Advances and Applications. *Electroanalysis* **2003**, 15, (2), 81-96.
17. Lukkari, J.; Meretoja, M.; Kartio, I.; Laajalehto, K.; Rajamaki, M.; Lindstrom, M.; Kankare, J., Organic thiosulfates (Bunte salts): Novel surface-active sulfur compounds for the preparation of self-assembled monolayers on gold. *Langmuir* **1999**, 15, (10), 3529-3537.
18. Bain, C. D.; Troughton, E. B.; Tao, Y. T.; Evall, J.; Whitesides, G. M.; Nuzzo, R. G., Formation of Monolayer Films by the Spontaneous Assembly of Organic Thiols from Solution onto Gold. *Journal of the American Chemical Society* **1989**, 111, (1), 321-335.
19. Troughton, E. B.; Bain, C. D.; Whitesides, G. M.; Nuzzo, R. G.; Allara, D. L.; Porter, M. D., Monolayer Films Prepared by the Spontaneous Self-Assembly of Symmetrical and Unsymmetrical Dialkyl Sulfides from Solution onto Gold Substrates - Structure, Properties, and Reactivity of Constituent Functional-Groups. *Langmuir* **1988**, 4, (2), 365-385.
20. Nuzzo, R. G.; Allara, D. L., Adsorption of Bifunctional Organic Disulfides on Gold Surfaces. *Journal of the American Chemical Society* **1983**, 105, (13), 4481-4483.
21. Hsueh, C. C.; Lee, M. T.; Freund, M. S.; Ferguson, G. S., Electrochemically Directed Self-Assembly on Gold. *Angewandte Chemie-International Edition* **2000**, 39, (7), 1228-1230.
22. Liao, S.; Shnidman, Y.; Ulman, A., Adsorption kinetics of rigid 4-mercaptobiphenyls on gold. *Journal of the American Chemical Society* **2000**, 122, (15), 3688-3694.
23. Ma, F. Y.; Lennox, R. B., Potential-assisted deposition of alkanethiols on Au: Controlled preparation of single- and mixed-component SAMs. *Langmuir* **2000**, 16, (15), 6188-6190.

24. Meyers, R. A., *Encyclopedia of analytical chemistry : applications, theory, and instrumentation*. Wiley: Chichester; New York, 2000.
25. Byloos, M.; Al-Maznai, H.; Morin, M., Formation of a Self-Assembled Monolayer via the Electrospreading of Physisorbed Micelles of Thiolates. *Journal of Physical Chemistry B* **1999**, 103, (31), 6554-6561.
26. Cheng, L.; Yang, J. P.; Yao, Y. X.; Price, D. W.; Dirk, S. M.; Tour, J. M., Comparative Study of Electrochemically Directed Assembly Versus Conventional Self-Assembly of Thioacetyl-Terminated Oligo(phenylene ethynylene)s on Gold and Platinum Surface. *Langmuir* **2004**, 20, (4), 1335-1341.
27. Ron, H.; Rubinstein, I., Self-assembled monolayers on oxidized metals. 3. Alkylthiol and dialkyl disulfide assembly on gold under electrochemical conditions. *Journal of the American Chemical Society* **1998**, 120, (51), 13444-13452.
28. Hatchett, D. W.; Stevenson, K. J.; Lacy, W. B.; Harris, J. M.; White, H. S., Electrochemical Oxidative Adsorption of Ethanethiolate on Ag(111). *Journal of the American Chemical Society* **1997**, 119, (28), 6596-6606.
29. Stevenson, K. J.; Mitchell, M.; White, H. S., Oxidative adsorption of n-alkanethiolates at mercury. Dependence of adsorption free energy on chain length. *Journal of Physical Chemistry B* **1998**, 102, (7), 1235-1240.
30. Paik, W. K.; Eu, S.; Lee, K.; Chon, S.; Kim, M., Electrochemical reactions in adsorption of organosulfur molecules on gold and silver: Potential dependent adsorption. *Langmuir* **2000**, 16, (26), 10198-10205.
31. Brett, C. M. A.; Kresak, S.; Hianik, T.; Brett, A. M. O., Studies on Self-Assembled Alkanethiol Monolayers Formed at Applied Potential on Polycrystalline Gold Electrodes. *Electroanalysis* **2003**, 15, (5-6), 557-565.
32. Weisshaar, D. E.; Lamp, B. D.; Porter, M. D., Thermodynamically Controlled Electrochemical Formation of Thiolate Monolayers at Gold - Characterization and Comparison to Self-Assembled Analogs. *Journal of the American Chemical Society* **1992**, 114, (14), 5860-5862.
33. Lee, M. T.; Hsueh, C. C.; Freund, M. S.; Ferguson, G. S., Electrochemical self-assembly of monolayers from alkylthiosulfates on gold. *Langmuir* **2003**, 19, (13), 5246-5253.
34. Buttry, D. A.; Ward, M. D., Measurement of Interfacial Processes at Electrode Surfaces with the Electrochemical Quartz Crystal Microbalance. *Chemical Reviews* **1992**, 92, (6), 1355-1379.

35. Schumacher, R., The Quartz Microbalance - A Novel-Approach to the Insitu Investigation of Interfacial Phenomena at the Solid Liquid Junction. *Angewandte Chemie-International Edition in English* **1990**, 29, (4), 329-343.
36. Degennes, P. G., Wetting - Statics and Dynamics. *Reviews of Modern Physics* **1985**, 57, (3), 827-863.
37. Kwok, D. Y.; Gietzelt, T.; Grundke, K.; Jacobasch, H. J.; Neumann, A. W., Contact angle measurements and contact angle interpretation .1. Contact angle measurements by axisymmetric drop shape analysis and a goniometer sessile drop technique. *Langmuir* **1997**, 13, (10), 2880-2894.
38. Blosssey, R., Self-Cleaning Surfaces - Virtual Realities. *Nature Materials* **2003**, 2, (5), 301-306.
39. Yang, J.; Han, J. M.; Isaacson, K.; Kwok, D. Y., Effects of surface defects, polycrystallinity, and nanostructure of self-assembled monolayers for octadecanethiol adsorbed onto Au on wetting and its surface energetic interpretation. *Langmuir* **2003**, 19, (22), 9231-9238.
40. Bard, A. J.; Faulkner, L. R., *Electrochemical Methods and Applications*. Wiley-Interscience: New York; London, **2000**.
41. Zhong, C. J.; Woods, N. T.; Dawson, G. B.; Porter, M. D., Formation of thiol-based monolayers on gold: implications from open circuit potential measurements. *Electrochemistry Communications* **1999**, 1, (1), 17-21.
42. Chon, S.; Paik, W. K., Adsorption of self-assembling sulfur compounds through electrochemical reactions: Effects of potential, acid and oxidizing agents. *Physical Chemistry Chemical Physics* **2001**, 3, (16), 3405-3410.
43. Cohen-Atiya, M.; Mandler, D., Studying thiol adsorption on Au, Ag and Hg surfaces by potentiometric measurements. *Journal of Electroanalytical Chemistry* **2003**, 550, 267-276.
44. Janek, R. P.; Fawcett, W. R.; Ulman, A., Impedance spectroscopy of self-assembled monolayers on Au(111): Sodium ferrocyanide charge transfer at modified electrodes. *Langmuir* **1998**, 14, (11), 3011-3018.
45. Finklea, H. O.; Snider, D. A.; Fedyk, J.; Sabatani, E.; Gafni, Y.; Rubinstein, I., Characterization of Octadecanethiol-Coated Gold Electrodes as Microarray Electrodes by Cyclic Voltammetry and Ac-Impedance Spectroscopy. *Langmuir* **1993**, 9, (12), 3660-3667.
46. Downard, A. J.; Prince, M. J., Barrier Properties of Organic Monolayers on Glassy Carbon Electrodes. *Langmuir* **2001**, 17, (18), 5581-5586.

47. Karpovich, D. S.; Blanchard, G. J., Direct Measurement of the Adsorption-Kinetics of Alkanethiolate Self-Assembled Monolayers on a Microcrystalline Gold Surface. *Langmuir* **1994**, 10, (9), 3315-3322.
48. Briggs, D.; Grant, J. T.; SurfaceSpectra Limited., *Surface Analysis by Auger and x-ray Photoelectron Spectroscopy*. IM Publications: Chichester, 2003.
49. Hollander, J. M.; Jolly, W. L., X-Ray Photoelectron Spectroscopy. *Accounts of Chemical Research* **1970**, 3, (6), 193-200.
50. Kondo, T.; Yanagida, M.; Shimazu, K.; Uosaki, K., Determination of thickness of a self-assembled monolayer of dodecanethiol on Au(111) by angle-resolved X-ray photoelectron spectroscopy. *Langmuir* **1998**, 14, (19), 5656-5658.
51. Hollande.Jm; Jolly, W. L., X-Ray Photoelectron Spectroscopy. *Accounts of Chemical Research* **1970**, 3, (6), 193-&.
52. Ishida, T.; Choi, N.; Mizutani, W.; Tokumoto, H.; Kojima, I.; Azehara, H.; Hokari, H.; Akiba, U.; Fujihira, M., High-Resolution X-ray Photoelectron Spectra of Organosulfur Monolayers on Au(111): S(2p) Spectral Dependence on Molecular Species. *Langmuir* **1999**, 15, (20), 6799-6806.
53. Castner, D. G.; Hinds, K.; Grainger, D. W., X-ray Photoelectron Spectroscopy Sulfur 2p Study of Organic Thiol and Disulfide Binding Interactions with Gold Surfaces. *Langmuir* **1996**, 12, (21), 5083-5086.
54. Lamp, B. D.; Hobara, D.; Porter, M. D.; Niki, K.; Cotton, T. M., Correlation of the structural decomposition and performance of pyridinethiolate surface modifiers at gold electrodes for the facilitation of cytochrome c heterogeneous electron-transfer reactions. *Langmuir* **1997**, 13, (4), 736-741.
55. Huang, J. Y.; Hemminger, J. C., Photooxidation of Thiols in Self-Assembled Monolayers on Gold. *Journal of the American Chemical Society* **1993**, 115, (8), 3342-3343.
56. Lee, M. T.; Hsueh, C. C.; Freund, M. S.; Ferguson, G. S., Air oxidation of self-assembled monolayers on polycrystalline gold: The role of the gold substrate. *Langmuir* **1998**, 14, (22), 6419-6423.
57. Gates, B. D.; Xu, Q. B.; Stewart, M.; Ryan, D.; Willson, C. G.; Whitesides, G. M., New Approaches to Nanofabrication: Molding, Printing, and Other Techniques. *Chemical Reviews* **2005**, 105, (4), 1171-1196.
58. Finklea, H. O., Electrochemistry of Organized Monolayers of Thiols and Related Molecules on Electrodes. In *Electroanalytical Chemistry: A Series of Advances, Vol 19*, 1996; Vol. 19, pp 109-335.

59. Porter, M. D.; Bright, T. B.; Allara, D. L.; Chidsey, C. E. D., Spontaneously Organized Molecular Assemblies .4. Structural Characterization of Normal-Alkyl Thiol Monolayers on Gold by Optical Ellipsometry, Infrared-Spectroscopy, and Electrochemistry. *Journal of the American Chemical Society* **1987**, 109, (12), 3559-3568.
60. Flink, S.; van Veggel, F.; Reinhoudt, D. N., Sensor Functionalities in Self-Assembled Monolayers. *Advanced Materials* **2000**, 12, (18), 1315-1328.
61. Mirsky, V. M., New electroanalytical applications of self-assembled monolayers. *Trac-Trends in Analytical Chemistry* **2002**, 21, (6-7), 439-450.
62. Tsukruk, V. V., Molecular lubricants and glues for micro- and nanodevices. *Advanced Materials* **2001**, 13, (2), 95-108.
63. Maboudian, R.; Carraro, C., Surface chemistry and tribology of MEMS. *Annual Review of Physical Chemistry* **2004**, 55, 35-54.
64. Yamamoto, Y.; Nishihara, H.; Aramaki, K., Self-Assembled Layers of Alkanethiols on Copper for Protection against Corrosion. *Journal of the Electrochemical Society* **1993**, 140, (2), 436-443.
65. Zamborini, F. P.; Crooks, R. M., Corrosion passivation of gold by n-alkanethiol self-assembled monolayers: Effect of chain length and end group. *Langmuir* **1998**, 14, (12), 3279-3286.
66. Jennings, G. K.; Munro, J. C.; Yong, T. H.; Laibinis, P. E., Effect of chain length on the protection of copper by n-alkanethiols. *Langmuir* **1998**, 14, (21), 6130-6139.
67. Kumar, A.; Biebuyck, H. A.; Whitesides, G. M., Patterning Self-Assembled Monolayers - Applications in Materials Science. *Langmuir* **1994**, 10, (5), 1498-1511.
68. Lahann, J.; Mitragotri, S.; Tran, T. N.; Kaido, H.; Sundaram, J.; Choi, I. S.; Hoffer, S.; Somorjai, G. A.; Langer, R., A reversibly switching surface. *Science* **2003**, 299, (5605), 371-374.
69. Wink, T.; vanZuilen, S. J.; Bult, A.; vanBennekom, W. P., Self-assembled monolayers for biosensors. *Analyst* **1997**, 122, (4), R43-R50.
70. Datwani, S. S.; Vijayendran, R. A.; Johnson, E.; Biondi, S. A., Mixed Alkanethiol Self-Assembled Monolayers as Substrates for Microarraying Applications. *Langmuir* **2004**, 20, (12), 4970-4976.

71. Liedberg, B.; Tengvall, P., Molecular Gradients of Omega-Substituted Alkanethiols on Gold - Preparation and Characterization. *Langmuir* **1995**, *11*, (10), 3821-3827.
72. McCreery, R. L.; Bergren, A. J., Progress with Molecular Electronic Junctions: Meeting Experimental Challenges in Design and Fabrication. *Advanced Materials* **2009**, *21*, (43), 4303-4322.
73. Carroll, R. L.; Gorman, C. B., The genesis of molecular electronics. *Angewandte Chemie-International Edition* **2002**, *41*, (23), 4379-4400.
74. Chen, F.; Hihath, J.; Huang, Z. F.; Li, X. L.; Tao, N. J., Measurement of single-molecule conductance. *Annual Review of Physical Chemistry* **2007**, *58*, 535-564.
75. Wynne, K. J.; Street, G. B., Conducting Polymers - a Short Review. *Industrial & Engineering Chemistry Product Research and Development* **1982**, *21*, (1), 23-28.
76. Nalwa, H. S., *Handbook of Organic Conductive Molecules and Polymers; Conductive Polymers: Synthesis and Electrical Properties*. J. Wiley & Sons: Chichester, **1997**; Vol. 2.
77. Skotheim, T., *Handbook of conducting polymers vol. 1*. Taylor & Francis, Inc: New York, 1986.
78. Inzelt, G., *Conducting Polymers: A New Era in Electrochemistry*. Springer: Berlin; Heidelberg, **2008**.
79. Frommer, J. E., Conducting Polymer-Solutions. *Accounts of Chemical Research* **1986**, *19*, (1), 2-9.
80. Freund, M. S.; Deore, B., *Self-Doped Conducting Polymers*. Wiley: Chichester, England; Hoboken, NJ, 2007.
81. Heeger, A. J., Semiconducting and metallic polymers: The fourth generation of polymeric materials (Nobel lecture). *Angewandte Chemie-International Edition* **2001**, *40*, (14), 2591-2611.
82. MacDiarmid, A. G., "Synthetic metals": A novel role for organic polymers (Nobel lecture). *Angewandte Chemie-International Edition* **2001**, *40*, (14), 2581-2590.
83. Shirakawa, H., The discovery of polyacetylene film: The dawning of an era of conducting polymers (Nobel lecture). *Angewandte Chemie-International Edition* **2001**, *40*, (14), 2575-2580.
84. McQuade, D. T.; Pullen, A. E.; Swager, T. M., Conjugated polymer-based chemical sensors. *Chemical Reviews* **2000**, *100*, (7), 2537-2574.

85. Smela, E., Microfabrication of PPy Microactuators and Other Conjugated Polymer Devices. *Journal of Micromechanics and Microengineering* **1999**, 9, (1), 1-18.
86. Chiang, C. K.; Jr., F., C. R.; Park, Y. W.; Heeger, A. J.; Shirakawa, H.; Louis, E. J.; Gau, S. C.; MacDiarmid, A. G., Electrical Conductivity in Doped Polyacetylene. *Physical Review Letters* **1977**, 39, 1098-1101.
87. Sonmez, G.; Sonmez, H. B.; Shen, C. K. E.; Wudl, F., Red, green, and blue colors in polymeric electrochromics. *Advanced Materials* **2004**, 16, (21), 1905-1908.
88. Pei, Q. B.; Yu, G.; Zhang, C.; Yang, Y.; Heeger, A. J., Polymer Light-Emitting Electrochemical-Cells. *Science* **1995**, 269, (5227), 1086-1088.
89. Jager, E. W. H.; Smela, E.; Inganas, O., Microfabricating Conjugated Polymer actuators. *Science* **2000**, 290, (5496), 1540-1545.
90. Burroughes, J. H.; Jones, C. A.; Friend, R. H., New Semiconductor-Device Physics in Polymer Diodes and Transistors. *Nature* **1988**, 335, (6186), 137-141.
91. Chao, S.; Wrighton, M. S., Solid-State Microelectrochemistry - Electrical Characteristics of a Solid-State Microelectrochemical Transistor Based on Poly(3-Methylthiophene). *Journal of the American Chemical Society* **1987**, 109, (7), 2197-2199.
92. Novak, P.; Muller, K.; Santhanam, K. S. V.; Haas, O., Electrochemically active polymers for rechargeable batteries. *Chemical Reviews* **1997**, 97, (1), 207-281.
93. Angelopoulos, M., Conducting Polymers in Microelectronics. *Ibm Journal of Research and Development* **2001**, 45, (1), 57-75.
94. Lefebvre, M.; Qi, Z. G.; Rana, D.; Pickup, P. G., Chemical synthesis, characterization, and electrochemical studies of poly(3,4-ethylenedioxythiophene)/poly(styrene-4-sulfonate) composites. *Chemistry of Materials* **1999**, 11, (2), 262-268.
95. Roncali, J., Conjugated Poly(Thiophenes) - Synthesis, Functionalization, and Applications. *Chemical Reviews* **1992**, 92, (4), 711-738.
96. Diaz, A. F., Bargon, J, Electrochemical Synthesis of Conducting Polymers. In *Handbook of Conducting Polymers*, Skotheim, T., Ed. Taylor & Francis, Inc: New York, **1986**; Vol. 1.
97. Street, G. B., Polypyrrole: From Powders to Plastics. In *Handbook of Conducting Polymers vol. 1*, Skotheim, T., Ed. Marcel Dekker, Inc: New York, **1986**.

98. Sadki, S.; Schottland, P.; Brodie, N.; Sabouraud, G., The mechanisms of pyrrole electropolymerization. *Chemical Society Reviews* **2000**, 29, (5), 283-293.
99. Kang, E. T.; Neoh, K. G.; Ong, Y. K.; Tan, K. L.; Tan, B. T. G., X-Ray Photoelectron Spectroscopic Studies of Polypyrrole Synthesized with Oxidative Fe(III) Salts. *Macromolecules* **1991**, 24, (10), 2822-2828.
100. Machida, S.; Miyata, S.; Techagumpuch, A., Chemical Synthesis of Highly Electrically Conductive Polypyrrole. *Synthetic Metals* **1989**, 31, (3), 311-318.
101. Lewis, T. W.; Wallace, G. G.; Kim, C. Y.; Kim, D. Y., Studies of the overoxidation of polypyrrole. *Synthetic Metals* **1997**, 84, (1-3), 403-404.
102. Genies, E. M.; Bidan, G.; Diaz, A. F., Spectroelectrochemical Study of Polypyrrole Films. *Journal of Electroanalytical Chemistry* **1983**, 149, (1-2), 101-113.
103. Diaz, A. F.; Crowley, J.; Bargon, J.; Gardini, G. P.; Torrance, J. B., Electrooxidation of Aromatic Oligomers and Conducting Polymers. *Journal of Electroanalytical Chemistry* **1981**, 121, (APR), 355-361.
104. Andrieux, C. P.; Audebert, P.; Hapiot, P.; Saveant, J. M., Identification of the 1st Steps of the Electrochemical Polymerization of Pyrroles by Means of Fast Potential Step Techniques. *Journal of Physical Chemistry* **1991**, 95, (24), 10158-10164.
105. Torresi, R. M.; Detorresi, S. I. C.; Matencio, T.; Depaoli, M. A., Ionic Exchanges in Dodecylbenzenesulfonate-Doped Polypyrrole .2. Electrochemical Quartz-Crystal Microbalance Study. *Synthetic Metals* **1995**, 72, (3), 283-287.
106. Smela, E.; Gadegaard, N., Surprising volume change in PPy(DBS): An atomic force microscopy study. *Advanced Materials* **1999**, 11, (11), 953-957.
107. Smela, E., Conjugated polymer actuators for biomedical applications. *Advanced Materials* **2003**, 15, (6), 481-494.
108. Kupila, E. L.; Kankare, J., Electropolymerization of Pyrrole - Effects of Ph and Anions on the Conductivity and Growth-Kinetics of Polypyrrole. *Synthetic Metals* **1993**, 55, (2-3), 1402-1405.
109. Gandhi, M. R.; Murray, P.; Spinks, G. M.; Wallace, G. G., Mechanism of Electromechanical Actuation in Polypyrrole. *Synthetic Metals* **1995**, 73, (3), 247-256.
110. Pillai, R. G.; Zhao, J. H.; Freund, M. S.; Thomson, D. J., Field-induced carrier generation in conjugated polymer semiconductors for dynamic, asymmetric junctions. *Advanced Materials* **2008**, 20, (1), 49-53.

111. Zhao, J. H.; Thomson, D. J.; Pillai, R. G.; Freund, M. S., Dynamic resistive crossbar memory based on conjugated polymer composite. *Applied Physics Letters* **2009**, 94, (9).
112. Tourillon, G., Polythiophenes and Its Derivatives. In *Handbook of Conducting Polymers*, Skotheim, T. A.; Elsenbaumer, R. L.; Reynolds, J. R., Eds. M. Dekker: New York; Basel, **1998**; Vol. 1.
113. Groenendaal, B. L.; Jonas, F.; Freitag, D.; Pielartzik, H.; Reynolds, J. R., Poly(3,4-ethylenedioxythiophene) and its Derivatives: Past, Present, and Future. *Advanced Materials* **2000**, 12, (7), 481-494.
114. Heywang, G.; Jonas, F., Poly(Alkylenedioxythiophene)S - New, Very Stable Conducting Polymers. *Advanced Materials* **1992**, 4, (2), 116-118.
115. McCullough, R. D., The chemistry of conducting polythiophenes. *Advanced Materials* **1998**, 10, (2), 93-116.
116. Daoust, G.; Leclerc, M., Structure Property Relationships in Alkoxy-Substituted Polythiophenes. *Macromolecules* **1991**, 24, (2), 455-459.
117. Jonas, F.; Schrader, L., Conductive Modifications of Polymers with Polypyrroles and Polythiophenes. *Synthetic Metals* **1991**, 41, (3), 831-836.
118. Crispin, X.; Jakobsson, F. L. E.; Crispin, A.; Grim, P. C. M.; Andersson, P.; Volodin, A.; van Haesendonck, C.; Van der Auweraer, M.; Salaneck, W. R.; Berggren, M., The Origin of the High Conductivity of Poly(3,4-ethylenedioxythiophene)-poly(styrenesulfonate) (PEDOT- PSS) Plastic Electrodes. *Chemistry of Materials* **2006**, 18, (18), 4354-4360.
119. DeLongchamp, D. M.; Vogt, B. D.; Brooks, C. M.; Kano, K.; Obrzut, J.; Richter, C. A.; Kirillov, O. A.; Lin, E. K., Influence of a Water Rinse on the Structure and Properties of Poly(3,4-ethylene dioxythiophene): poly(styrene sulfonate) Films. *Langmuir* **2005**, 21, (24), 11480-11483.
120. Mirkin, C. A.; Ratner, M. A., Molecular Electronics. *Annual Review of Physical Chemistry* **1992**, 43, 719-754.
121. Tour, J. M., Molecular electronics. Synthesis and testing of components. *Accounts of Chemical Research* **2000**, 33, (11), 791-804.
122. McCreery, R. L., Molecular electronic junctions. *Chemistry of Materials* **2004**, 16, (23), 4477-4496.
123. Akkerman, H. B.; de Boer, B., Electrical conduction through single molecules and self-assembled monolayers. *Journal of Physics-Condensed Matter* **2008**, 20, (1).

124. Akkerman, H. B.; Blom, P. W. M.; de Leeuw, D. M.; de Boer, B., Towards molecular electronics with large-area molecular junctions. *Nature* **2006**, 441, (7089), 69-72.
125. Haick, H.; Cahen, D., Contacting organic molecules by soft methods: Towards molecule-based electronic devices. *Accounts of Chemical Research* **2008**, 41, (3), 359-366.
126. Kushmerick, J. G.; Naciri, J.; Yang, J. C.; Shashidhar, R., Conductance scaling of molecular wires in parallel. *Nano Letters* **2003**, 3, (7), 897-900.
127. Zhou, C.; Deshpande, M. R.; Reed, M. A.; Jones, L.; Tour, J. M., Nanoscale metal self-assembled monolayer metal heterostructures. *Applied Physics Letters* **1997**, 71, (5), 611-613.
128. Wang, W. Y.; Lee, T.; Reed, M. A., Mechanism of electron conduction in self-assembled alkanethiol monolayer devices. *Physical Review B* **2003**, 68, (3).
129. Slowinski, K.; Chamberlain, R. V.; Miller, C. J.; Majda, M., Through-bond and chain-to-chain coupling. Two pathways in electron tunneling through liquid alkanethiol monolayers on mercury electrodes. *Journal of the American Chemical Society* **1997**, 119, (49), 11910-11919.
130. Haag, R.; Rampi, M. A.; Holmlin, R. E.; Whitesides, G. M., Electrical Breakdown of Aliphatic and Aromatic Self-Assembled Monolayers Used as Nanometer-Thick Organic Dielectrics. *Journal of the American Chemical Society* **1999**, 121, (34), 7895-7906.
131. Chaki, N. K.; Aslam, M.; Gopakumar, T. G.; Sharma, J.; Pasricha, R.; Mulla, I. S.; Vijayamohanan, K., Effect of Chain Length and the Nature of the Monolayer on the Electrical Behavior of Hydrophobically Organized Gold Clusters. *Journal of Physical Chemistry B* **2003**, 107, (49), 13567-13574.
132. Rieley, H.; Kendall, G. K.; Zemicael, F. W.; Smith, T. L.; Yang, S. H., X-ray studies of self-assembled monolayers on coinage metals. 1. Alignment and photooxidation in 1,8-octanedithiol and 1-octanethiol on Au. *Langmuir* **1998**, 14, (18), 5147-5153.
133. Bergren, A. J.; Harris, K. D.; Deng, F. J.; McCreery, R. L., Molecular Electronics Using Diazonium-Derived Adlayers on Carbon with Cu Top Contacts: Critical Analysis of Metal Oxides and Filaments. *Journal of Physics-Condensed Matter* **2008**, 20, (37).
134. Lu, W.; Lieber, C. M., Nanoelectronics from the bottom up. *Nature Materials* **2007**, 6, (11), 841-850.

135. Park, H.; Lim, A. K. L.; Alivisatos, A. P.; Park, J.; McEuen, P. L., Fabrication of metallic electrodes with nanometer separation by electromigration. *Applied Physics Letters* **1999**, 75, (2), 301-303.
136. Noguchi, Y.; Nagase, T.; Kubota, T.; Kamikado, T.; Mashiko, S., Fabrication of Au-molecule-Au junctions using electromigration method. *Thin Solid Films* **2006**, 499, (1-2), 90-94.
137. Reed, M. A.; Zhou, C.; Muller, C. J.; Burgin, T. P.; Tour, J. M., Conductance of a molecular junction. *Science* **1997**, 278, (5336), 252-254.
138. Grave, C.; Tran, E.; Samori, P.; Whitesides, G. M.; Rampi, M. A., Correlating Electrical Properties and Molecular Structure of SAMs Organized Between Two Metal Surfaces. *Synthetic Metals* **2004**, 147, (1-3), 11-18.
139. Bumm, L. A.; Arnold, J. J.; Dunbar, T. D.; Allara, D. L.; Weiss, P. S., Electron Transfer Through Organic Molecules. *Journal of Physical Chemistry B* **1999**, 103, (38), 8122-8127.
140. Andres, R. P.; Bein, T.; Dorogi, M.; Feng, S.; Henderson, J. I.; Kubiak, C. P.; Mahoney, W.; Osifchin, R. G.; Reifenberger, R., "Coulomb staircase" at room temperature in a self-assembled molecular nanostructure. *Science* **1996**, 272, (5266), 1323-1325.
141. Wold, D. J.; Frisbie, C. D., Formation of metal-molecule-metal tunnel junctions: Microcontacts to alkanethiol monolayers with a conducting AFM tip. *Journal of the American Chemical Society* **2000**, 122, (12), 2970-2971.
142. Akkerman, H. B.; Naber, R. C. G.; Jongbloed, B.; van Hal, P. A.; Blom, P. W. M.; de Leeuw, D. M.; de Boer, B., Electron tunneling through alkanedithiol self-assembled monolayers in large-area molecular junctions. *Proceedings of the National Academy of Sciences of the United States of America* **2007**, 104, (27), 11161-11166.
143. Akkerman, H. B.; Kronemeijer, A. J.; Harkema, J.; van Hal, P. A.; Smits, E. C. P.; de Leeuw, D. M.; Blom, P. W. M., Stability of large-area molecular junctions. *Organic Electronics* **2010**, 11, (1), 146-149.

## Chapter 2:

### Self-Assembly of Alkylthiosulfates on Gold: Role of Electrolyte and Trace Water in the Solvent

### **Authors' Contributions**

All experiments pertaining to this work were designed and conducted by R. G. Pillai. All figures and manuscript drafts were prepared by R. G. Pillai. Dr. M. S. Freund and R. G. Pillai were responsible for revisions and final editing of the manuscript.

# Self-Assembly of Alkylthiosulfates on Gold: Role of Electrolyte and Trace Water in the Solvent

Rajesh G. Pillai<sup>1</sup> and Michael S. Freund<sup>1, 2</sup>

<sup>1</sup>Department of Chemistry and <sup>2</sup>Department of Electrical & Computer Engineering,  
University of Manitoba, Winnipeg, Manitoba R3T 2N2, Canada

## **Abstract**

Spontaneous self-assembly of alkylthiosulfates on gold produce monolayers similar to the corresponding alkanethiols. Alkylthiosulfate self-assembly from THF solutions is inhibited in the presence of tetrabutylammonium tetrafluoroborate electrolyte. However, the mechanism of alkylthiosulfate self-assembly and the role of electrolyte is not well understood. Open-circuit potential and redox electron transfer experiments support the hypothesis that trace water present in the solvent facilitate alkylthiosulfate monolayer formation on gold.

## Introduction

Self assembled monolayers (SAMs) provide a simple method to form highly ordered two dimensional organic assemblies.<sup>1-4</sup> These monolayers have been used as prototypes for fundamental studies in the areas of tribology,<sup>5</sup> surface patterning,<sup>6</sup> bio and analytical sensors<sup>7-9</sup> and molecular electronics.<sup>10</sup> Among the various self assembling systems, alkanethiolate monolayers on gold surfaces are getting wide attention.<sup>4</sup> Spontaneous self-assembly of alkylthiosulfates (Bunte salts) on gold have been reported to form SAMs similar to that of alkanethiols and alkyldisulfides.<sup>11</sup> A novel method for the selective formation of SAMs on gold electrodes was reported using electrochemical oxidation of alkylthiosulfates under solution conditions where spontaneous self-assembly is inhibited.<sup>12</sup> In this particular system the monolayer formation depends on many factors including the applied potential, solvent, substrate and electrolyte.<sup>13</sup> Spontaneous chemisorption of alkylthiosulfates on gold was found to be inhibited by the presence of an electrolyte, tetrabutylammonium tetrafluoroborate (TBATFB), enabling electrochemically directed self-assembly.<sup>12</sup> This behavior was attributed to the tetrafluoroborate anion and was not observed with other tetrabutylammonium salts including tetrabutylammonium hexafluorophosphate and tetrabutylammonium perchlorate (TBAP).<sup>12, 13</sup>

The mechanism of alkylthiosulfate chemisorption on gold is not well understood. Lukkari and coworkers reported a heterolytic cleavage of the alkylthiosulfate molecule on gold surface, under anaerobic conditions, results in a sulfite ion and the

corresponding alkylthiolate.<sup>11</sup> The XPS spectra for the SAMs of dodecylthiosulfate and dodecanethiol on gold were practically identical suggesting S-SO<sub>3</sub> bond cleavage.<sup>11</sup> Shon and Murray reported that the monolayer protected clusters (MPCs) of gold prepared from dodecanethiol and dodecylthiosulfate, characterized by NMR, FTIR and XPS techniques, were nearly indistinguishable.<sup>14</sup> Alkylthiosulfates have also been used to form passivating monolayers on copper surfaces.<sup>15</sup> Impedance analysis on the alkylthiosulfate monolayers formed in toluene or water showed poorer passivation of the copper surface than those formed in THF or ethanol.<sup>15</sup> The poor monolayer quality may be due to lower solubility of dodecylthiosulfate in water and toluene, compared to other solvents used.

The present work investigates the influence of solvent and electrolytes on the spontaneous self-assembly of alkylthiosulfates on gold. Open circuit potential (OCP) measurements are used to study possible charge transfer associated with the alkylthiosulfate adsorption on gold. The quality of SAM was determined by contact angle measurements and electron transfer blocking experiments using redox probes. Contact angle goniometry provides valuable information regarding the wetting properties of the monolayers. For example, a well ordered monolayer of alkanethiols or alkylthiosulfates on gold gives hexadecane advancing contact angles ( $\theta_a$ ) close to 44-46° and the  $\theta_a$  values will be less than 10° when no monolayer is formed.<sup>11, 13</sup> Electron transfer blocking experiments using redox probes (e.g., ferricyanide/ferrocyanide couple) are an indirect means for monitoring adsorption and surface passivation.<sup>16, 17</sup> In cases where adsorption results in a passivating layer, electron transfer between the electrode surface and the

redox species in solution will be attenuated. This is a common technique used for characterizing monolayer formation and their quality since the presence of disorder or pinholes will result in a measurable redox current from solution species.<sup>16</sup> The results are compared to SAMs formed from the corresponding alkanethiol. Ferguson and coworkers have proposed that the spontaneous adsorption of monolayers on gold from solutions containing alkyl thiosulfates in organic solvents occurs via hydrolysis by trace water, and that this process is inhibited in the presence of tetrafluoroborate ion by sequestration of that water in clusters with the ion.<sup>18, 19</sup> The experiments in this chapter tested these hypotheses. Determining the role of TBATFB on the inhibition of alkylthiosulfate monolayer formation is important for extending this selective self-assembly technique to other systems. Furthermore, a better understanding of alkylthiosulfate self-assembly on gold surface is necessary for their applications in molecular electronics and sensors.

## **2.2 Experimental**

**2.2.1 Synthesis of Alkylthiosulfates:** Sodium salts of alkylthiosulfates (Bunte Salts),  $\text{CH}_3(\text{CH}_2)_n\text{S}_2\text{O}_3\text{Na}$  ( $n= 7, 11, 13, 15, 17, 19$ ) were synthesized by the previously reported procedure.<sup>13</sup> For example, 1-bromododecane (5 mmol) dissolved in 20 mL of ethanol was added to a solution of sodium thiosulfate (5 mmol) in 20 mL of water, and the mixture was brought to reflux until the solution become homogeneous. The solution was then cooled and filtered. The precipitated Bunte salt was recrystallized twice from absolute alcohol. The white crystals of Bunte salts were dried and stored at  $-20^\circ\text{C}$ .

$^1\text{H}$  NMR (300 MHz, MeOH- $\text{D}_4$ ,  $\delta$ , ppm):  $\text{CH}_3(\text{CH}_2)_9\text{CH}_2\text{CH}_2\text{SSO}_3\text{Na}$ , 0.86 (t, 3H,  $3J=6.9$  Hz,  $\text{CH}_3$ ), 1.26-1.46 (m, 18H,  $(\text{CH}_2)_9$ ), 1.70 (m, 2H,  $\text{CH}_2$ ), 3.02 (t, 2H,  $3J=7.5$  Hz,  $\text{CH}_2\text{SSO}_3\text{Na}$ );  $\text{CH}_3(\text{CH}_2)_{11}\text{CH}_2\text{CH}_2\text{SSO}_3\text{Na}$ , 0.86 (t, 3H,  $3J=7.0$  Hz,  $\text{CH}_3$ ), 1.26-1.46 (m, 18H,  $(\text{CH}_2)_9$ ), 1.69 (m, 2H,  $\text{CH}_2$ ), 3.02 (t, 2H,  $3J=7.4$  Hz,  $\text{CH}_2\text{SSO}_3\text{Na}$ );  $\text{CH}_3(\text{CH}_2)_{13}\text{CH}_2\text{CH}_2\text{SSO}_3\text{Na}$ , 0.86 (t, 3H,  $3J=6.9$  Hz,  $\text{CH}_3$ ), 1.26-1.46 (m, 26H,  $(\text{CH}_2)_9$ ), 1.70 (m, 2H,  $\text{CH}_2$ ); 3.03 (t, 2H,  $3J=7.4$  Hz,  $\text{CH}_2\text{SSO}_3\text{Na}$ );  $\text{CH}_3(\text{CH}_2)_{15}\text{CH}_2\text{CH}_2\text{SSO}_3\text{Na}$ , 0.86 (t, 3H,  $3J=7.4$  Hz,  $\text{CH}_3$ ), 1.26-1.46 (m, 26H,  $(\text{CH}_2)_9$ ), 1.69 (m, 2H,  $\text{CH}_2$ ); 3.02 (t, 2H,  $3J=6.9$  Hz,  $\text{CH}_2\text{SSO}_3\text{Na}$ );  $\text{CH}_3(\text{CH}_2)_{17}\text{CH}_2\text{CH}_2\text{SSO}_3\text{Na}$ , 0.87 (t, 3H,  $3J=7.4$  Hz,  $\text{CH}_3$ ), 1.26-1.46 (m, 18H,  $(\text{CH}_2)_9$ ), 1.70 (m, 2H,  $\text{CH}_2$ ), 3.02 (t, 2H,  $3J=6.9$  Hz,  $\text{CH}_2\text{SSO}_3\text{Na}$ ).

**2.2.2 Electrochemistry:** Electrochemical experiments were carried out using a Bioanalytical Systems BAS-100B potentiostat or CH Instrument electrochemical workstation (CHI 760C) with a conventional three electrode configuration. Working electrodes were gold disk electrodes (CH Instruments, CHI 101) or gold (~200 nm thick) sputtered on glass having a thin adhesion layer of titanium (~20 nm thick). A platinum wire is used as the counter electrode. The potentials for all the experiments in non-aqueous solvents are referred to  $\text{Ag}/\text{Ag}^+$  reference electrode (3 mM  $\text{Ag}/\text{AgNO}_3$ , 0.1 M TBATFB in acetonitrile), unless otherwise specified.

Redox electron transfer blocking experiments were carried out using aqueous potassium hexacyanoferrate solution (3 mM) with 0.1 M potassium chloride. The solutions were purged for at least 15 minutes with high purity nitrogen prior to their use in voltammetry experiments. The potentials were referred to an aqueous reference electrode ( $\text{Ag}/\text{AgCl}$  with saturated KCl).

Open-circuit potential (OCP) measurements were performed at 1s intervals with Agilent 34970A Data Acquisition unit controlled by a PC using BenchLink data logger software or CH Instrument electrochemical workstation (CHI 760c). Prior to OCP measurements, the solutions were filtered through an inorganic membrane filter (Whatman Anotop 25, 0.02 $\mu$ m) to remove any fine particles. The nitrogen purged solutions were kept in a closed glass vial and stirred with a micro stirrer bar. For all OCP measurements, the concentration of the organosulfur compound in the final solutions was approximately 10 mM.

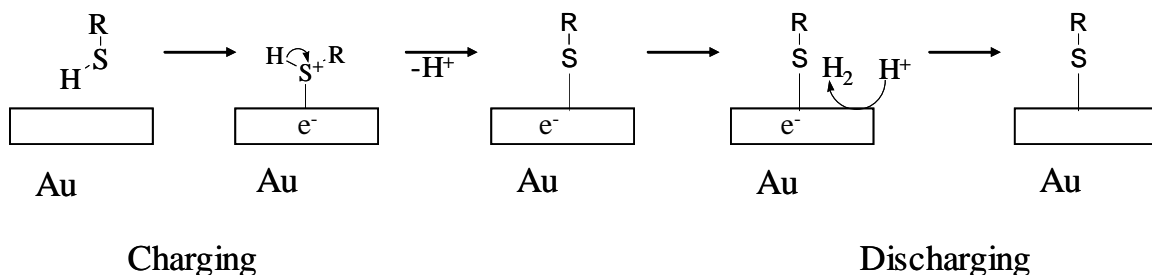
**2.2.3 Contact Angle Measurements:** Advancing hexadecane contact angles were measured with Rame-Hart NRL model 100 goniometer. The measurements were performed on sputter deposited gold electrodes ( $\sim$  200 nm thick) on glass with titanium adhesion layer (20 nm thick) having a dimension of 1 cm x 2.5 cm each. A minimum of five measurements on three independent drops were made for each sample.

## 2.3 Results and Discussion

### 2.3.1 Mechanism of Alkylthiosulfate Self-Assembly on Gold

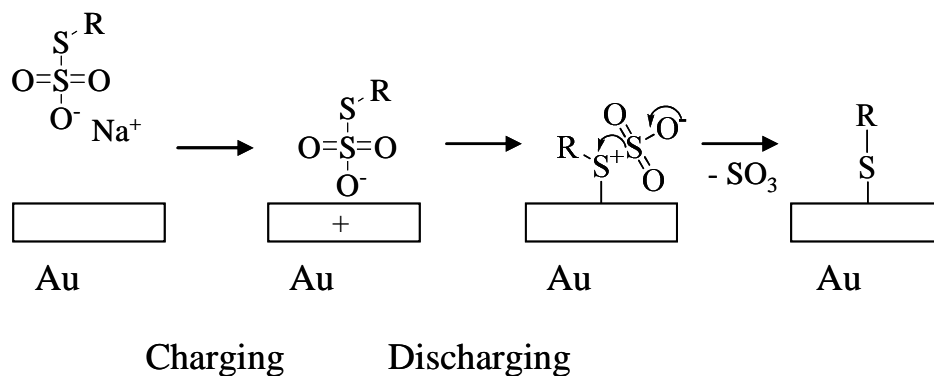
The mechanism of charge transfer processes accompanying alkanethiol adsorption on gold surface has been explored through *in-situ* OCP measurements.<sup>20-23</sup> The results suggest an electrochemical charge transfer step associated with the adsorption of alkanethiols and dialkyldisulfides on gold.<sup>23</sup> A negative shift in the OCP upon the addition of alkanethiol (Figure 2.1) is consistent with the charge transfer from thiol to gold, leading to Au-S bond formation.<sup>20, 23</sup> In presence of a protic solvent or

oxygen, the negative shift in the OCP is followed by a gradual positive shift due to discharging of the negative charge on gold (Scheme 2.1).<sup>20</sup> A similar mechanism has



**Scheme 2.1.** Proposed mechanism for alkanethiol<sup>20</sup> adsorption on gold surface.

The change in OCP of a bare gold electrode in THF upon the addition of sodium dodecylthiosulfate and dodecanethiol is shown in Figure 2.1. The initial negative shift in the OCP with the addition of dodecanethiol is in agreement with previous studies.<sup>20, 23</sup> The residual negative charge on the gold electrode can be discharged in presence of any oxidizing agents (e.g., oxygen, proton) present in the solution.<sup>20, 21</sup>



**Scheme 2.2.** Proposed mechanism for alkylthiosulfate adsorption on gold surface

been proposed for alkylthiosulfates (Scheme 2.2) since they form monolayers similar to the corresponding alkanethiols. According to this mechanism a positive shift in OCP is

expected due to the polarization of gold electrode by alkylthiosulfate anion. A negative shift in OCP is expected when discharging of the electrode takes place after alkylthiosulfate adsorption. A sudden positive shift in the OCP of the gold electrode followed by a gradual return of the potential in the negative direction is observed after the addition of dodecylthiosulfate. The positive shift in OCP is consistent with changes observed upon the addition of sodium dodecylsulfate (SDS) surfactant on gold.<sup>24</sup> In the case of dodecylthiosulfate or dodecylsulfate, the anion generates a positive image charge on the gold surface that results in a positive shift in the OCP. The gradual return of the OCP in the negative direction is consistent with the discharging mechanism, shown in Scheme 2.2.

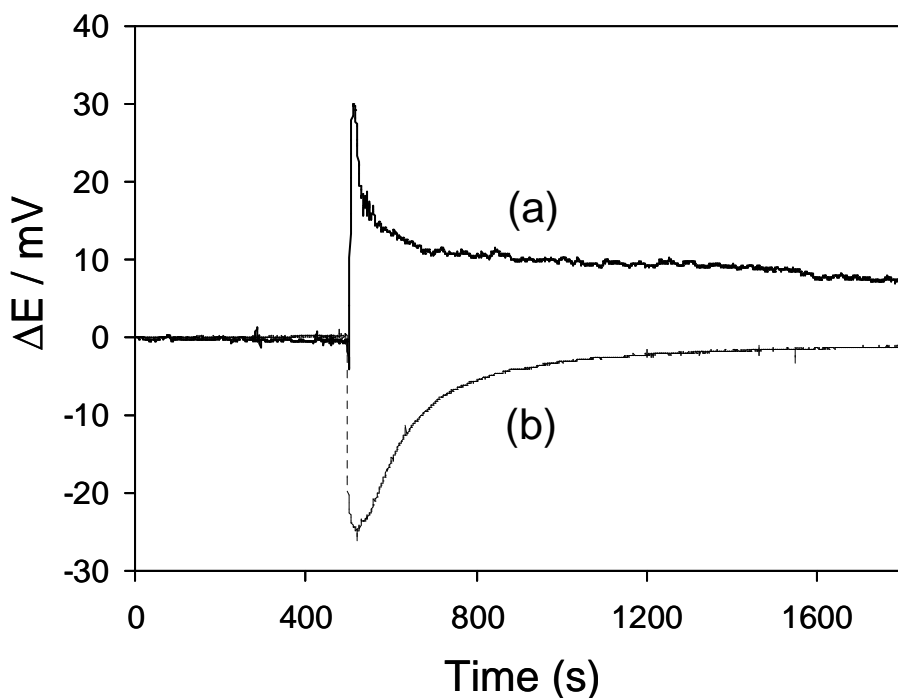


**Figure 2.1.** OCP vs. time response of a gold electrode in THF (no electrolyte) upon the addition of a) dodecylthiosulfate b) dodecanethiol

In presence of TBATFB and TBAP electrolytes, the change in OCP of a gold electrode after the addition of alkylthiosulfates show significant differences (Figure 2.2). The OCP change in presence of TBAP is similar to that in Figure 2.1 where a sudden positive shift in the potential is observed followed by a gradual negative shift, presumably due to Au-S bond formation (Scheme 2.2). However, in the presence of TBATFB, the discharging of the electrode is not observed after the addition of thiosulfate. The absence of a negative shift in OCP shows that the Au-S bond formation process is either not occurring or is very slow.

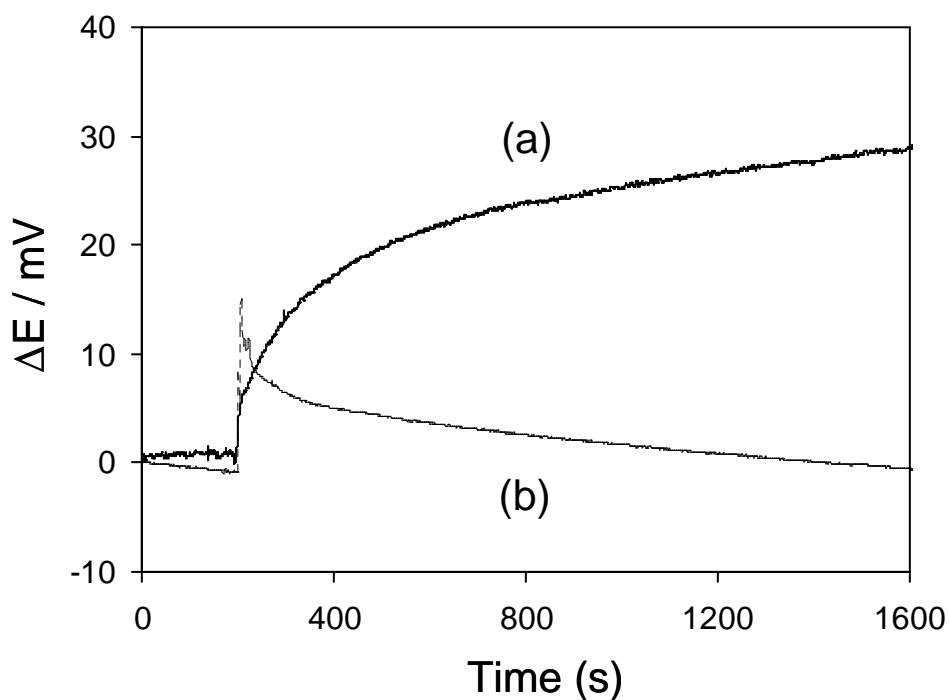


**Figure 2.2.** OCP vs. time response of a gold electrode in THF containing 0.1 M a) TBATFB b) TBAP after the addition of dodecylthiosulfate

### 2.3.2. Role of Electrolyte

Inhibition of alkylthiosulfate self-assembly by the electrolyte, TBATFB, has been previously reported.<sup>12</sup> However, the mechanism of electrolyte inhibition on

alkylthiosulfate self-assembly is not well understood. Figure 2.3 shows the effect of electrolytes on alkylthiosulfate adsorption, explored by electron transfer blocking experiments using ferricyanide/ferrocyanide redox couple. Spontaneous adsorption of dodecylthiosulfate on gold electrode from THF in presence of TBATFB for 30 minutes yields only partial monolayer formation (Figure 2.3a). Dodecylthiosulfate adsorption shows less passivation than that of dodecanethiol on gold, possibly due to the slow rate of monolayer formation of alkylthiosulfate compared to thiol.<sup>11</sup> Consistent with the previous reports,<sup>13</sup> adsorption of dodecanethiol on gold was found to be unaffected by the presence of electrolytes (Figure 2.2b). The above results show that the mechanism of TBATFB inhibition on alkylthiosulfate self-assembly is more complex than expected.

Since alkylthiosulfates, not thiols, adsorption is preferentially inhibited, the electrolyte may be interfering with any of the adsorption steps mentioned in Scheme 2.2. Therefore, it has been hypothesised that the inhibition of alkylthiosulfate self-assembly by TBATFB may be due to one or more of the following; a) physical blocking b) electrostatic repulsions c) trace water in the solvent. Considering the surface passivation of gold in presence of alkylthiosulfates and TBAP, the physical blocking of the electrode by electrolyte adsorption can be ruled out. Figure 2.4 shows the OCP shift of a gold electrode in THF upon the addition of two tetrabutylammonium electrolytes having different anionic species. The gold electrode becomes positively polarized after the addition of TBAP whereas a negative polarization of the electrode observed with the addition of TBATFB. This excess negative charge on the electrode may electrostatically repel the incoming alkylthiosulfate anion and prevent monolayer formation. Inhibition

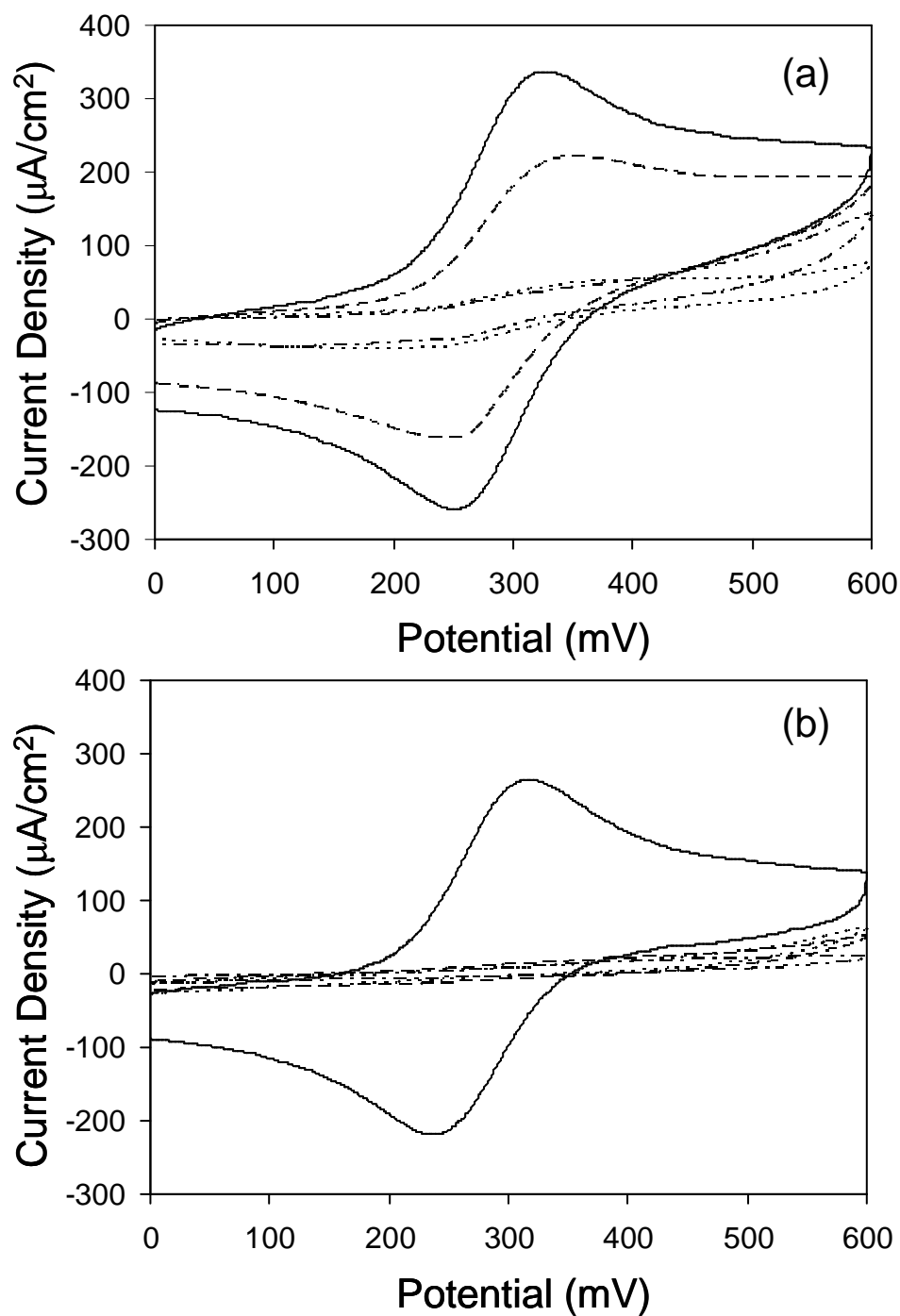


**Figure 2.3.** Cyclic voltammograms (1.0 mM  $K_3Fe(CN)_6$ , 0.1 M KCl, scan rate  $100\text{ mV s}^{-1}$ ; saturated Ag/AgCl reference electrode) of gold electrode before and after modification (30 min) with 10 mM a) sodium dodecylthiosulfate b) dodecanethiol in THF in the absence and presence of electrolytes; (—) bare electrode, (---) TBATFB, (.....) TBAP, (-·-·-) no electrolyte.

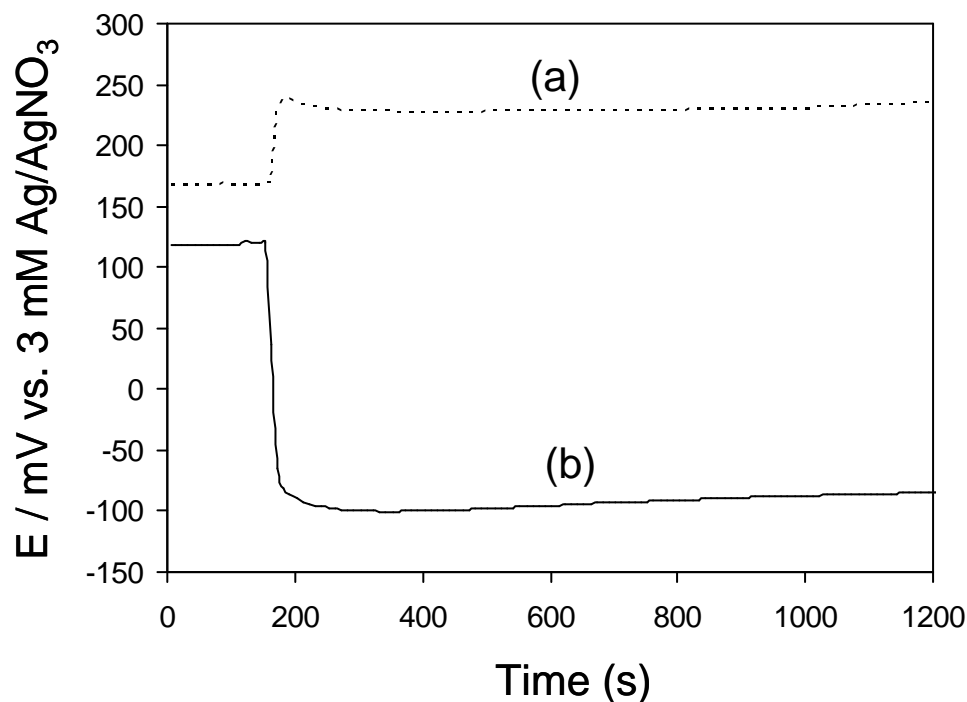


**Figure 2.4.** OCP vs. time response of a gold electrode in THF upon the addition of a) TBAP b) TBATFB electrolytes

of monolayer formation is also expected on gold electrodes kept in THF and TBAP at negative potentials equivalent to the OCP of gold electrode in presence of TBATFB. To test this hypothesis, a clean gold electrode was kept in THF with 10mM dodecylthiosulfate and 0.1 M TBAP for 30 minutes at -0.3 V. After 30 minutes, the electrode was taken out, washed with THF and water. The electron transfer blocking experiment in ferricyanide/ferrocyanide solution shows passivation of the electrode due to monolayer formation. Therefore, electrostatic interactions may not play a significant role in preventing alkylthiosulfate monolayer formation on gold in presence of TBATFB.

### 2.3.3 Role of Trace Water in the Solvent

The reactions involving alkylthiosulfate and water have been previously reported.<sup>25</sup> For example, hydrolysis of alkylthiosulfates in presence of dilute acids gives their corresponding thiols.<sup>26</sup> However, the reaction is reported to occur at elevated temperatures and the solution must generally be heated for several hours for complete conversion to the corresponding thiols.<sup>25</sup>

**Table 2.1.** Advancing hexadecane contact angle ( $\theta_a$ )\* on a gold electrode treated with 10 mM hexadecylthiosulfate in THF for 30 minute under different conditions.

	Ordinary THF (>0.02% water)	Anhydrous THF (<0.002% water)
Without TBATFB	44.2±0.6	17.4±1.8
With TBATFB	14.8±1.9	< 10

\*Contact angles are mean values ±standard deviations based on three measurements

Preliminary experiments suggest that alkylthiosulfate adsorption is influenced by trace water present in the solvent. The SAM formation in anhydrous conditions was performed inside a nitrogen filled glovebox where water and oxygen concentrations were less than 20 ppm (0.002%). Table 2.1 shows the advancing hexadecane contact angle on hexadecylthiosulfate SAMs formed under ambient and anhydrous solvent (THF) conditions. Self-assembly was not observed for alkylthiosulfates in THF except in

the case where a trace amount of water was present and TBATFB was absent. In contrast, a good monolayer (Hexadecane,  $\theta_a = \sim 44$ ) was observed in the spontaneous self-assembly of alkanethiols under the conditions mentioned in Table 2.1. These results indicate that water plays a critical role in the spontaneous self-assembly process. The addition of hygroscopic TBATFB apparently mitigates the presence of trace water in the solvent (THF), otherwise available for alkylthiosulfate self-assembly, possibly due to the formation of stable tetrafluoroborate-water clusters.<sup>19, 27</sup>

Tetraalkylammonium salts are reported to form stable water clusters that contain at least three molecules of water.<sup>27</sup> These clusters can be neutral or double-ionic and are stabilized by hydrogen bonding. The clusters of tetrabutylammonium salts and water can be represented as  $(C_4H_9)_3N \cdots (C_4H_9)A \cdots (H_2O)_3$  (neutral) and  $(C_4H_9)_4N^+ \cdots (H_2O)_3 \cdots A^-$  (double-ionic), where  $A^-$  represent the counter ion.<sup>27</sup> The stability of these clusters largely depends on the nature of the counter ion. For example, the double-ionic cluster of tetrabutylammonium tetrafluoroborate is more stable than tetrabutylammonium perchlorate.<sup>27</sup> Also, the presence of a polar aprotic solvent like THF may stabilize these double-ionic clusters. This additional stability of the tetrafluoroborate water clusters may explain inhibition of alkylthiosulfate self-assembly in presence of tetrafluoroborate and not in the presence of perchlorate.

The role of trace water in the solvent on alkylthiosulfate self-assembly is further explored using electron transfer blocking experiments with ferricyanide/ferrocyanide redox couple. SAMs were formed on clean gold electrodes kept in solutions containing 10mM dodecylthiosulfate and 0.1 M TBATFB in anhydrous grade THF with varying water

content. After 30 minutes, electrodes were taken out, washed with THF and water. Then electron transfer blocking experiments were performed in a de-aerated solution of 3 mM  $K_4[Fe(CN)_6]$  aqueous solution with 0.1 M KCl. Figure 2.5 shows the variation of oxidation peak current is plotted as a function of added water to THF. The surface

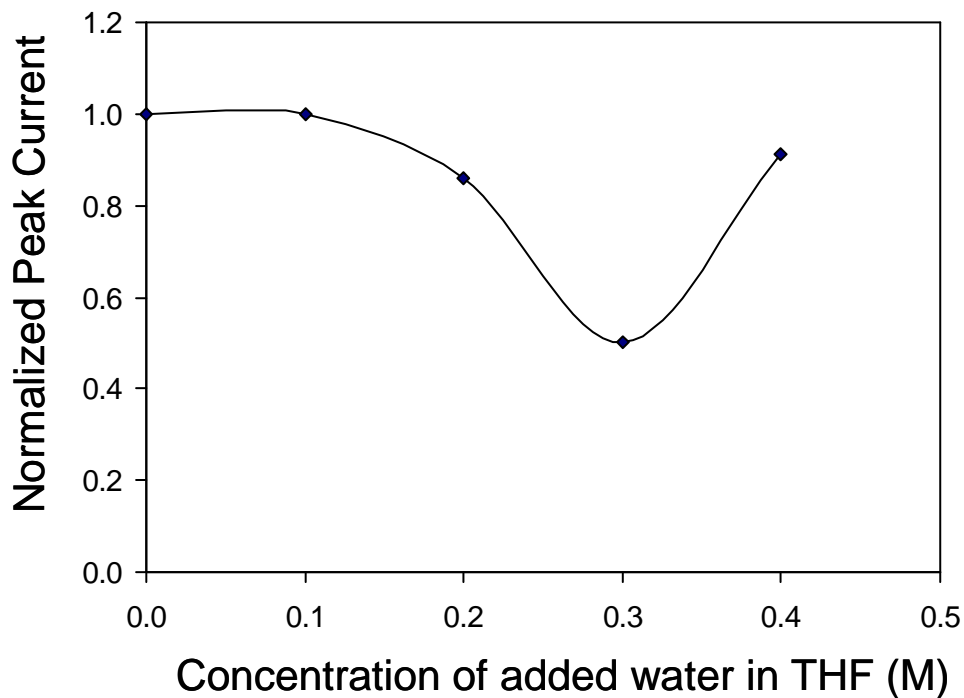


**Figure 2.5.** Variation of Ferrocyanide/Ferricyanide oxidation peak current for gold electrodes kept in THF solution (30 minutes) containing 10mM dodecylthiosulfate and 0.1 M TBATFB with varying water content. The peak currents are normalized with that of bare gold electrode.

passivation of the electrode found to increase with the amount of water present in the solution and shows a maximum at 0.3 M water added to THF. At this concentration (0.3 M), the TBATFB (0.1 M) present in the solvent may be saturated with water due to the formation of clusters with three water molecules per TBATFB; and the water already present in the anhydrous solvent (0.001 M) becomes available for the monolayer

formation of alkylthiosulfate on gold. Solutions having more than 0.3 M water show decrease in surface passivation due to poor solubility of alkylthiosulfates in presence of excess water. These results are also in agreement with the previous reports that inhibition of alkylthiosulfate self-assembly shows TBATFB concentration dependence.<sup>13</sup>

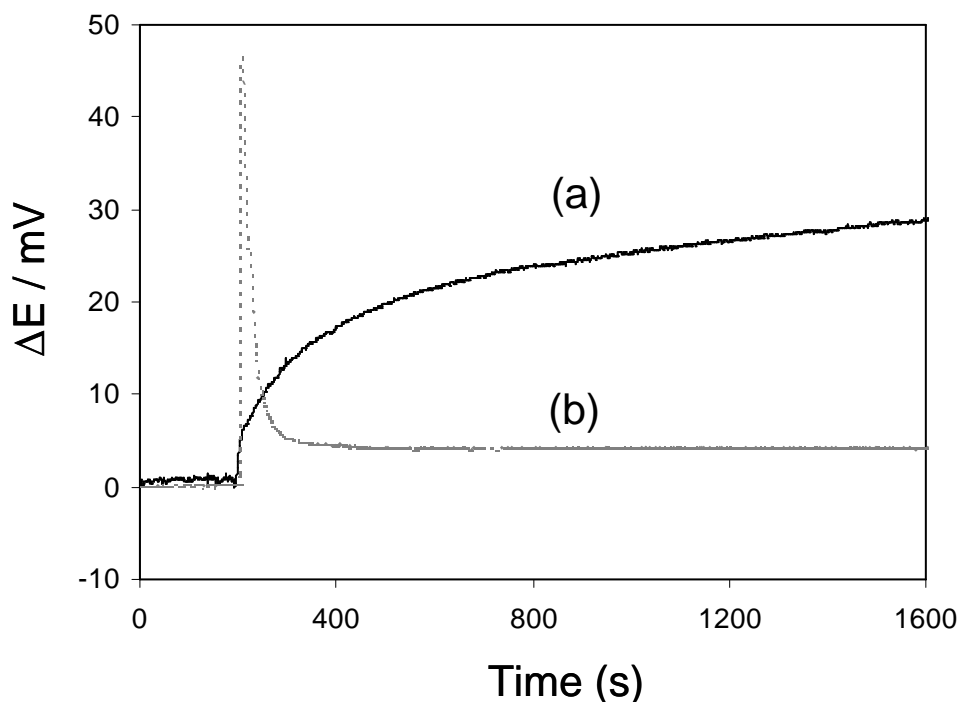
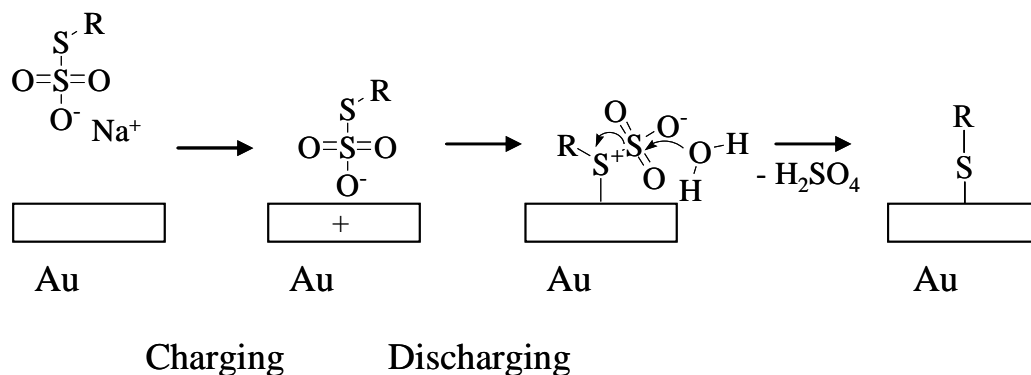


**Figure 2.6.** OCP vs. time response of a gold electrode after the addition of dodecylthiosulfate to a solution of 0.1 M TBATFB and a) THF b) THF with 0.3 M water.

Figure 2.6 shows the effect of added water on the OCP change for gold electrode in THF solution with 10mM dodecylthiosulfate and 0.1M T BATFB. In presence of 0.3 M water, the discharging of the electrode is observed after dodecylthiosulfate addition. Similar discharging of the electrodes was observed after dodecylthiosulfate addition in the absence of electrolyte (Figure 2.1) and TBAP (Figure 2.2), where a good monolayer is formed. The excess water available for alkylthiosulfate self-assembly may facilitate the

dissociation of S-S bond and hence the discharging of the electrode as shown in Scheme 2.3.



**Scheme 2.3.** Proposed mechanism for alkylthiosulfate adsorption on gold surface in presence of trace water in the solvent.

## 2.4 Conclusions

Spontaneous self-assembly of alkylthiosulfates on gold surfaces is influenced by electrolyte and solvent. The redox electron transfer blocking, OCP and contact angle experiments show that alkylthiosulfate self-assembly on gold from THF is inhibited by TBATFB, however alkanethiol adsorption is independent of the presence of electrolytes. Alkylthiosulfate adsorption on gold is facilitated by trace water present in the solvent. In presence of TBATFB, alkylthiosulfate self-assembly is inhibited since the electrolyte sequesters trace water in the solvent, otherwise available for alkylthiosulfate monolayer formation, by forming stable TBATFB-water clusters. A mechanism for alkylthiosulfate self-assembly under these conditions has been proposed. The results of our studies are consistent with Ferguson's proposed mechanism for the spontaneous adsorption of monolayers from solutions of alkyl thiosulfates and inhibition of that process by  $\text{BF}_4^-$ .

These results are particularly important since they conclude that solvent must be sufficiently dry to get good selectivity in monolayer formation by electrochemically directed self-assembly.

## References

1. Nuzzo, R. G.; Allara, D. L., Adsorption of Bifunctional Organic Disulfides on Gold Surfaces. *Journal of the American Chemical Society* **1983**, 105, (13), 4481-4483.
2. Bain, C. D.; Troughton, E. B.; Tao, Y. T.; Evall, J.; Whitesides, G. M.; Nuzzo, R. G., Formation of Monolayer Films by the Spontaneous Assembly of Organic Thiols from Solution onto Gold. *Journal of the American Chemical Society* **1989**, 111, (1), 321-335.
3. Ulman, A., Formation and structure of self-assembled monolayers. *Chemical Reviews* **1996**, 96, (4), 1533-1554.
4. Love, J. C.; Estroff, L. A.; Kriebel, J. K.; Nuzzo, R. G.; Whitesides, G. M., Self-assembled monolayers of thiolates on metals as a form of nanotechnology. *Chemical Reviews* **2005**, 105, (4), 1103-1169.
5. Carpick, R. W.; Salmeron, M., Scratching the surface: Fundamental investigations of tribology with atomic force microscopy. *Chemical Reviews* **1997**, 97, (4), 1163-1194.
6. Kumar, A.; Biebuyck, H. A.; Whitesides, G. M., Patterning Self-Assembled Monolayers - Applications in Materials Science. *Langmuir* **1994**, 10, (5), 1498-1511.
7. Ferretti, S.; Paynter, S.; Russell, D. A.; Sapsford, K. E.; Richardson, D. J., Self-assembled monolayers: a versatile tool for the formulation of bio-surfaces. *Trends in Analytical Chemistry* **2000**, 19, (9), 530-540.
8. Wink, T.; vanZuilen, S. J.; Bult, A.; vanBennekom, W. P., Self-assembled monolayers for biosensors. *Analyst* **1997**, 122, (4), R43-R50.
9. Wettig, S. D.; Li, C. Z.; Long, Y. T.; Kraatz, H. B.; Lee, J. S., M-DNA: a self-assembling molecular wire for nanoelectronics and biosensing. *Analytical Sciences* **2003**, 19, (1), 23-26.

10. Tour, J. M., Molecular electronics. Synthesis and testing of components. *Accounts of Chemical Research* **2000**, 33, (11), 791-804.
11. Lukkari, J.; Meretoja, M.; Kartio, I.; Laajalehto, K.; Rajamaki, M.; Lindstrom, M.; Kankare, J., Organic thiosulfates (Bunte salts): Novel surface-active sulfur compounds for the preparation of self-assembled monolayers on gold. *Langmuir* **1999**, 15, (10), 3529-3537.
12. Hsueh, C. C.; Lee, M. T.; Freund, M. S.; Ferguson, G. S., Electrochemically directed self-assembly on gold. *Angewandte Chemie-International Edition* **2000**, 39, (7), 1228-1230.
13. Lee, M. T.; Hsueh, C. C.; Freund, M. S.; Ferguson, G. S., Electrochemical self-assembly of monolayers from alkylthiosulfates on gold. *Langmuir* **2003**, 19, (13), 5246-5253.
14. Shon, Y. S.; Gross, S. M.; Dawson, B.; Porter, M.; Murray, R. W., Alkanethiolate-protected gold clusters generated from sodium S-dodecylthiosulfate (Bunte salts). *Langmuir* **2000**, 16, (16), 6555-6561.
15. Lusk, A. T.; Jennings, G. K., Characterization of self-assembled monolayers formed from sodium S-alkyl thiosulfates on copper. *Langmuir* **2001**, 17, (25), 7830-7836.
16. Janek, R. P.; Fawcett, W. R.; Ulman, A., Impedance spectroscopy of self-assembled monolayers on Au(111): Sodium ferrocyanide charge transfer at modified electrodes. *Langmuir* **1998**, 14, (11), 3011-3018.
17. Finklea, H. O.; Snider, D. A.; Fedyk, J.; Sabatani, E.; Gafni, Y.; Rubinstein, I., Characterization of Octadecanethiol-Coated Gold Electrodes as Microarray Electrodes by Cyclic Voltammetry and Ac-Impedance Spectroscopy. *Langmuir* **1993**, 9, (12), 3660-3667.
18. G. S. Ferguson, personal communication of results prior to publication.
19. Farcasiu, D.; Lukinskas, P., The stability of the hydronium tetrafluoroborate dimer determined by theoretical calculations. Implications for water protonation in nonpolar solvents and on solid acids. *Physical Chemistry Chemical Physics* **2000**, 2, (18), 4219-4224.
20. Cohen-Atiya, M.; Mandler, D., Studying thiol adsorption on Au, Ag and Hg surfaces by potentiometric measurements. *Journal of Electroanalytical Chemistry* **2003**, 550, 267-276.

21. Chon, S.; Paik, W. K., Adsorption of self-assembling sulfur compounds through electrochemical reactions: Effects of potential, acid and oxidizing agents. *Physical Chemistry Chemical Physics* **2001**, 3, (16), 3405-3410.
22. Zhong, C. J.; Woods, N. T.; Dawson, G. B.; Porter, M. D., Formation of thiol-based monolayers on gold: implications from open circuit potential measurements. *Electrochemistry Communications* **1999**, 1, (1), 17-21.
23. Paik, W. K.; Eu, S.; Lee, K.; Chon, S.; Kim, M., Electrochemical reactions in adsorption of organosulfur molecules on gold and silver: Potential dependent adsorption. *Langmuir* **2000**, 16, (26), 10198-10205.
24. Soares, D. M.; Gomes, W. E.; Tenan, M. A., Sodium dodecyl sulfate adsorbed monolayers on gold electrodes. *Langmuir* **2007**, 23, (8), 4383-4388.
25. Distler, H., Chemistry of Bunte Salts. *Angewandte Chemie-International Edition* **1967**, 6, (6), 544-553
26. Kice, J. L., A Kinetic Study of Acid Hydrolysis of a Bunte Salt. *Journal of Organic Chemistry* **1963**, 28, (4), 957-961.
27. Zielinski, R.; Szymusiak, H., Structure of stable double-ionic model water clusters of quaternary alkylammonium surfactants with some monovalent counterions as derived by the DFT method. *International Journal of Quantum Chemistry* **2004**, 99, (5), 724-734.

## Chapter 3:

Electrochemically Assisted Self-Assembly of Alkylthiosulfates and Alkanethiols on Gold: The Role of Gold Oxide Formation and Corrosion

### **Authors' Contributions**

All experiments, except the exchange experiments with alkylthiosulfates, pertaining to this work were designed and conducted by R. G. Pillai. M. D. Braun performed the exchange experiments, conceptualized by Dr. M. S. Freund. All figures and manuscript drafts were prepared by R. G. Pillai. Dr. M. S. Freund and R. G. Pillai were responsible for revisions and final editing of the manuscript, prior to its publication in the ACS journal '*Langmuir*'.

Electrochemically Assisted Self-Assembly of Alkylthiosulfates and Alkanethiols on Gold: The Role of Gold Oxide Formation and Corrosion

Rajesh G. Pillai,<sup>1</sup> Monica D. Braun,<sup>1</sup> and Michael S. Freund<sup>1,2</sup>

<sup>1</sup>Department of Chemistry and <sup>2</sup>Department of Electrical & Computer Engineering,  
University of Manitoba, Winnipeg, Manitoba R3T 2N2, Canada

Reproduced with permission from *Langmuir* **2010**, 26(1), 269–276

Copyright ©2009 American Chemical Society

## **Abstract**

Electrochemically directed self-assembly of alkylthiosulfates enables the selective formation of monolayers on gold surfaces. These monolayers are identical to those formed from the corresponding alkanethiols. However, the mechanistic details of monolayer formation under electrochemical conditions as well as the role of other variables and residual water in the solvent have not been extensively studied. A systematic investigation shows that self-assembly is not a result of an outer-sphere one-electron oxidation of alkylthiosulfate. Voltammetry and electrochemical quartz crystal microbalance techniques reveal that self-assembly involving alkylthiosulfates as well as alkanethiols under oxidative conditions proceed through direct reaction with gold oxide and in some cases is accompanied by corrosion. X-ray photoelectron spectroscopy indicates that monolayers can undergo rapid exchange with molecules in solution under electrochemically directed self-assembly conditions.

### 3.1 Introduction

Molecular-level self-assembly techniques have emerged as a versatile tool for controlling the surface properties of materials. Self-assembled monolayers (SAMs) have been the dominant approach, producing well-ordered molecular layers that are formed by the spontaneous organization of molecules on a surface.<sup>1, 2</sup> These monolayers have been used as model systems for fundamental studies in different areas including tribology,<sup>3</sup> surface patterning,<sup>4</sup> bio- and analytical sensors<sup>5</sup> as well as molecular electronics.<sup>6</sup> Among the various systems that display this behavior, SAMs formed from the chemisorption of alkanethiols on gold have been the most widely studied and implemented system due to the ease of preparation and characterization.<sup>7, 8</sup> However, conventional self-assembly methods lack the ability for selective monolayer formation on spatially complex structures, such as electrode arrays or integrated circuits. For example, treatment of an array of gold electrodes with alkanethiol or disulfide results in monolayer formation on all of the electrodes. The spatial control over monolayer formation is critical for emerging technologies involving complex structures such as molecular electronics<sup>9</sup> and sensors.<sup>8</sup> While advances have been made in this field using the oxidation of alkanethiolates at gold electrodes to control the formation of SAMs,<sup>10, 11</sup> the reductive desorption of monolayers from a subset of modified electrodes<sup>12</sup> and the oxidation of alkylthiosulfates (also known as Bunte salts),<sup>13</sup> more detailed studies of these systems are required.

Although the details of alkanethiol and alkyl disulfide self-assembly on gold have been extensively studied, the chemical<sup>14</sup> and electrochemical reactions of

alkylthiosulfates with gold have been less well characterized.<sup>13</sup> It has been reported that spontaneous self-assembly of alkylthiosulfates on gold occurs in deaerated ethanol solutions resulting alkanethiol monolayers.<sup>15</sup> However, the rate of spontaneous self-assembly of alkylthiosulfates is dramatically reduced in THF in the presence of the electrolyte, tetrabutylammonium tetrafluoroborate (TBATFB), enabling electrochemically directed self-assembly.<sup>13</sup> Under these conditions, the electrolyte inhibits the spontaneous decomposition and chemisorption of alkylthiosulfate on gold to form SAMs, allowing the monolayers to be selectively formed only at sufficiently high anodic potentials. Hence this electrochemically directed self-assembly approach enables controlled monolayer formation on multicomponent substrates including electrode arrays and integrated circuits *via* potential control.<sup>13</sup>

The mechanistic details of the electrochemically directed self-assembly process remains to be investigated in detail. The originally proposed mechanism<sup>16</sup> involves the one electron oxidation of the alkylthiosulfate, followed by decomposition to form a thiolate radical, which is known to self-assemble on gold to form monolayers.<sup>10</sup> However, to date no systematic studies have been performed to support the mechanism or to explore the role of substrate or other variables present in the system such as residual water. In this study, a detailed investigation of electrochemically assisted self-assembly involving alkylthiosulfates as well as alkanethiols has been undertaken to develop a better understanding of the steps involved in both systems.

Previous reports<sup>15</sup> indicate that the absence of oxygen is desirable for the spontaneous adsorption of alkylthiosulfates on gold from protic solvents, due to

possible etching of gold in the presence of oxidizing agents. This is consistent with reports that solutions containing thiosulfate and an oxidant are considered as good etchants for gold.<sup>17</sup> Spontaneous self-assembly of alkanethiols is also reported to induce adsorbate assisted etching of gold in nondeaerated solutions. For example, Woll and co-workers reported the etching of gold in alkanethiol solution with measureable concentrations of dissolved gold species in the incubation bath as determined by atomic absorption spectroscopy.<sup>18</sup> The “holes” observed in STM images of monolayer modified gold surfaces were initially attributed to defects in the thiol monolayer or gold corrosion.<sup>19</sup> However this hypothesis was later challenged and the pits were ascribed to gold vacancies arising from the nonequilibrium surface rearrangements.<sup>20</sup> Cao and Gu used *in situ* electrochemical quartz crystal microbalance (EQCM) measurements to monitor gold corrosion during alkanethiol self-assembly from oxygen saturated THF solutions.<sup>21</sup> They found that approximately 6% of a gold monolayer is lost in THF as soluble products that they attribute to Au-SR or gold oxide. In a recent report, Repo and co-workers observed the dissolution of gold in a methanol solution of 4-pyridinethiol in presence of oxygen.<sup>22</sup> These studies indicate that spontaneous self-assembly of thiol species on gold under nondeaerated conditions is accompanied by gold corrosion, however the exact mechanism of the process and nature of the soluble gold species formed remains unclear.

The electrochemical dissolution of gold in presence of organic<sup>23</sup> and inorganic additives<sup>24, 25</sup> has been extensively studied. The nature of the process and amount of gold dissolved is influenced by various factors including applied potential, the presence

of additives, solvent and electrolyte. For example, tetramethylthiourea (TMTU) has been found to assist the anodic dissolution of gold in both protic and aprotic solvents including water and acetonitrile. Gothelf and co-workers used cyclic voltammetry and EQCM to study TMTU-induced etching of gold in acetonitrile.<sup>26</sup> Ritchie and co-workers used voltammetry to study of the effect of acidic thiourea solutions on gold, platinum and glassy carbon.<sup>27</sup> For each electrode, within the same potential window, an anodic peak was observed corresponding to the formation of disulfide and a cathodic peak due to the reduction of disulfide. However, an additional anodic peak was observed at lower potentials on the gold electrode and was attributed to the dissolution of gold as the  $\text{Au}(\text{thiourea})_2^+$  complex, which is reportedly reduced at potentials similar to the reduction of disulfide.

The motivation for the work presented herein was the observation that the process of electrochemically directed self-assembly of alkylthiosulfates enabled the formation of good monolayers on both clean and nominally “dirty” gold substrates.<sup>16</sup> The fact that the gold did not have to be rigorously cleaned suggested that some surface cleaning process is likely involved. Similarities between the electrochemical behavior of both alkylthiosulfates and alkanethiols, the possibility of corrosion, and the potential involvement of surface oxides<sup>28</sup> indicated that the process of electrochemically assisted self-assembly was complex and worthy of a more detailed investigation.

## 3.2 Experimental

**3.2.1 Materials:** High purity grade solvents and electrolytes were used for electrochemical studies. Tetrabutylammonium tetrafluoroborate (99%), tetrabutylammonium perchlorate (99%), tetrahydrofuran (THF, 99.9%), N, N-Dimethyl formamide (DMF, 99.8%), methanol (99.8%), 1-hexadecanethiol (92 %), 1-dodecanethiol (98+ %), 1-bromohexadecane (97%), 1-bromododecane (96%) were obtained from Aldrich and used as received. All water used in this work was purified with a Millipore Milli-Q water purifier system to a resistivity of  $18.2 \text{ M}\Omega\text{-cm}^{-1}$ .

**3.2.2 Synthesis:** Alkylthiosulfates (Bunte Salts),  $\text{CH}_3(\text{CH}_2)_n\text{S}_2\text{O}_3\text{Na}$  ( $n=7,11,15$ ) were synthesized following a previously reported procedure.<sup>16</sup> For example, 1-bromododecane (5 mmol) dissolved in 20 mL of ethanol was added to a solution of sodium thiosulfate (5 mmol) in 20 mL water, and the mixture was brought to reflux until the solution became homogenous. The solution was then cooled, filtered and recrystallized twice from absolute alcohol.

**3.2.3 Electrochemistry:** Electrochemical experiments were carried out using either a Bioanalytical Systems BAS-100B potentiostat or CH Instrument electrochemical workstation (CHI660) with a conventional three electrode configuration with a platinum wire used as counter electrode. Working electrodes used were gold, platinum or glassy carbon disk electrodes and gold ultramicroelectrode (UME) from CH Instruments. All the potentials were referred to a non aqueous reference electrode (3 mM Ag/AgNO<sub>3</sub> in acetonitrile).

**3.2.4 Electrochemical Quartz Crystal Microbalance (EQCM) Measurements:** EQCM measurements were performed on a CH Instrument electrochemical work station (CHI400) with AT-cut quartz crystals (ICM Company Inc., USA) having a resonance frequency of 7.995 MHz. The QCM crystals were calibrated using electrochemical deposition of silver<sup>29</sup> to give a sensitivity of 2.01 ng-Hz<sup>-1</sup>. The scan rates in all of the experiments using EQCM were 10 mV/s. The exposed gold surfaces on the EQCM crystals were cleaned with “piranha” solution (3:1 mixture of concentrated H<sub>2</sub>SO<sub>4</sub> and 30% H<sub>2</sub>O<sub>2</sub>; *CAUTION: Piranha solution reacts violently with most organic materials and should be handled with extreme care*), washed with Millipore water and dried in nitrogen.

**3.2.5 X-ray Photoelectron Spectroscopy (XPS) Analysis:** XPS analysis of samples of SAMs on gold was performed using a Kratos AXIS ULTRA spectrometer with a 300W monochromated Al K $\alpha$  source and a delay line detector. The survey and high resolution scans were recorded with pass energies of 160 eV and 20 eV respectively. All spectra were collected at 90 deg take off angle and referenced to the Au 4f<sub>7/2</sub> peak set at 84.0 eV. The background pressure in the analyzer chamber was  $\sim 10^{-9}$  Torr. For quantitative analysis sensitivity factors supplied by the instrument manufacturer were used: Au 4f<sub>7/2</sub>, 6.25; C 1s, 0.278.

### 3.3 Results and Discussion

Electrochemically directed self-assembly of alkylthiosulfates on gold surfaces form monolayers indistinguishable from those formed from the spontaneous self-

assembly of corresponding alkanethiols.<sup>13</sup> The indistinguishable nature of these monolayers is observed with contact angle, ellipsometry and XPS measurements.<sup>13, 16</sup> For example, electrochemically directed self-assembly of hexadecylthiosulfate on gold gives advancing contact angle of hexadecane (45-47°) and an ellipsometric thickness of approximately 13 Å, in agreement with those reported for complete and well-ordered SAMs prepared by self-assembly of hexadecanethiol.<sup>13</sup> High resolution XPS data of sulphur 2p region of these monolayers show a spin-orbit doublet at 162 and 163 eV characteristic of thiolate sulphur.<sup>16</sup> There is no evidence for any significant amount of oxygen in these monolayers washed with THF and water.<sup>16</sup> Also, the C/Au ratio calculated from the XPS peak intensities for electrochemically deposited dodecylthiosulfate SAM is in good agreement with that of dodecanethiol SAM prepared by conventional method. The C 1s /Au 4f<sub>7/2</sub> peak intensity ratio calculated for dodecylthiosulfate and dodecanethiol SAMs were 0.61 and 0.59 respectively.

During this self-assembly process, the voltammetry of alkylthiosulfates in THF and TBATFB exhibits an irreversible oxidation peak, which decreases with the number of potential cycles and reaches a steady-state value approximately 5-10 times lower than the first scan. This wave was initially assigned to the oxidation of alkylthiosulfate and subsequent monolayer formation on gold.<sup>16</sup> However, further investigations indicate that mechanism of electrochemically directed self-assembly may proceed by a different mechanism.

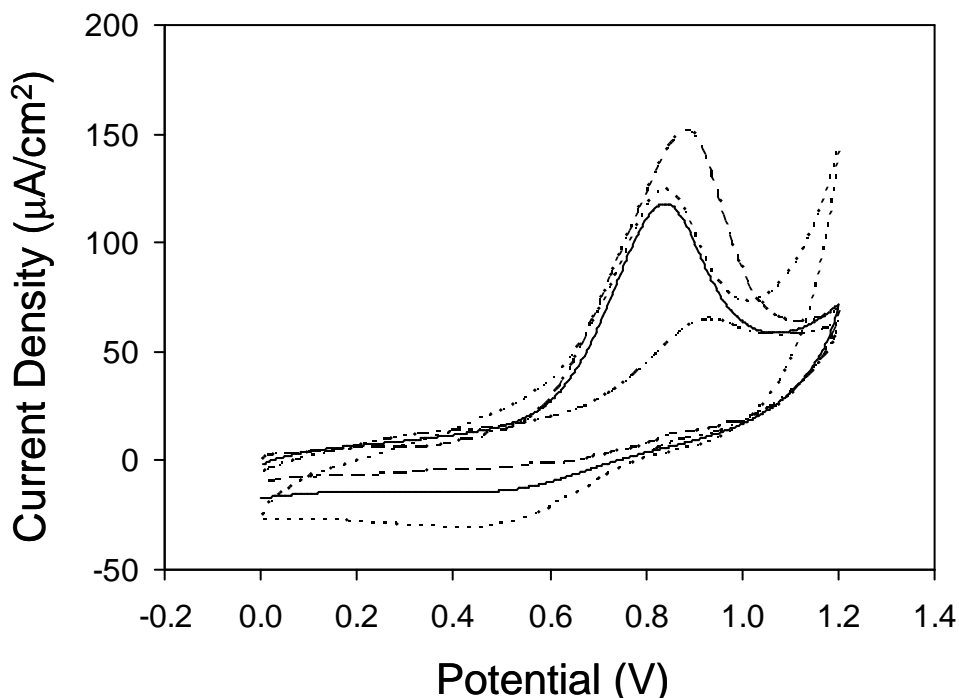


**Figure 3.1.** Cyclic voltammograms for dodecylthiosulfate in various solvents (0.1 M TBATFB, 100 mV/s) including THF (—), DMF (— · — · —), MeOH (---), and MeCN (·····) on gold disc electrodes. The data represent the first cycle on a clean gold electrode.

In order to explore alternative mechanisms the role of solvent and substrate has been explored. The voltammetry of alkylthiosulfates was performed in different non-aqueous solvents including THF, DMF, acetonitrile and methanol. Alkylthiosulfates exhibit excellent solubility in these solvents which are electrochemically stable in the potential window used for this study. Figure 3.1 shows the first potential cycle in the voltammograms of dodecylthiosulfate on gold in these organic solvents. The cyclic voltammograms in protic and aprotic solvents show similar behaviour. In previous work,<sup>16</sup> it was reported that the voltammetry of dodecylthiosulfate in THF shows no oxidation peaks on platinum and glassy carbon electrode (Figure 3.2), and that after the first cycle, electron transfer blocking experiments with a redox probe (ferricyanide/ferrocyanide couple) show no surface passivation on either platinum and

glassy carbon electrodes. However on gold, the current density decreases by approximately an order of magnitude after the first scan due to monolayer formation.

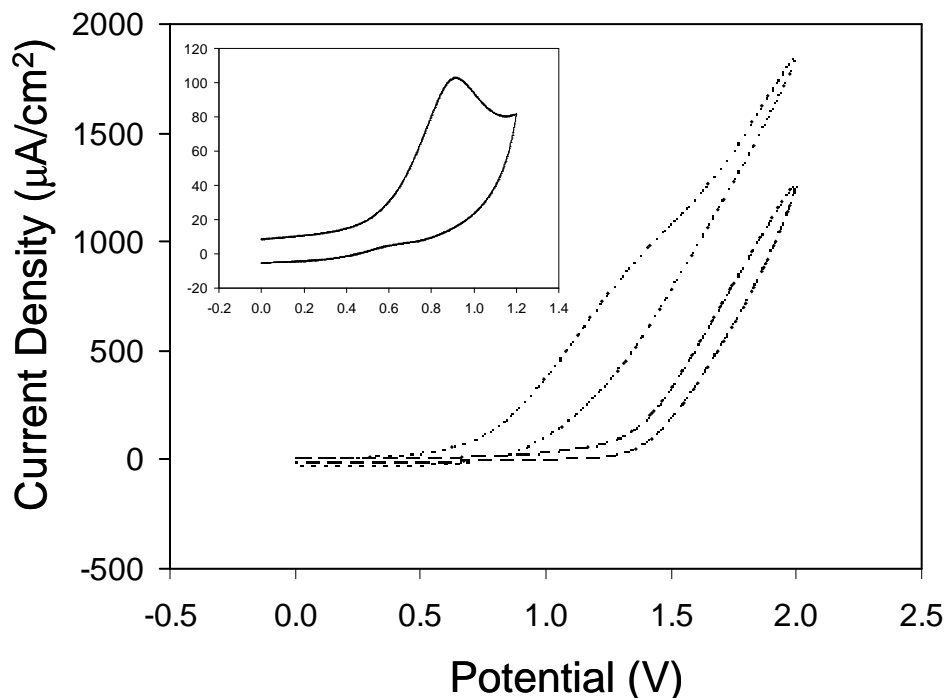


**Figure 3.2.** Cyclic voltammograms for dodecylthiosulfate in THF (0.1 M TBATFB, 100 mV/s) on different electrode substrates including gold (—), glassy carbon (-----), and platinum (-.-.-). The data represent the first cycle on a clean gold electrode.

These results demonstrate that alkylthiosulfates do not undergo a simple outersphere electron transfer reaction and that the oxidation, taking place only on gold, is ultimately responsible for the formation of any intermediates and ultimately monolayer formation.

To gain more insight into the difference between the observed alkylthiosulfate redox chemistry and that of alkanethiols, a direct comparison was made. For this purpose, voltammetric experiments were performed in a polar aprotic (THF) and polar protic (methanol). Potential assisted adsorption of alkanethiols has been reported to

form well ordered monolayers on gold electrodes held at anodic potentials.<sup>28, 30, 31</sup> The anodic reaction reportedly involves a single electron transfer per thiol molecule adsorbed on gold and possibly proceeds through an alkylsulfide radical intermediate<sup>10, 30</sup> as proposed in the mechanism for alkylthiosulfates.<sup>16</sup> The cyclic voltammograms of dodecylthiosulfate and dodecanethiol in THF as well as methanol show comparable anodic peaks under similar conditions (Figure 3.3(a) and 3.3(b)). These voltammograms indicate that a similar mechanism may be involved in the electrochemically assisted self-assembly of alkanethiols and alkylthiosulfates on gold. From the above results, the irreversible oxidation peak observed in the voltammetry of alkanethiols on gold can be assigned to one or more of the following electrochemical processes: a) oxidation of thiol present in the solution to form disulfide,<sup>30</sup> b) oxidative adsorption of thiol,<sup>28, 31, 32</sup> c) oxidative desorption of thiol monolayer formed on gold surface,<sup>33</sup> d) surface oxidation of gold at anodic potentials,<sup>28, 34</sup> or e) gold corrosion or dissolution induced by thiol molecules.<sup>21</sup> Different electrochemical characterization techniques including EQCM and ultramicroelectrode (UME) voltammetry can be used to identify the dominant electrochemical process corresponding to the anodic peak. Figure 3.4 shows voltammograms of alkanethiol and alkylthiosulfate oxidation on a gold UME as a function of concentration. Here the peak current decreases with increasing concentration. It is immediately clear that both systems exhibit similar responses characteristic of a surface confined redox reaction as opposed to a steady-state diffusion controlled response characteristic of UME.<sup>35</sup> However, the peak current does not exhibit a square root or direct dependence on scan rate (as in Figure 3.5) suggesting

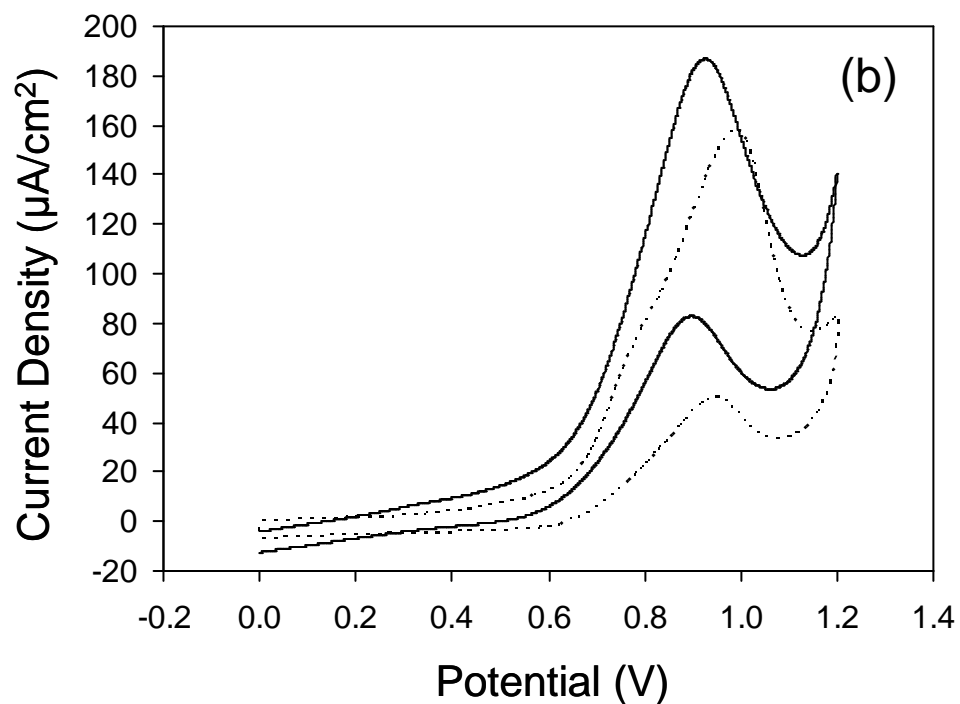
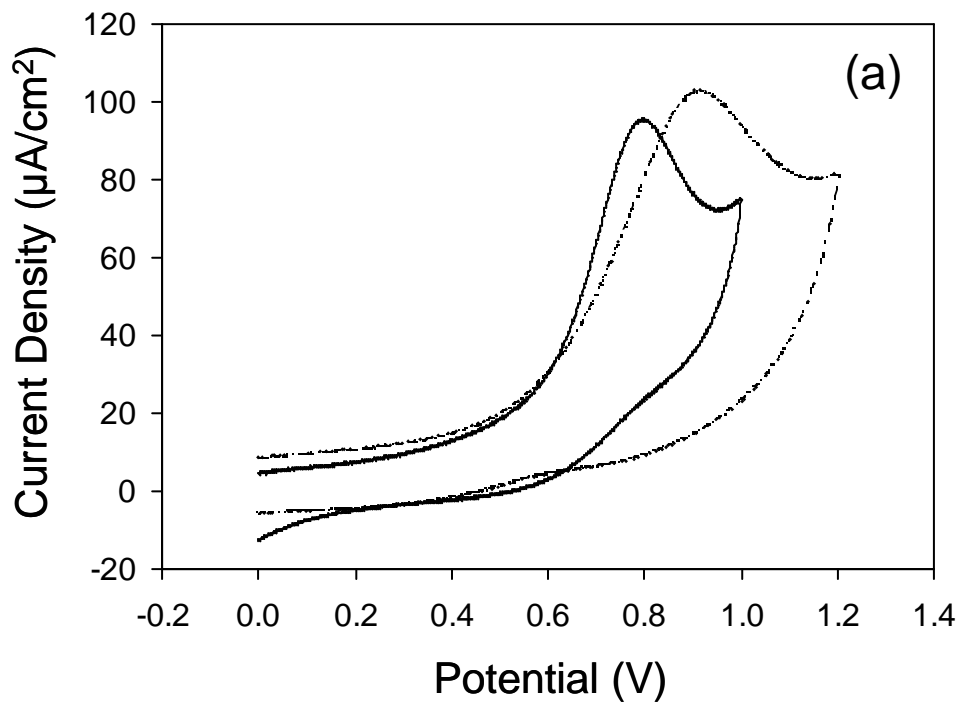


**Figure 3.3.** Cyclic voltammograms (0.1 M TBATFB, 100 mV/s) for dodecylthiosulfate (—) and dodecanethiol (-----) in a) THF and b) methanol using gold disc electrodes. The data represent the first cycle on a clean gold electrode.

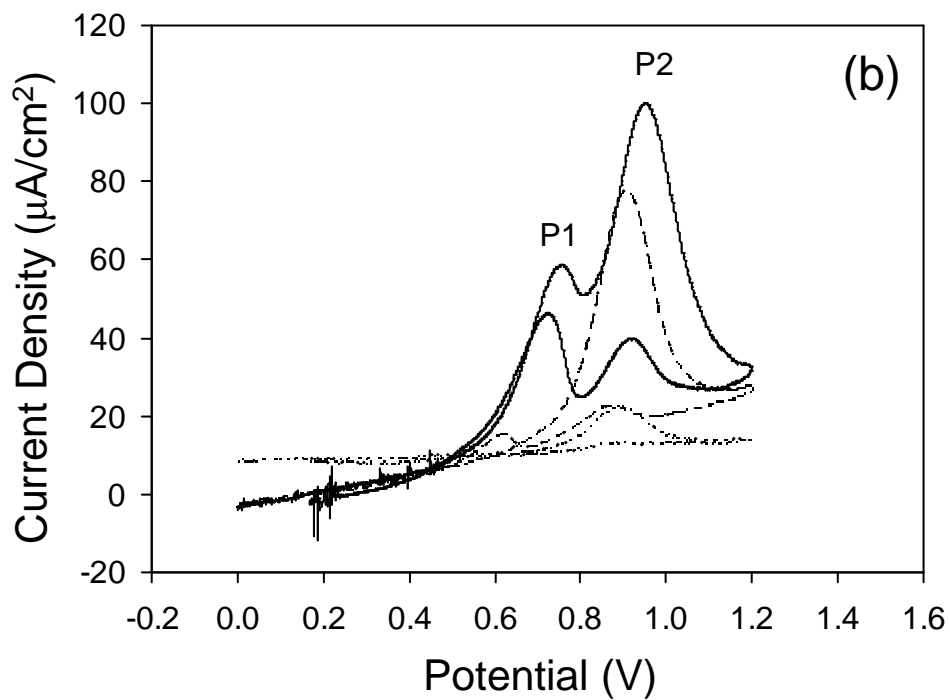
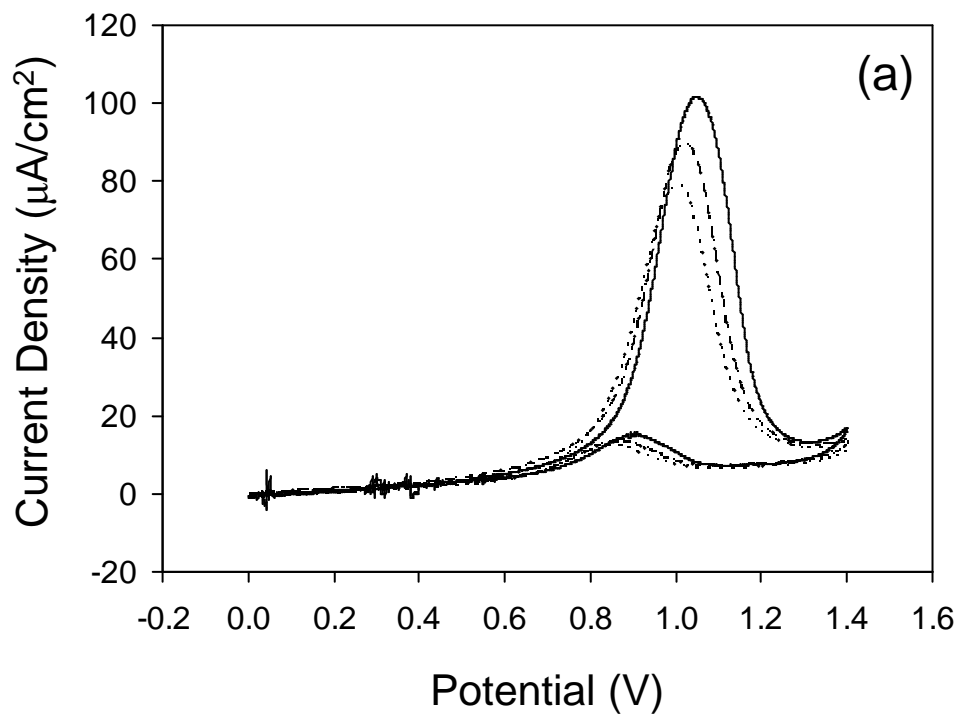


**Figure 3.4.** Cyclic voltammograms for a) dodecanethiol and b) dodecylthiosulfate in THF (0.1M TBATFB, 10 mV/s) on a gold UME at different concentrations; 10mM ( — ), 50mM ( - - - ) and 100mM ( ····· ). The data represent the first cycle on a clean gold electrode.

a rate determining step not involving electron transfer. The decrease in current near 1.1 V in the forward scan and the appearance of an anodic current near 1.0 V on the return scan is consistent with the reversible formation of blocking layers in both cases. For example, Ritchie and co-workers reported similar passivation and depassivation peaks with electrochemical oxidation of thiourea on gold.<sup>27</sup> They found that the passivation film is soluble in acidic thiourea solution but the composition of the film is unclear. In our case the depassivation peaks found with both thiols and alkylthiosulfates suggest that a similar surface film may be formed (Figure 3.4). It is interesting to note that both sets of peaks (P1 and P2) in the case of the thiosulfate have depassivation components,

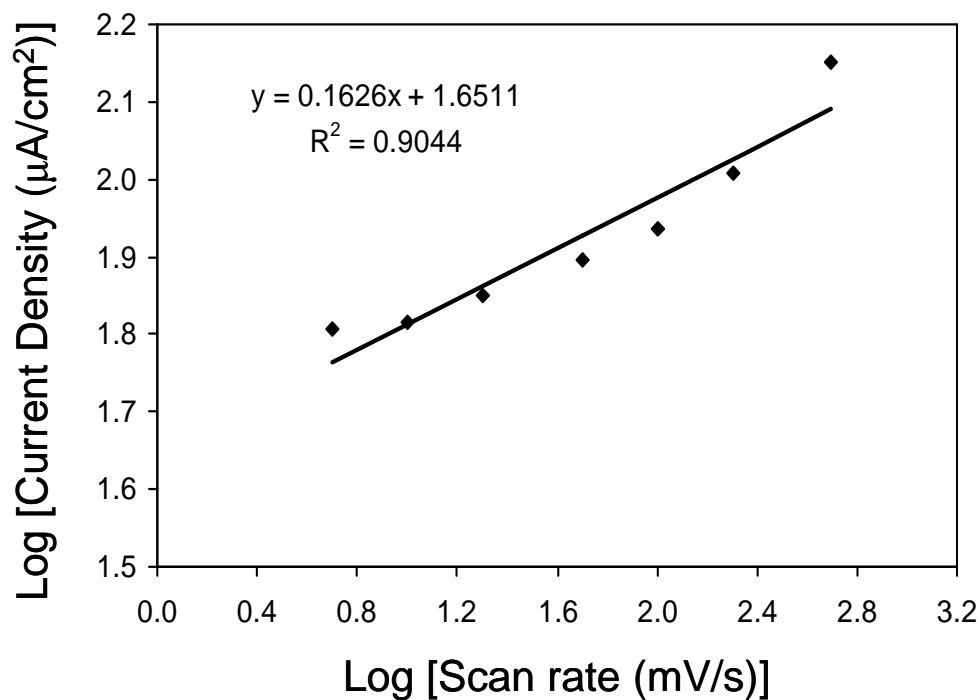


**Figure 3.5.** The peak currents in the cyclic voltammograms for 10 mM dodecanethiol in THF (with 0.1 M TBATFB) on gold EQCM electrode are plotted as a function of scan rate. The deviation of the slope from 0.5 shows that the process corresponds to the oxidation peak is not diffusion limited.

suggesting similar reactions at two distinct sites. Blank experiments on gold UME in aqueous solutions with no electrolyte show similar peaks due to gold surface oxide formation. Here the oxidation peaks are separated by approximately 200 mV as in the case of alkylthiosulfate voltammetry (Figure 3.4.b). The above results are consistent with previous reports<sup>36</sup> and these anodic peaks can be related to the first and second electron transfer steps in the oxidation of polycrystalline gold surface. Based on these reports the peak P1 corresponds to the electron transfer accompanying the deposition of a monolayer of OH ions to the gold surface and P2 corresponds to the second electron transfer to form the gold surface oxide. The peak potential and shape is related to the crystallinity of the gold surface.<sup>37</sup> In the case of alkanethiol voltammetry on UME, the first peaks are absent likely because of the difference in the nature of the monolayer and accessibility of water to the gold substrate. The depassivation peaks are absent in blank THF solution where there is no thiol or thiosulfate (Figure 3.6), which further supports the formation of a passivating gold oxide surface layer.

The lack of a diffusion-controlled response in Figure 3.4.(a) eliminates the possibility that alkanethiols are simply oxidized to disulfides (a). This assertion is further supported by the fact that the oxidation wave decreases with increasing concentration, contrary to what would be expected for (a).<sup>38</sup> The oxidative adsorption of thiols under these conditions (b) does not appear to be responsible for the irreversible oxidation wave observed in Figure 4a. As observed with *in situ* EQCM analysis<sup>39</sup> of alkanethiol oxidation (Figure 3.7), mass loss occurs as a gold electrode is cycled. These results are inconsistent with oxidative adsorption, but may result from oxidative desorption (c) or

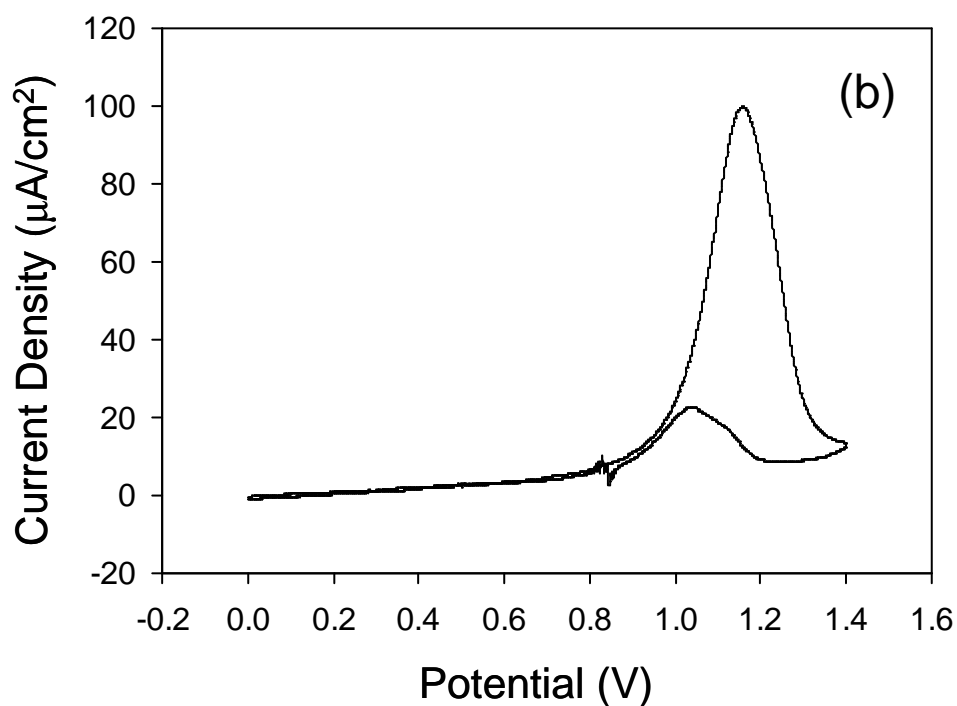
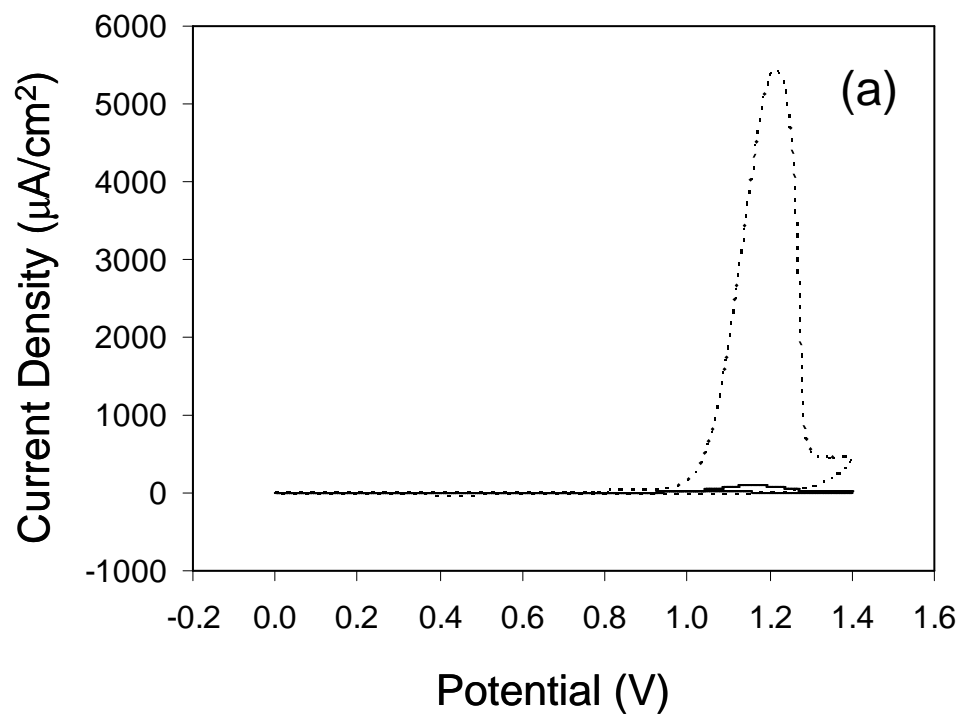


**Figure 3.6.** (a) Cyclic voltammograms for a blank THF solution (0.1 M TBATFB, 100 mV/s) containing approximately 1.5 mM of water on a polycrystalline gold electrode before (—) and after (-----) addition of 5 mM dodecanethiol. (b) The cyclic voltammogram in (a) after thiol addition is shown separately for clarity.

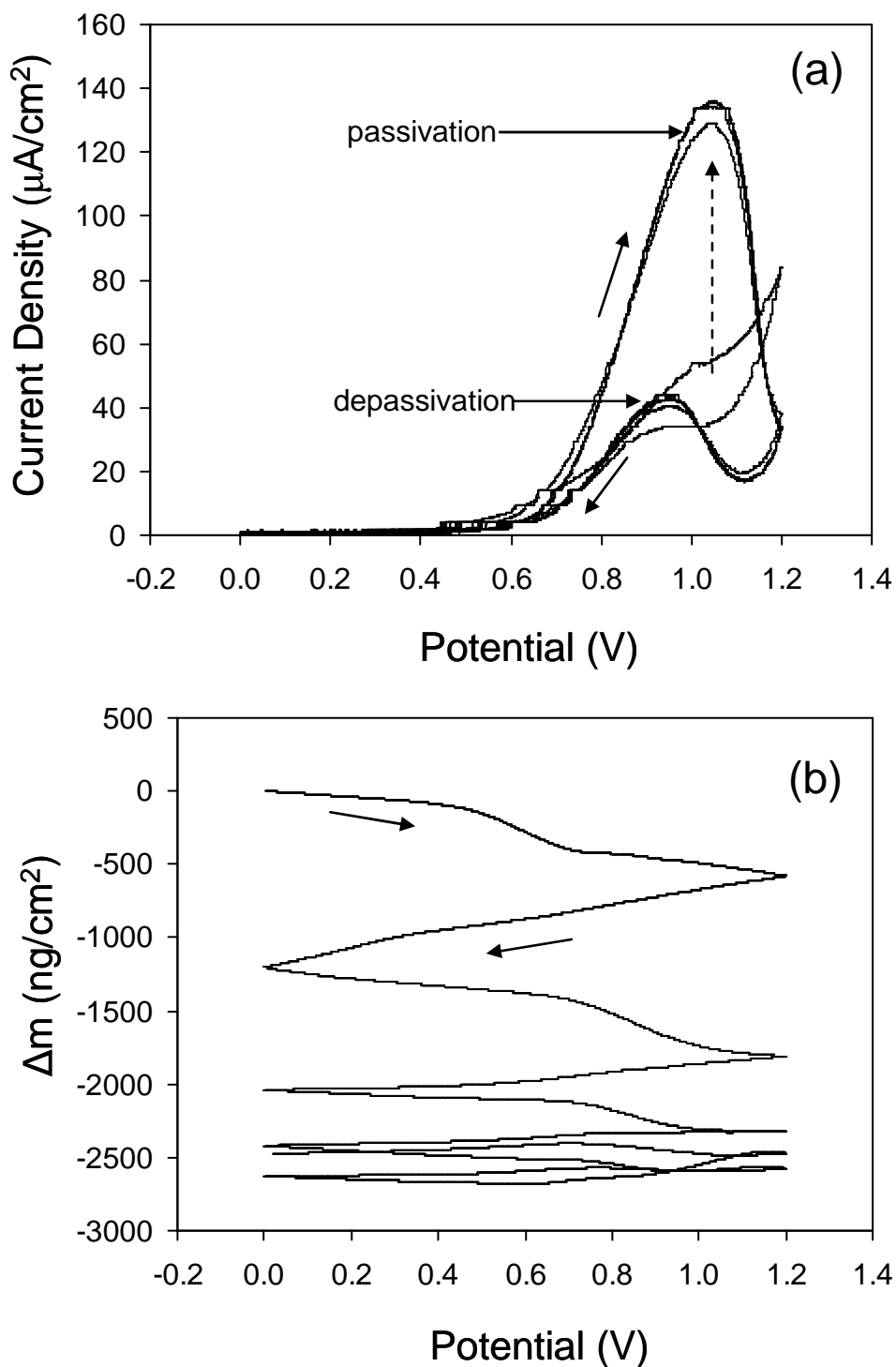


**Figure 3.7.** Cyclic voltammogram (a) and the corresponding frequency change (b) for a 10 mM solution of dodecanethiol in THF (0.1 M TBATFB, 10 mV/s) using a gold EQCM electrode. These measurements were made after equilibrating the QCM cell with the thiol solution and a preformed monolayer is already present.

corrosion (e). However, in the case of oxidative desorption of preformed thiol monolayers at higher potentials, no change or perhaps a slight increase in peak current would be expected in presence of higher alkanethiol concentration,<sup>33</sup> because the monolayer may be unchanged or slightly denser at higher thiol concentrations. The decrease in peak current with increasing thiol concentration observed in Figure 4a suggests that oxidative desorption of the monolayer (c) does not dominate the response under these conditions. This conclusion is further supported by the mass change observed in the EQCM measurement shown in Figure 3.7. After five cycles, the total frequency change is approximately 250 Hz which corresponds to  $2.55 \mu\text{g}/\text{cm}^2$  of gold lost from the surface of the gold coated QCM crystal. Assuming a density of  $1.5 \times 10^{15}$  atoms/ $\text{cm}^2$  for polycrystalline gold substrate,<sup>21</sup> the mass loss is equivalent to the removal of five atomic layers of gold. The surface density of a well packed thiol monolayer on gold surface is  $4.5 \times 10^{14}$  molecules/ $\text{cm}^2$ .<sup>8</sup> Using this value, the mass of one monolayer of dodecanethiolate adsorbed on gold surface is  $150 \text{ ng}/\text{cm}^2$ . This value is significantly lower than the mass change corresponding to the first cycle in Figure 3.7 (approximately  $1200 \text{ ng}/\text{cm}^2$ ) indicating that a significant amount of mass lost must be attributed to loss of gold or gold oxide.

Blank EQCM experiments with TBATFB electrolyte show no significant frequency change (less than  $\pm 10 \text{ Hz}$ ) compared to what observed with thiols ( $\sim +200 \text{ Hz}$ ). This demonstrates that our system is not suffering from the corrosion associated with halogen impurities in TBATFB as has been reported by Goncalves and Irene.<sup>40</sup> Therefore

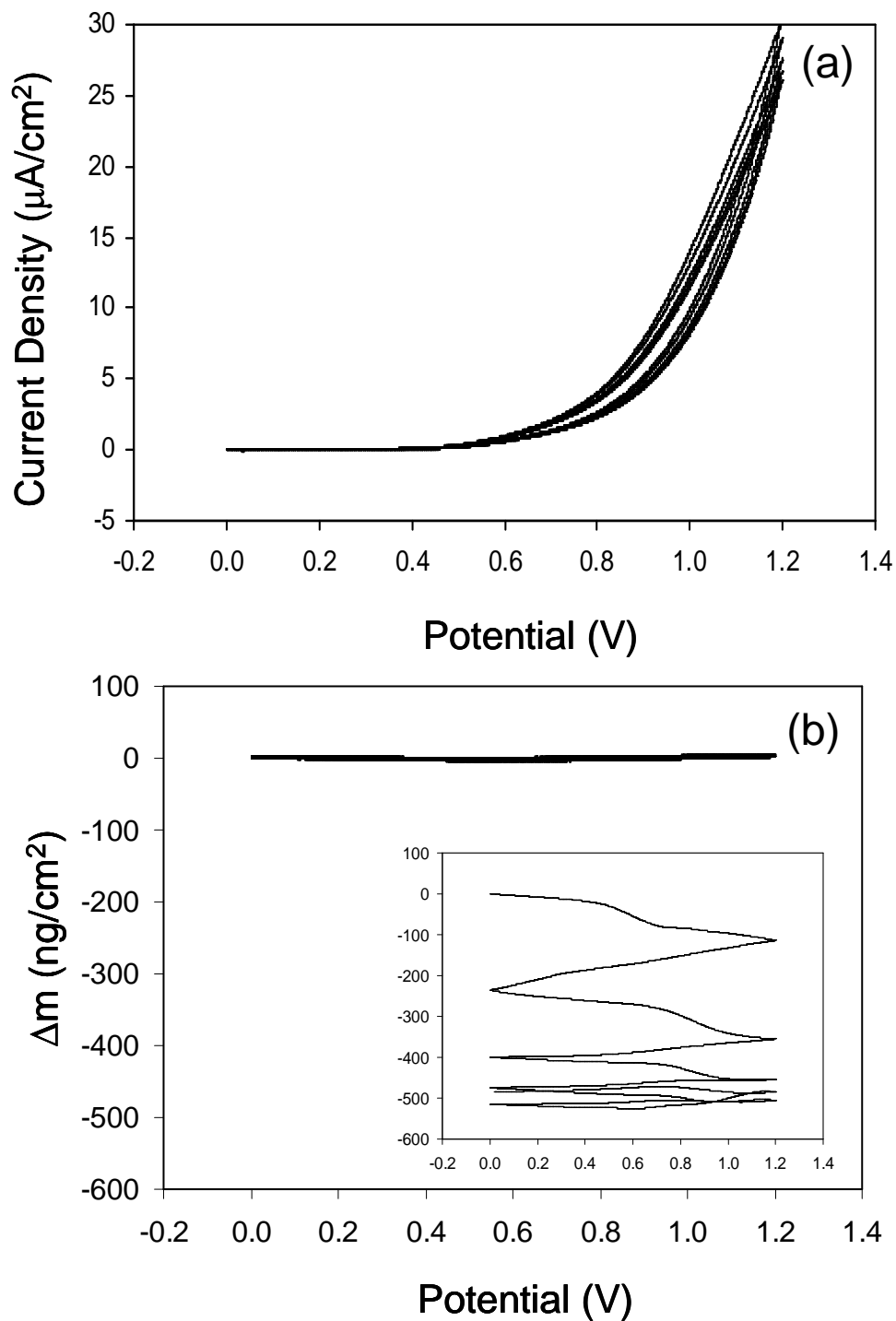


**Figure 3.8.** Cyclic voltammogram (a) and the corresponding frequency change (b) for a 10 mM solution of dodecanethiol in THF (0.1 M TBATFB, 10 mV/s) on a platinum coated gold EQCM electrode. These measurements were made after equilibrating the EQCM cell with the thiol solution. The gold EQCM response under the same conditions is given in inset of (b) for comparison.

it is concluded that the gold corrosion in our system is associated with thiol or thiosulfate. Voltammetry on platinum modified gold EQCM electrode in presence of dodecanethiol under identical conditions did not show oxidation peaks or mass loss (Figure 3.8). Based on these results we conclude that the peak current that is observed under these conditions is due to oxidation and corrosion of gold, not the oxidation of alkanethiol. The similarity in the behavior observed for alkanethiols and alkylthiosulfates suggest that gold oxidation and corrosion is likely occurring in this case as well, however, EQCM measurements were not possible due to the formation of insoluble sodium sulfate in THF, which masks any mass loss.<sup>16</sup>

In contrast to the results obtained in THF, EQCM measurements in methanol show no evidence of corrosion (Figure 3.9). On the contrary, a mass increase approaching that expected for a monolayer is observed in the first cycle (approximately  $150 \text{ ng/cm}^2$ ), while the oxidation wave decreases with scan. The measurements were performed after equilibrating the EQCM cell with thiol solution where a monolayer is presumably present at the beginning of the experiment. The magnitude of the peak current and mass change found to decrease with potential cycles while a better passivating monolayer is formed. The fact that the magnitude of oxidation is similar to that observed in THF suggests that while corrosion may be occurring in THF, the oxidation reaction precedes dissolution and that dissolution does not occur in the case of methanol, presumably due to solubility issues. The similarity in behaviour observed between alkanethiols and alkylthiosulfates raised the possibility that a common component may play a role in the redox behaviour observed. In order to explore the

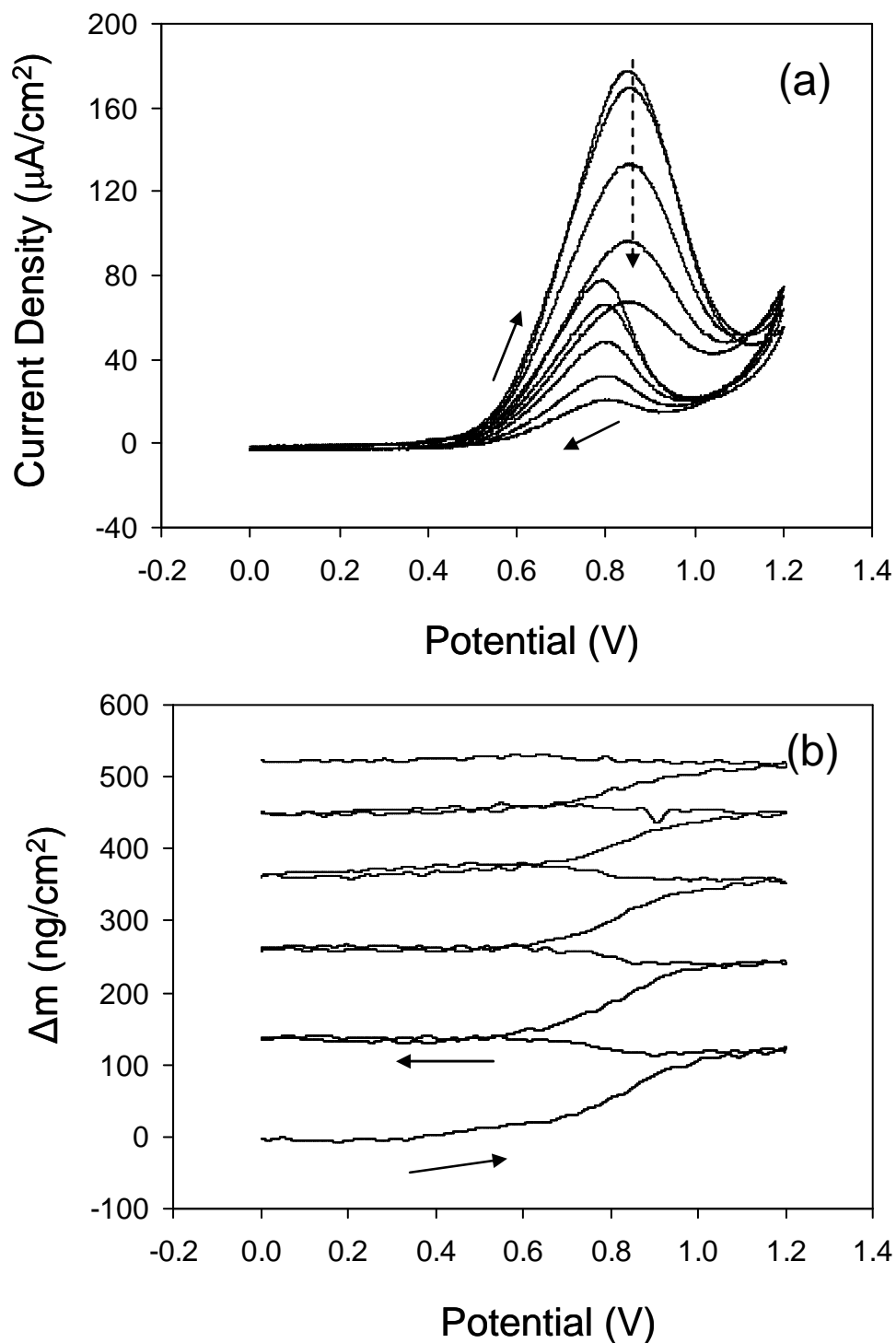
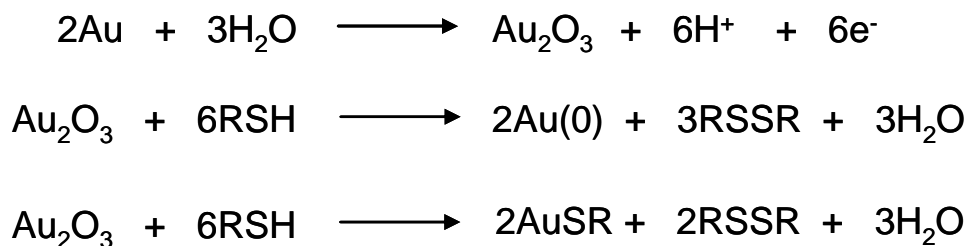


**Figure 3.9.** Cyclic voltammogram (a) and the corresponding frequency change (b) for a 10 mM solution of dodecanethiol in methanol (0.1 M TBATFB, 10 mV/s) using a gold EQCM electrode. These measurements were made after equilibrating the QCM cell with the thiol solution and a preformed monolayer is already present.

potential role of water in the observed behaviour, experiments were performed under dry solvent conditions. Extensive drying of THF and performing voltammetry under strictly dry conditions in a glove box showed more than a 50% reduction in the oxidation peak current compared to standard conditions where THF contains trace amounts of water (~ 0.01 mM), suggesting the role of gold oxide formation due to trace water and its subsequent reaction with alkanethiol and alkythiosulfates.<sup>28</sup>

### 3.3.1 Gold Oxide Formation and Corrosion

Gold oxidation is associated with the electrosorption of hydroxyl ions at anodic potentials to form hydrated gold oxide, which undergoes structural rearrangements to form hydrated or anhydrous gold oxide (Scheme 3.1).<sup>41</sup> Electrochemical oxidation of gold has been reported in non-aqueous solvents containing trace water.<sup>28</sup> The presence



(Rubinstein *et al.*, *J. Am. Chem. Soc.*, **1998**, 120, 13444)



**Scheme 3.1.** Mechanism of alkanethiol and alkythiosulfate monolayer formation on gold at anodic potentials through the reduction of gold surface oxide

of a small peak in blank THF solution containing trace water ( $\sim 0.01$  mM) on an UME (Figure 3.10) is consistent with these reports. Here, the peak appears at the same potential (approximately 1.0 V) as that of anodic peak observed in the voltammogram for alkanethiol on gold in relatively anhydrous THF. Additions of small amounts of water to a blank THF solution increases the peak current which reaches a limiting value around 1.5 mM, further supporting oxidation of gold in presence of trace water. In the presence

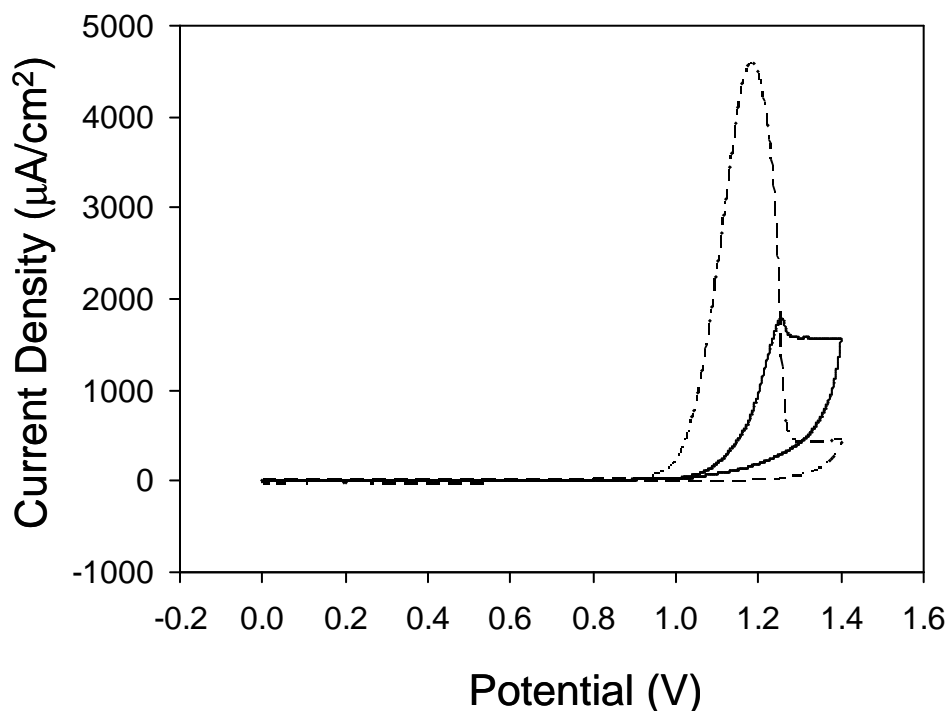
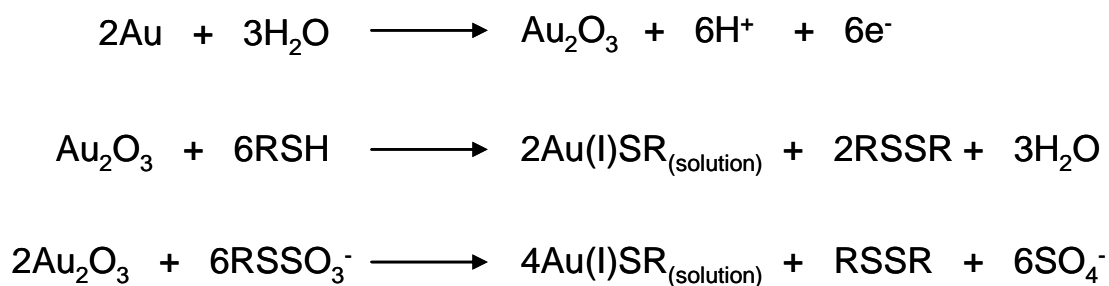


**Figure 3.10.** Cyclic voltammograms on a gold UME electrode in blank THF (0.1 M TBATFB, 10mV/s) solution with  $\sim 0.005$  mM (-----) and  $\sim 1.5$  mM (—) water.

of alkanethiols or alkylthiosulfates, the cyclic voltammograms in THF show a depassivation peak<sup>27</sup> in the reverse scan (Figure 3.8 ) on both micro and ultramicro electrodes. This suggests that a part of the passive layer of gold oxide dissolves away<sup>27</sup>

(Scheme 3.2) consistent with thiol<sup>21</sup> or thiosulfate<sup>42</sup> induced gold corrosion. In all of these cases, the peak expected for the gold oxide reduction in the reverse scan is absent, presumably due to thiol or thiosulfate induced reduction of gold oxide and monolayer formation (Scheme 3.1). These results further suggest that gold surface oxidation is the major source of the irreversible anodic peak in the voltammograms, and not thiol or thiosulfate oxidation. Gold corrosion may then occur at these anodic potentials in the presence of strong ligands like thiol<sup>31</sup> and thiosulfates<sup>42</sup> depending on the nature of the solvent.



**Scheme 3.2.** Gold corrosion induced by electrochemically directed self-assembly of alkanethiol and alkylthiosulfate on gold

The gold corrosion is consistent with past reports<sup>21, 26, 27</sup> and likely explains the formation of good monolayers on nominally “dirty” gold surfaces.<sup>13</sup> This mechanism can also account for the facile formation of well-ordered, low-defect monolayers in a relatively short period of time.<sup>13</sup> The initial corrosion that occurs in THF will remove contaminants and expose a freshly etched gold surface. Any unpassivated defects in the gold surface can then be oxidized and etched in subsequent oxidation steps until a

relatively defect free surface is formed. The morphology of gold surface has been characterized using AFM, before and after the electrochemical treatment, however no noticeable changes in surface roughness were observed. This is not unexpected given the small amount of gold removed (~5 monolayers) during cycling.

As established above, the monolayer formation at oxidative potentials is not a result of a simple outersphere electron transfer reaction between gold and thiol or thiosulfate. Instead, it appears that the reaction in both cases occurs between gold oxide and thiol<sup>28</sup> or thiosulfate. To investigate this possibility, following the method of Paik *et al.*,<sup>31</sup> amperometric measurements were performed after holding the electrode below and at the oxidation potential of gold (at 0.3 V and 1.2 V respectively) in THF solution with TBATFB as electrolyte. At 0.3 V, addition of thiol shows transient anodic currents (Figure 3.9) consistent with previous reports indicating the oxidation of alkanethiol to form well ordered monolayers on gold.<sup>31</sup> The monolayer formation is also in agreement with previous results<sup>16</sup> that the electrolyte TBATFB does not inhibit alkanethiol self-assembly on gold. Contrary to alkanethiol, addition of alkylthiosulfate at 0.3 V did not show any significant variation in current. The absence of a current transient following alkylthiosulfate addition suggests no significant oxidation of thiosulfate on gold at this potential, consistent with previous reports that alkylthiosulfate self-assembly on gold is retarded in presence of TBATFB at open circuit or lower applied potentials.<sup>16</sup> Electrode blocking experiments with a solution phase redox couple (ferricyanide) confirmed that no significant blocking of the gold surface due to monolayer formation.

For a gold electrode held at 1.2 V (at the surface oxidation potential of gold) addition of dodecanethiol or dodecylthiosulfate shows a decrease in current (Figure 3.11) due to surface passivation by monolayer formation. Further addition of thiol or thiosulfate did not give any noticeable response confirming that a passivating monolayer is formed in both cases. No oxidative current is observed with either alkanethiol or alkylthiosulfate addition suggesting that the redox reaction takes place between gold oxide and thiol with no net electron flow through the external circuit. The drop in current after thiol or thiosulfate addition is due to the surface passivation of gold associated with the formation of a thiol monolayer. The current transients are larger than expected from a simple change in double-layer capacitance and PZC upon self-assembly. For example, the double layer capacitance for bare gold and gold with a monolayer of dodecanethiol is 11.8 and 3.2  $\mu\text{F}/\text{cm}^2$  respectively.<sup>43</sup> A change in double layer capacitance of 8.6  $\mu\text{F}/\text{cm}^2$  while applying 1.5 V would result in 12.9  $\mu\text{C}/\text{cm}^2$ , almost two orders of magnitude smaller than the charge passed in Figure 3.11(b) ( $\sim 2 \text{ mC}/\text{cm}^2$ ). In the event of a significant shift in PZC upon monolayer formation, which as been reported to be approximately 1 V under aqueous conditions<sup>44</sup> (larger than expected under our non-aqueous conditions), at most one would expect the passage of somewhere between 11.8 and 3.2  $\mu\text{C}/\text{cm}^2$ . Again, this is about two orders of magnitude less charge than observed in Figure 3.11(b). These results are consistent with previous reports demonstrating alkanethiol monolayer formation on oxidized gold surfaces.<sup>28, 45</sup> and suggests that alkylthiosulfates undergo a similar redox reaction with gold oxide.

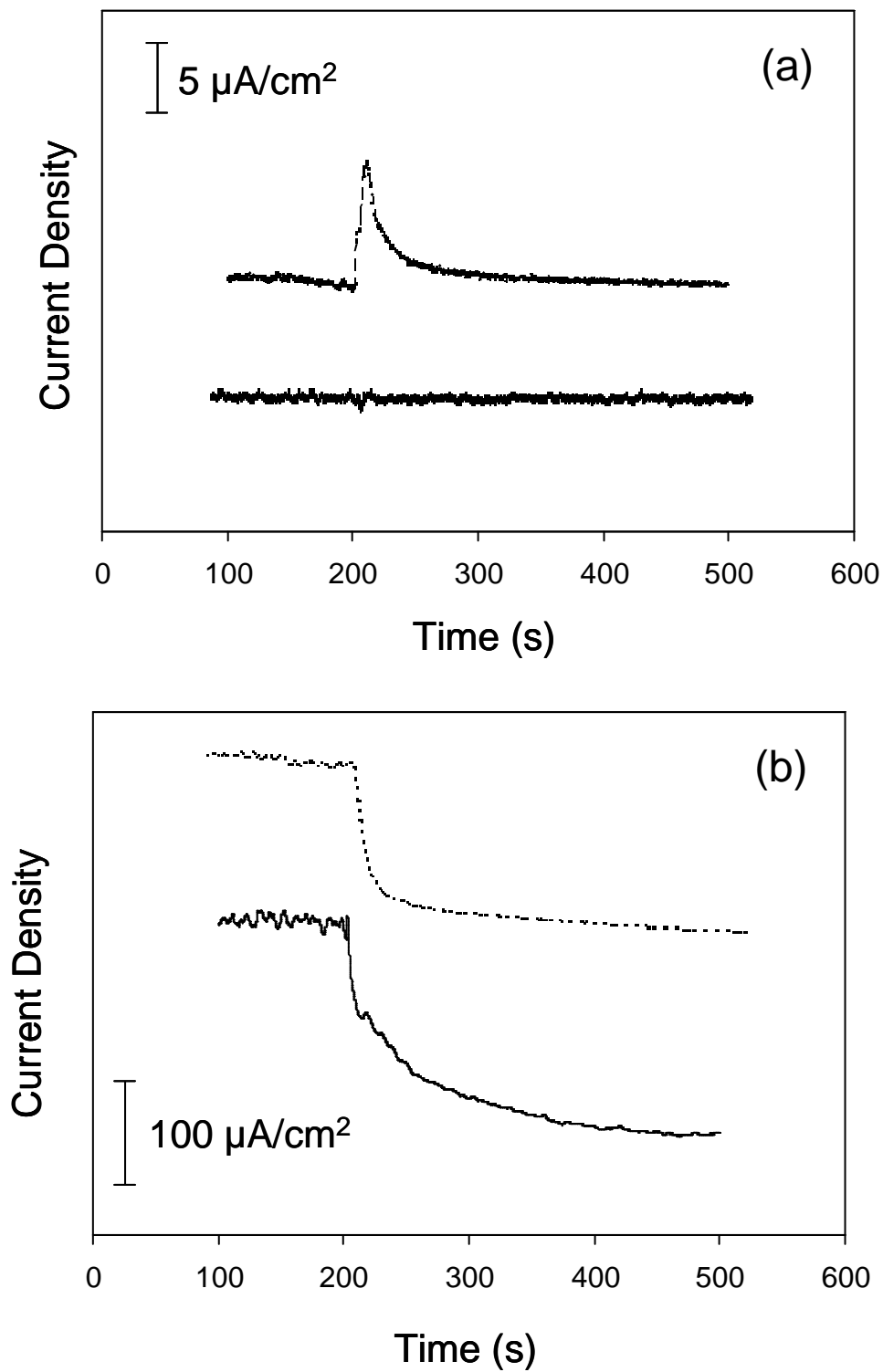


**Figure 3.11.** Amperometric current-time data for gold disc electrodes held at a) 0.3 V and b) 1.2 V after addition of 10 mM dodecanethiol ( - - - - - ) and 10 mM dodecylthiosulfate ( ——— ).

### 3.3.2 Electrochemical Stability and Exchange of Monolayers

Alkanethiol monolayers on gold undergo exchange reactions to form mixed monolayers under spontaneous self-assembly conditions. The rate of the exchange process depends upon several factors including the hydrocarbon chain length, solubility of the thiols in the solvent used, nature of the chain-terminating groups and temperature.<sup>46</sup> For example, the exchange between 1-dodecanethiol and 11-mercapto-1-undecanol on gold was found to increase with immersion time and temperature.<sup>47</sup> However, the exchange process is very slow at lower temperatures and only around 15% of the molecules in the SAM of 11-mercapto-1-undecanol are exchanged with 1-dodecanethiol molecules in solution at 20<sup>0</sup>C, even after an immersion time of 72 hours. Alkanethiol monolayers on gold are reported to exhibit good electrochemical stability towards desorption between -0.6 and +0.6 V (vs. SHE) under neutral, aqueous conditions.<sup>48</sup> In acetonitrile and dichloromethane, the potential window for monolayer stability is greater, from -1.0 to +0.5 V (vs Ag/AgCl (saturated KCl)) and is independent of the type of gold substrates, i.e., gold foil and thermally evaporated gold films.<sup>49</sup> The monolayer instability at anodic potentials may be due to gold surface oxide formation in presence of trace water in the solvents.

EQCM measurements in THF (Figure 3.7) show that the thiol monolayer - gold interface is initially dynamic, losing a significant mass, but eventually stabilizes. Despite the mass stability, a noticeable oxidation wave remains. This behavior is significantly different than that observed in methanol which shows a continual decrease

in the oxidation wave and no mass loss. Here the fraction of the gold oxide peak current observed is significantly (approximately one order of magnitude) less than what would be expected in the absence of a monolayer.

It is unclear, however if the monolayer is stable or in a dynamic equilibrium that results in no net mass loss but rapid exchange with thiols in solution. To investigate this possibility, exchange experiments were performed using alkylthiosulfates and characterized by XPS. These experiments were followed on gold surfaces with a preformed dodecanethiolate monolayer exposed to a solution containing hexadecylthiosulfate in THF. Assuming similar behavior for alkanethiols and alkylthiosulfate, the preformed dodecanethiolate monolayer was deposited under conditions where there is no further mass change with EQCM after deposition, indicating the presence of a passivating, well ordered monolayer that is stable with potential cycling.

**Table 1.** XPS peak area ratios of C 1s and Au 4f<sub>7/2</sub> peak of dodecylthiosulfate (C12-TS) and hexadecylthiosulfate (C16-TS) monolayers on gold electrode. The percentage change in the C1s/ Au 4f<sub>7/2</sub> ratio was calculated with respect to the C 1s/ Au 4f<sub>7/2</sub> ratio of C12-TS.

	C/Au	% change in C 1s/ Au 4f <sub>7/2</sub> ratio
C12-TS on Au	0.61	---
C16-TS on Au	0.81	+ 31.8 %
C12-TS on Au after 10 cycles in C16-TS/THF/0.1M TBATFB	0.86	+ 40.5 %

After ten potential cycles in hexadecylthiosulfate between 0 to 1.2 V, gold electrode surfaces were characterized with XPS. The carbon to gold ratio determined from the XPS analysis of the monolayers were used as a tool to study these electrochemical exchange reactions (Table 1).<sup>50</sup> The hexadecanethiolate monolayer exhibited a C 1s/Au 4f<sub>7/2</sub> ratio of 0.81 which is 31% higher than that for a dodecanethiolate monolayer. This value is reasonable considering the expected 33% higher number of carbon atoms in hexadecanethiolate monolayer. A comparable value of 0.86 obtained after cycling the dodecanethiolate modified gold surface in hexadecylthiosulfate suggesting that complete replacement of the former by a hexadecylthiosulfate monolayer. These results suggest exchange of monolayer takes place during potential cycling in the presence of alkylthiosulfate in solution.

### **3.4 Conclusions**

Electrochemically directed self-assembly of alkylthiosulfates on gold follow a more complex mechanism of monolayer formation than originally recognized. No redox process is observed associated with the alkanethiol or alkylthiosulfate directly, but instead is due to gold. The electrochemically assisted self-assembly process is accompanied by gold surface oxidation in presence of trace water in the solvent and monolayer formation is accompanied by reduction of the gold oxide and gold corrosion. EQCM results support this mechanism. The gold corrosion, limited by the surface oxide formation, may act as a surface cleaning process and explain the previous report of monolayer formation on soiled gold substrate under electrochemically directed self-

assembly conditions. The XPS analysis of the exchange of monolayers with alkylthiosulfates in solution shows the dynamic nature of the monolayer under electrochemically directed self-assembly conditions.

## Acknowledgements

Financial support is gratefully acknowledged from the Natural Sciences and Engineering Research Council (NSERC) of Canada, the Canada Research Chairs (CRC) Program, the Canada Foundation for Innovation (CFI), the Manitoba Research and Innovation Fund, and the University of Manitoba. Also acknowledge the Manitoba Regional Materials and Surface Characterization Facility for access to XPS and Dr. Sergei Rudenja for performing XPS analysis.

## References

1. Nuzzo, R. G.; Zegarski, B. R.; Dubois, L. H., Fundamental-Studies of the Chemisorption of Organosulfur Compounds on Au(111) - Implications for Molecular Self-Assembly on Gold Surfaces. *Journal of the American Chemical Society* **1987**, 109, (3), 733-740.
2. Whitesides, G. M.; Mathias, J. P.; Seto, C. T., Molecular Self-Assembly and Nanochemistry - a Chemical Strategy for the Synthesis of Nanostructures. *Science* **1991**, 254, (5036), 1312-1319.
3. Carpick, R. W.; Salmeron, M., Scratching the Surface: Fundamental Investigations of Tribology with Atomic Force Microscopy. *Chemical Reviews* **1997**, 97, (4), 1163-1194.
4. Kumar, A.; Biebuyck, H. A.; Whitesides, G. M., Patterning Self-Assembled Monolayers - Applications in Materials Science. *Langmuir* **1994**, 10, (5), 1498-1511.
5. Mirsky, V. M., New Electroanalytical Applications of Self-Assembled Monolayers. *Trac-Trends in Analytical Chemistry* **2002**, 21, (6-7), 439-450.

6. Tour, J. M., Molecular Electronics. Synthesis and Testing of Components. *Accounts of Chemical Research* **2000**, 33, (11), 791-804.
7. Ulman, A., Formation and structure of self-assembled monolayers. *Chemical Reviews* **1996**, 96, (4), 1533-1554.
8. Love, J. C.; Estroff, L. A.; Kriebel, J. K.; Nuzzo, R. G.; Whitesides, G. M., Self-Assembled Monolayers of Thiolates on Metals as a form of Nanotechnology. *Chemical Reviews* **2005**, 105, (4), 1103-1169.
9. Chen, F.; Hihath, J.; Huang, Z. F.; Li, X. L.; Tao, N. J., Measurement of Single-Molecule Conductance. *Annual Review of Physical Chemistry* **2007**, 58, 535-564.
10. Weisshaar, D. E.; Lamp, B. D.; Porter, M. D., Thermodynamically Controlled Electrochemical Formation of Thiolate Monolayers at Gold - Characterization and Comparison to Self-Assembled Analogs. *Journal of the American Chemical Society* **1992**, 114, (14), 5860-5862.
11. Tender, L. M.; Worley, R. L.; Fan, H. Y.; Lopez, G. P., Electrochemical Patterning of Self-Assembled Monolayers onto Microscopic Arrays of Gold Electrodes Fabricated by Laser Ablation. *Langmuir* **1996**, 12, (23), 5515-5518.
12. Walczak, M. M.; Popenoe, D. D.; Deinhammer, R. S.; Lamp, B. D.; Chung, C. K.; Porter, M. D., Reductive Desorption of Alkanethiolate Monolayers at Gold - a Measure of Surface Coverage. *Langmuir* **1991**, 7, (11), 2687-2693.
13. Hsueh, C. C.; Lee, M. T.; Freund, M. S.; Ferguson, G. S., Electrochemically Directed Self-Assembly On Gold. *Angewandte Chemie-International Edition* **2000**, 39, (7), 1228-+.
14. Kice, J. L., A Kinetic Study of Acid Hydrolysis of a Bunte Salt. *Journal of Organic Chemistry* **1963**, 28, (4), 957-&.
15. Lukkari, J.; Meretoja, M.; Kartio, I.; Laajalehto, K.; Rajamaki, M.; Lindstrom, M.; Kankare, J., Organic Thiosulfates (Bunte Salts): Novel Surface-Active Sulfur Compounds for the Preparation of Self-Assembled Monolayers on Gold. *Langmuir* **1999**, 15, (10), 3529-3537.
16. Lee, M. T.; Hsueh, C. C.; Freund, M. S.; Ferguson, G. S., Electrochemical Self-Assembly of Monolayers from Alkylthiosulfates on Gold. *Langmuir* **2003**, 19, (13), 5246-5253.
17. Burdinski, D.; Bles, M. H., Thiosulfate- and Thiosulfonate-Based Etchants for the Patterning of Gold Using Microcontact Printing. *Chemistry of Materials* **2007**, 19, (16), 3933-3944.
18. Edinger, K.; Golzhauser, A.; Demota, K.; Woll, C.; Grunze, M., Formation of Self-Assembled Monolayers of N-Alkanethiols on Gold - a Scanning Tunneling Microscopy Study on the Modification of Substrate Morphology. *Langmuir* **1993**, 9, (1), 4-8.

19. Schonenberger, C.; Sondaghuethorst, J. A. M.; Jorritsma, J.; Fokkink, L. G. J., What Are the Holes in Self-Assembled Monolayers of Alkanethiols on Gold. *Langmuir* **1994**, 10, (3), 611-614.
20. VanPatten, P. G.; Noll, J. D.; Myrick, M. L., Formation of Holes In Alkanethiol Monolayers on Gold - Comment. *Journal of Physical Chemistry B* **1997**, 101, (39), 7874-7875.
21. Cao, Z.; Xiao, Z. L.; Gu, N.; Gong, F. C.; Yang, D. W.; Zhu, Z. P., Corrosion Behaviors on Polycrystalline Gold Substrates in Self-Assembled Processes of Alkanethiol Monolayers. *Analytical Letters* **2005**, 38, (8), 1289-1304.
22. Raisanen, M. T.; Kemell, M.; Leskela, M.; Repo, T., Oxidation of Elemental Gold in Alcohol Solutions. *Inorganic Chemistry* **2007**, 46, (8), 3251-3256.
23. Goolsby, A. D.; Sawyer, D. T., Electrochemistry of Gold(1) and Its Complexes in Acetonitrile. *Analytical Chemistry* **1968**, 40, (13), 1978-&.
24. Chandra, I.; Jeffrey, M. I., A Fundamental Study of Ferric Oxalate for Dissolving Gold in Thiosulfate Solutions. *Hydrometallurgy* **2005**, 77, (3-4), 191-201.
25. Kissner, R., Halide Catalysis of the Electrochemical Oxidation of Gold in Acetonitrile. *Journal of Electroanalytical Chemistry* **1995**, 385, (1), 71-75.
26. Larsen, A. G.; Johannsen, K.; Gothelf, K. V., An Electrochemical Quartz Crystal Microbalance Study of the Etching of Gold Surfaces in the Presence of Tetramethylthiourea. *Journal of Colloid and Interface Science* **2004**, 279, (1), 158-166.
27. Zhang, H. G.; Ritchie, I. M.; La Brooy, S. R., Electrochemical Oxidation of Gold and Thiourea in Acidic Thiourea Solutions. *Journal of the Electrochemical Society* **2001**, 148, (10), D146-D153.
28. Ron, H.; Rubinstein, I., Self-Assembled Monolayers on Oxidized Metals. 3. Alkylthiol and Dialkyl Disulfide Assembly on Gold under Electrochemical Conditions. *Journal of the American Chemical Society* **1998**, 120, (51), 13444-13452.
29. Burgess, J. D.; Hawkrigde, F. M., Octadecyl Mercaptan Sub-Monolayers on Silver Electrodeposited on Gold Quartz Crystal Microbalance Electrodes. *Langmuir* **1997**, 13, (14), 3781-3786.
30. Borsari, M.; Cannio, M.; Gavioli, G., Electrochemical Behavior of Diphenyl Disulfide and Thiophenol on Glassy Carbon and Gold Electrodes in Aprotic Media. *Electroanalysis* **2003**, 15, (14), 1192-1197.
31. Paik, W. K.; Eu, S.; Lee, K.; Chon, S.; Kim, M., Electrochemical Reactions in Adsorption of Organosulfur Molecules on Gold and Silver: Potential Dependent Adsorption. *Langmuir* **2000**, 16, (26), 10198-10205.

32. Ma, F. Y.; Lennox, R. B., Potential-Assisted Deposition of Alkanethiols on Au: Controlled Preparation of Single- and Mixed-Component SAMs. *Langmuir* **2000**, 16, (15), 6188-6190.
33. Yang, D. F.; AlMaznai, H.; Morin, M., Vibrational Study of the Fast Reductive and the Slow Oxidative Desorptions of a Nonanethiol Self-Assembled Monolayer from a Au(111) Single Crystal Electrode. *Journal of Physical Chemistry B* **1997**, 101, (7), 1158-1166.
34. Brett, C. M. A.; Kresak, S.; Hianik, T.; Brett, A. M. O., Studies on Self-Assembled Alkanethiol Monolayers Formed at Applied Potential on Polycrystalline Gold Electrodes. *Electroanalysis* **2003**, 15, (5-6), 557-565.
35. Heinze, J., Ultramicroelectrodes in Electrochemistry. *Angewandte Chemie-International Edition in English* **1993**, 32, (9), 1268-1288.
36. Angersteinkozłowska, H.; Conway, B. E.; Hamelin, A.; Stoicoviciu, L., Elementary Steps of Electrochemical Oxidation of Single-Crystal Planes of Au .1. Chemical Basis of Processes Involving Geometry of Anions and the Electrode Surfaces. *Electrochimica Acta* **1986**, 31, (8), 1051-1061.
37. Hamelin, A., Cyclic Voltammetry at Gold Single-Crystal Surfaces .1. Behaviour At Low-Index Faces. *Journal of Electroanalytical Chemistry* **1996**, 407, (1-2), 1-11.
38. Qu, D.; Morin, M., The Effect of Concentration on the Oxidative Deposition of a Monolayer of Alkylthiolate on Gold: From Island Formation To Random Adsorption. *Journal of Electroanalytical Chemistry* **2004**, 565, (2), 235-242.
39. Buttry, D. A.; Ward, M. D., Measurement of Interfacial Processes at Electrode Surfaces with the Electrochemical Quartz Crystal Microbalance. *Chemical Reviews* **1992**, 92, (6), 1355-1379.
40. Goncalves, D.; Irene, E. A., A Study of Gold-Coated Glass as Electrodes for Electropolymerization of 3-Methylthiophene. *Langmuir* **2001**, 17, (16), 5031-5038.
41. Angersteinkozłowska, H.; Conway, B. E.; Hamelin, A.; Stoicoviciu, L., Elementary Steps of Electrochemical Oxidation of Single-Crystal Planes of Au .2. A Chemical and Structural Basis of Oxidation of the (111) Plane. *Journal of Electroanalytical Chemistry* **1987**, 228, (1-2), 429-453.
42. Zhang, S. C.; Nicol, M. J., An Electrochemical Study Of The Dissolution of Gold In Thiosulfate Solutions - Part I: Alkaline Solutions. *Journal of Applied Electrochemistry* **2003**, 33, (9), 767-775.
43. Petrovic, Z.; Metikos-Hukovic, M.; Babic, R., Potential-Assisted Assembly of 1-Dodecanethiol on Polycrystalline Gold. *Journal of Electroanalytical Chemistry* **2008**, 623, (1), 54-60.

44. Kakiuchi, T.; Usui, H.; Hobara, D.; Yamamoto, M., Voltammetric Properties of the Reductive Desorption Of Alkanethiol Self-Assembled Monolayers from a Metal Surface. *Langmuir* **2002**, 18, (13), 5231-5238.
45. Ron, H.; Matlis, S.; Rubinstein, I., Self-Assembled Monolayers on Oxidized Metals. 2. Gold Surface Oxidative Pretreatment, Monolayer Properties, and Depression Formation. *Langmuir* **1998**, 14, (5), 1116-1121.
46. Groat, K. A.; Creager, S. E., Self-Assembled Monolayers in Organic-Solvents - Electrochemistry at Alkanethiolate-Coated Gold in Propylene Carbonate. *Langmuir* **1993**, 9, (12), 3668-3675.
47. Baralia, G. G.; Duwez, A. S.; Nysten, B.; Jonas, A. M., Kinetics of Exchange of Alkanethiol Monolayers Self-Assembled on Polycrystalline Gold. *Langmuir* **2005**, 21, (15), 6825-6829.
48. Beulen, M. W. J.; Kastenbergh, M. I.; van Veggel, F.; Reinhoudt, D. N., Electrochemical Stability of Self-Assembled Monolayers on Gold. *Langmuir* **1998**, 14, (26), 7463-7467.
49. Everett, W. R.; Fritschfaules, I., Factors That Influence the Stability of Self-Assembled Organothiols on Gold under Electrochemical Conditions. *Analytica Chimica Acta* **1995**, 307, (2-3), 253-268.
50. Manolova, M.; Ivanova, V.; Kolb, D. M.; Boyen, H. G.; Ziemann, P.; Buttner, M.; Romanyuk, A.; Oelhafen, P., Metal Deposition onto Thiol-Covered Gold: Platinum on a 4-Mercaptopyridine SAM. *Surface Science* **2005**, 590, (2-3), 146-153.

## Chapter 4:

### Field-Induced Carrier Generation in Conjugated Polymer Semiconductors for Dynamic, Asymmetric Junctions

### **Authors' Contributions**

The work described in this chapter was performed in collaboration with Electrical and Computer Engineering Department at the University of Manitoba. The idea of designing a conjugated polymer hybrid material with potential electronic applications was first conceived by Dr. M. S. Freund and Dr. D. J. Thomson. All electrochemical experiments mentioned in this work were designed and conducted by R. G. Pillai. J. H. Zhao, supervised by Dr. D. J. Thomson, performed the testing of the memory device. The electrical characterization experiments were conceptualized by Dr. D.J. Thomson and Dr. M.S Freund; designed and performed by R. G. Pillai. Dr. M. S. Freund wrote the first draft of the paper. The figures were prepared by J.H. Zhao and R. G. Pillai. All the authors contributed equally for revisions and final editing of the manuscript before its acceptance for publication in the WILEY-VCH journal '*Advanced Material*'.

## Field-Induced Carrier Generation in Conjugated Polymer Semiconductors for Dynamic, Asymmetric Junctions

Rajesh G. Pillai,<sup>1</sup> Jun Hui Zhao,<sup>2</sup> Michael S. Freund<sup>1,2</sup> and Douglas J. Thomson<sup>2</sup>

<sup>1</sup>Department of Chemistry and <sup>2</sup>Department of Electrical & Computer Engineering,  
University of Manitoba, Winnipeg, Manitoba R3T 2N2, Canada

Published: *Adv. Mater.* **2008**, 20, 49-53

Copyright ©2008 WILEY-VCH Verlag GmbH & Co. KGaA, Weinheim

## Abstract

Electronically conducting polymers have had a major impact in diverse technological fields ranging from sensing to organic-based electronics to microrobotics. The excitement and activity surrounding this class of material is based on its unique properties arising from the coupling of polymer chemistry and electronic structure. These properties include the ability to alter band structure by changing the molecular structure of the polymer as well as the high mobility of the counter ions (also referred to as dopant) that stabilize charge carriers within the polymer. While the semiconducting properties of these materials have also been exploited for the fabrication of more conventional electronic components such as transistors, field-induced drift of dopants can be exploited as a mechanism for creating electronic components in a way that has to date been completely unexplored. A new approach that exploits this property and allows the creation of electronic components that operate *via* a completely different mechanism involving ion drift within the bulk polymer is discussed. Using this method a functioning dynamic memory device has been demonstrated. This approach has more favorable scaling of properties in comparison to interfacial phenomena observed with Si-based devices.

## 4.1. Introduction

The impact of conjugated polymer semiconductors continues to increase in a wide range of emerging technologies from polymer-based electronics<sup>1</sup> to microrobotics.<sup>2</sup> An attractive feature of these materials that has been exploited very successfully is the ability to manipulate electronic properties by altering their molecular structure.<sup>3</sup> The conduction mechanism (p-type or n-type) can be altered by immobilizing ions within the semiconducting polymer enabling the creation of p-n junctions<sup>4</sup> analogous to inorganic semiconductors. Unique to conjugated polymer semiconductors is the ability to rapidly change the carrier density electrochemically in the presence of mobile counter ions. To date, these properties have received relatively little attention in the field of organic-based electronics; however they provide entirely new mechanisms for time-dependent and field-dependent responses that can form the basis of electronic devices that are less complex, less expensive and scalable down to smaller dimensions. For example, current approaches in electronic design create devices through the production of complex architectures of relatively simple, homogeneous materials. An alternative paradigm involves engineering complex, functional materials at the molecular level that enable the creation of architecturally simple structures with equivalent functionality. In this report we provide an example demonstrating a conjugated semiconducting polymer composite containing immobile anions that act as a counter ion for the oxidized (more conductive) form of the polymer and highly mobile cations that can balance the charge of the immobile anions in the presence of the reduced (less conductive)

form of the polymer. This material exhibits a field-dependent resistance in the solid state with a time dependence that is a function of the mobility of the cation. Using this approach, we have created a functioning dynamic memory device. These findings should open up new directions for the development of organic-based electronics that utilize field- and time-dependent behavior of organic semiconducting composites.

Since the original reports on the conductivity of polyacetylene,<sup>5</sup> there have been considerable efforts to develop semiconducting polymers for use in electronic devices.<sup>6</sup> The primary focus has been on chemical modification in order to tune the band gap<sup>7</sup> as well as to control the carrier type (p and n-type)<sup>8</sup> and the carrier concentrations.<sup>9</sup> Emphasis has been placed on developing materials that function in a manner that is analogous to inorganic semiconductors and on creating devices with traditional architectures such as transistors,<sup>10</sup> p-n junctions<sup>11</sup> and organic light emitting diodes (OLEDs).<sup>12</sup> At the same time, considerable focus has been placed on understanding and controlling the movement of counter ions into and out of semiconducting polymers in contact with electrolyte, and a wide range of devices have been developed based on redox switching such as batteries, supercapacitors and electrochromic devices.<sup>13</sup> Control over the identity of the ionic charge carrier can be imposed by immobilizing anions within the polymer either covalently<sup>14</sup> or by physical entrapment,<sup>15</sup> thereby forcing charge to be carried by smaller and more mobile cations.

In typical conjugated polymer systems, current conduction can be either electrode or bulk limited. For most conducting polymers, such as polypyrrole (PPy), with Au electrodes, the current is expected to be bulk limited.<sup>16</sup> Several mechanisms

of bulk conduction of charge can be dominant depending on geometry, field strength and carrier mobility among other things.<sup>16, 17</sup> At lower potentials between contact electrodes, ohmic behaviour is expected. As the potential between the electrodes increases space charge limited currents (SCLC) often become dominant.<sup>16</sup> With space charge limited current the injected charge carriers create a potential that limits the flow of charge.<sup>16</sup> This results in a current which is nonlinear and increases as  $V^2$  and  $1/L^3$  in conventional semiconductors, in the absence of traps. However unlike conventional semiconductors, in conjugated polymers the mobility of the charge carriers increases with the applied field.<sup>16, 17</sup> This results in the current increasing more rapidly with voltage than would be predicted in the absence of field enhanced mobility.<sup>16, 17</sup> The present work explore the modulation of field generated carriers by introducing ion pairs into a neutral conjugated polymer. The much slower time-dependent mobility of ions relative to injected holes is expected to result in the formation of transient structures that can be probed by applying a potential change and observing the current passing through the structure.

## **4.2. Experimental**

**4.2.1. Preparation of IDA/Polymer Structures:** The gold interdigitated array electrodes (IDAs) were obtained from Biomedical Microsensors Laboratory at North Carolina State University. Each of these arrays contains 2.8 mm x 0.075 mm gold electrodes with a gap width of 20  $\mu\text{m}$  having a total exposed area of 6.09  $\text{mm}^2$ . The polypyrrole (PPy) films were grown across the IDA electrodes using an aqueous solution of freshly distilled pyrrole monomer (100 mM) and an electrolyte (100 mM, NaDBS or  $\text{LiClO}_4$ ) at a constant potential of +0.65 V vs. Ag/AgCl. The thickness of the

polypyrrole films were controlled by passing specific amount of charge ( $200 \text{ mC/cm}^2$  for  $1 \text{ }\mu\text{m}$  thick film)<sup>18</sup> during the electrodeposition. In each case,  $1.23 \text{ C/cm}^2$  of charge was passed to achieve complete bridging of the IDA electrodes and resulted in a film thickness close to  $6 \text{ }\mu\text{m}$  as seen in Figure 4.1.

All electrochemical experiments were performed using a CHI660 electrochemical workstation (CH Instruments) and solutions were purged with nitrogen for at least 15 minutes prior to electrochemical measurements. The current-voltage (I-V) properties of the PPy-IDA devices were characterized under a nitrogen atmosphere with CHI660 electrochemical workstation (CH Instruments) or a Hewlett Packard 4145A semiconductor parameter analyzer.

**4.2.2. Scanning Electron Microscopy (SEM) Analysis:** For SEM characterization, samples were prepared by mechanical cutting and shaving of the PPy-IDA cross-sectional interface using a razor blade. The finely cut samples were sputter-coated (Edwards) with a thin layer of gold and the images were acquired with a Cambridge Stereoscan 120 Scanning Electron Microscope.

**4.2.3 X-ray Photoelectron Spectroscopy (XPS) Analysis:** XPS analysis of samples of electrochemically deposited PPy composites on gold was performed using a Kratos AXIS ULTRA spectrometer with a 300W monochromated Al K $\alpha$  source and a delay line detector. The survey and high resolution scans were recorded with pass energies of 160 eV and 20 eV respectively. All spectra were collected at 90 deg take off angle and referenced to the Au 4f<sub>7/2</sub> peak set at 84.0 eV. The background pressure in the analyzer chamber was  $\sim 10^{-9}$  Torr. For quantitative analysis relative sensitivity factors

supplied by the instrument manufacturer were used: Au  $4f_{7/2}$ , 6.25; C 1s, 0.278; N 1s, 0.477; S 2p, 0.668; Na 1s, 1.685.

**4.2.4. Construction and Testing of Memory Device:** As shown schematically in Figure 4.8, an electronic circuit was constructed for capturing memory data given by two distinctive states of current vs. time. The voltage applied to the PPy device in series with a resistor ( $R = 50 \Omega$ ) was supplied with a DS345 Synthesized Function Generator, and its synchronous signal (CLK1) was used to trigger pulses (CLK2, CLK3 and CLK4) generated by the HP 8016A word generator. The current flowing through the device was read out from voltage across the resistor, which was then amplified 10 times by a differential amplifier (Op AMP AD621). Furthermore, two sample and hold amplifiers (LF398A) were used to record initial and stable states of the current, and their values were compared using comparator (LM311). At the final stage, a dual D-type flip/flop (SN74LS74A) was used to capture the memory data.

### 4.3 Results and Discussion

In order to produce a neutral conjugated polymer structure containing ion pairs, a PPy composite material containing immobilized dodecylbenzenesulfonate ( $\text{DBS}^-$ ) and lithium ( $\text{Li}^+$ ) has been created in the form of a thin film spanning two metal electrodes (Figure 4.1) in an interdigitated electrode array (IDA) configuration. By performing the electrochemical polymerization of pyrrole in the presence of NaDBS as electrolyte,  $\text{DBS}^-$  is incorporated into the polymer ( $\sim 10^{21}/\text{cm}^3$ ) at a level capable of stabilizing the oxidized (conducting) form of the polymer. Subsequent reduction of the polymer, in the presence of NaDBS or lithium perchlorate as

electrolyte, results in the generation of  $\text{Na}^+\text{DBS}^-$  or  $\text{Li}^+\text{DBS}^-$  in the neutral (nonconducting) form of the polymer, respectively.

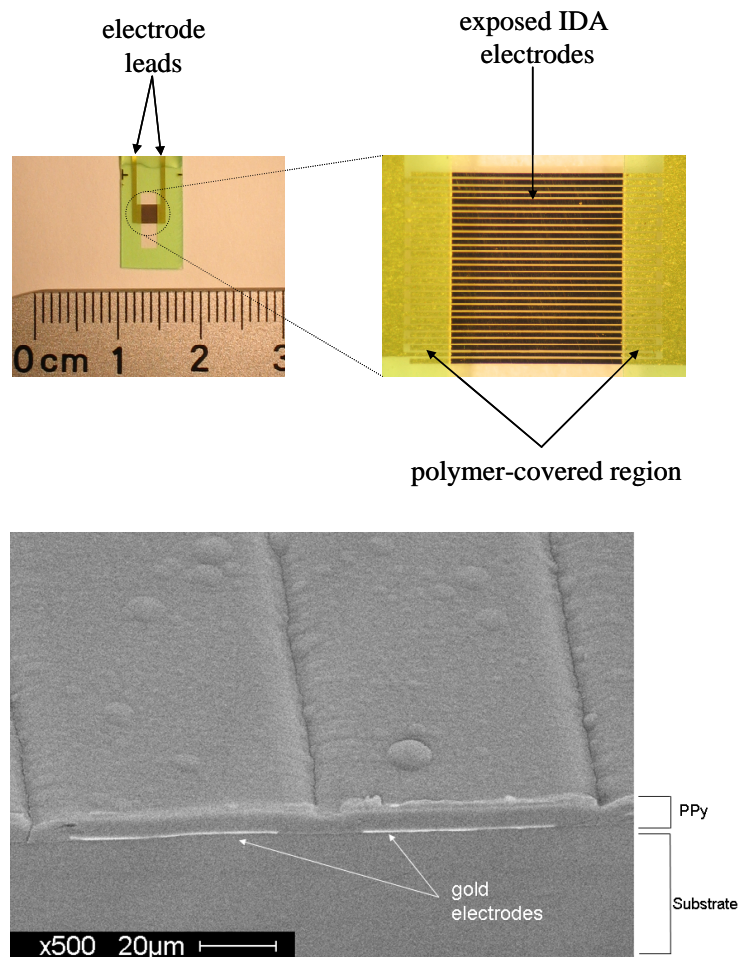
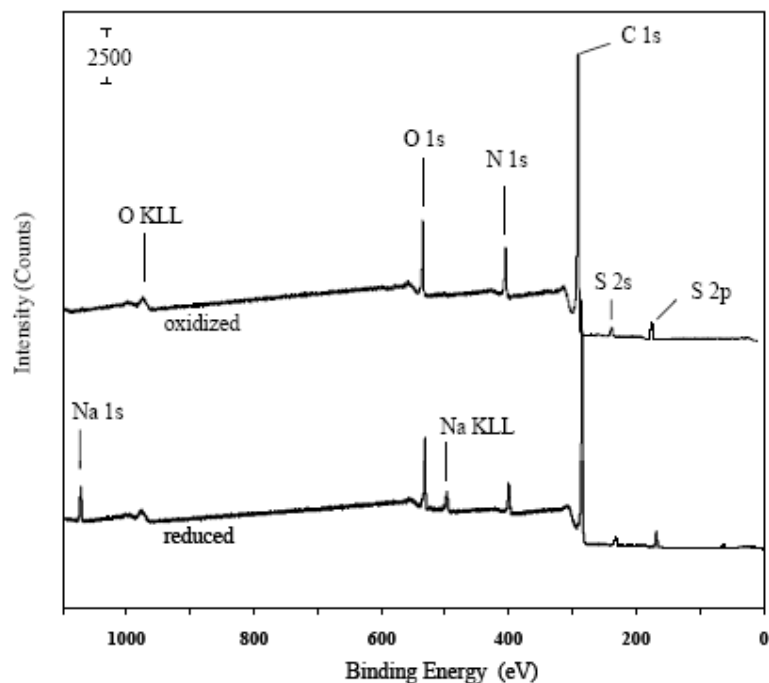


**Figure 4.1.** Optical micrographs of the IDA electrodes (top) and SEM micrograph of the cross-section of an IDA (bottom) showing two gold electrodes covered by a ca.  $6\mu\text{m}$  thick polypyrrole film.

XPS analysis of the PPy composites confirms the presence of  $\text{PPy}^0\text{Na}^+\text{DBS}^-$  or  $\text{PPy}^0\text{Li}^+\text{DBS}^-$  structures in the reduced polymer (Figure 4.2). During the electrochemical polymerization of pyrrole in the presence of NaDBS as electrolyte,

the deposited polymer is oxidized. The ratio of nitrogen (in the pyrrole unit) to sulphur (in DBS<sup>-</sup>) is approximately 5-to-1 as expected for the case where polypyrrole



	Integrated Peak Intensity <sup>a</sup>			Atomic ratios	
	N 1s	S 2p	Na 1s	N:S	Na:S
Oxidized	3022.8	542.9	-	5.5	-
Reduced	2540.0	627.8	635.1	4.0	1.0

<sup>a</sup> corrected with the relative sensitivity factors of the corresponding elements.

**Figure 4.2.** XPS spectra and the corresponding integrated peak intensity data calculated for electrochemically prepared PPy composite films on gold.

is oxidized and DBS<sup>-</sup> is present as a counter ion. Upon reduction of the polypyrrole in the presence of electrolyte, the cation enters the polymer to balance the charge of the DBS<sup>-</sup>, which is immobile in the polymer. In this particular case, Na<sup>+</sup> was used

instead of  $\text{Li}^+$  due to the higher sensitivity of XPS for Na relative to Li. The XPS results demonstrate that DBS remains within the film at approximately the same level (N: S, 4:1) and that  $\text{Na}^+$  is incorporated at a level equal to that of DBS<sup>-</sup> (Na:S, 1:1).

In the PPy composite ( $\text{PPy}^0\text{Li}^+\text{DBS}^-$ ), when a potential is applied across the material,  $\text{Li}^+$  can drift in the field, leaving behind  $\text{DBS}^-$ , which can in turn stabilize the injection of holes and the formation of a region of higher conductivity ( $\text{PPy}^+\text{DBS}^-$ ),

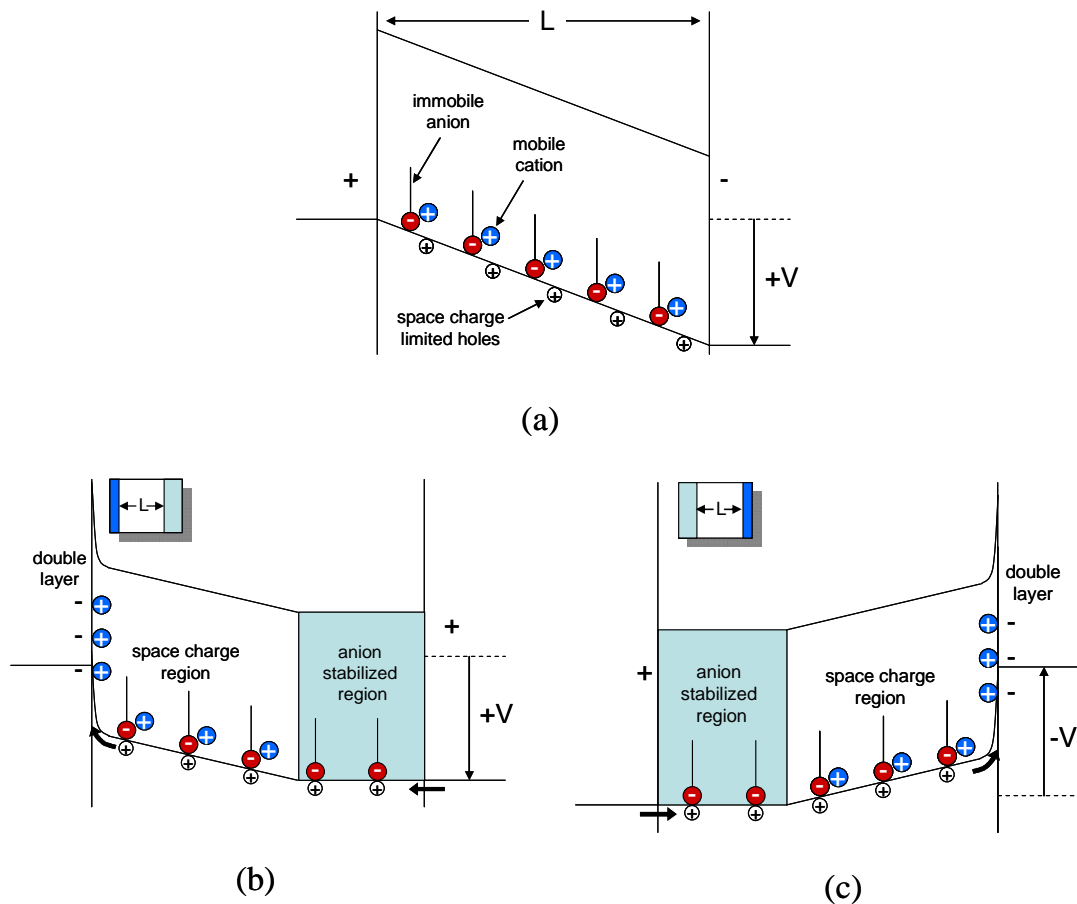


**Figure 4.3.** Schematic electron energy level diagram for a reduced PPy polymer that contains immobile anions compensated by mobile cations. Here (a) represents the instantaneous condition after the application of the voltage, (b) represents the condition after the cations have moved and (c) is upon voltage reversal after the ions have moved.

resulting in a smaller effective  $L$  as illustrated in Figure 4.3. As grown, the polymer contains sufficient immobilized anions to compensate holes that would be present in its fully oxidized state; however, in the reduced state shown, mobile cations are present to maintain charge neutrality. Upon application of a potential, initially, the field decays linearly across the gap between electrodes separated by distance  $L$  and a SCLC flows between the electrodes (Figure 4.3a). In response to the field, cations drift to result in the formation of a double layer, which allows hole injection and the formation of an anion-stabilized region with lower resistance, thereby reducing the effective  $L$  through which SCLC flows (Figure 4.3b). Reversal of the polarity results in the field driven movement of cations dispersing the double layer and reformation at the opposite electrode (Figure 4.3c). When the potential step is asymmetric, the evolution of  $L$  with time will be a function of the previous potential applied and thus contains a 'memory effect'.

**4.3.1. Electrical Characterization of PPy Devices:** The bulk-limited current behaviour of the PPy devices can be observed in current versus voltage curves (Figure 4.4). In the control device, where the polymer has been reduced without the presence of an immobilized anion (PPy<sup>0</sup>), behaviour is almost completely linear with little evidence for space charge limited current. In the composite device (PPy<sup>0</sup>Li<sup>+</sup>DBS<sup>-</sup>), at low voltages the current also increases linearly as expected, although characteristic of a higher resistance presumably associated with the presence of LiDBS (~57 % LiDBS by weight). However, when the voltage exceeds 0.2 V the current begins to increase super linearly and can be fit to a  $V^2$  relationship with field dependant mobility, which is in agreement with other work on conjugated polymers.<sup>16, 17</sup> As the voltage

increases past approximately 1 V the device enters a regime where it is no longer a static material, but begins to change the internal configuration of ionic species through drift<sup>19</sup> resulting in a region containing anion-stabilized charge carriers. This process is completely reversible in a nitrogen environment and under vacuum. Shaded areas indicate ohmic behavior characterized with a slope of 1, SCLC behavior with a slope of approximately 2, and field generated carrier current (FGCC) behavior with a slope approaching 4.

The time-dependant behaviour of the current through these devices offers further evidence of this internal reconfiguration leading to a structure as shown in Figure 4.3a. After the application of a potential, current begins to flow as shown in Figure 4.5. At potentials below that at which drift becomes significant, the temporal behaviour of the current (Figure 4.5) remains constant. At higher applied potentials

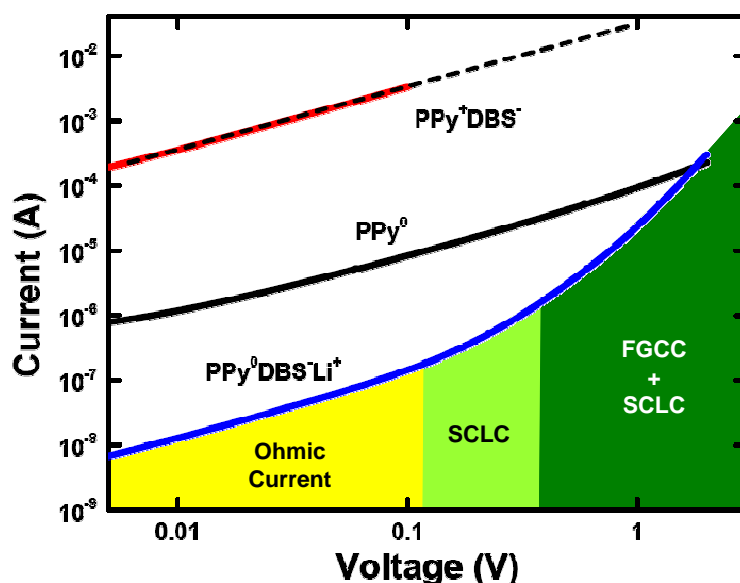


**Figure 4.4.**  $I$ - $V$  behavior (scan rate of  $0.01 \text{ Vs}^{-1}$ ) of a PPY composite device in the oxidized state as grown prior to reduction ( $\text{PPy}^+\text{DBS}^-$ ) and in the reduced state with  $\text{Li}^+$  incorporated into the film ( $\text{PPy}^0\text{DBS}^-\text{Li}^+$ ). A reduced PPY film deposited in the same way but with no surfactant present is shown ( $\text{PPy}^0$ ) for reference.

the temporal behavior changes and the current increases with time before approaching a new equilibrium. This behaviour is attributed to the drift of the cations resulting in a concomitant increase in anion-stabilized conducting region shown in Figure 4.3a and a decrease in the effective distance between electrodes and hence an increase in the current. Using a simple one-dimensional model, the current changes observed in these junctions correspond to an effective change in length of about 5 – 20 %.

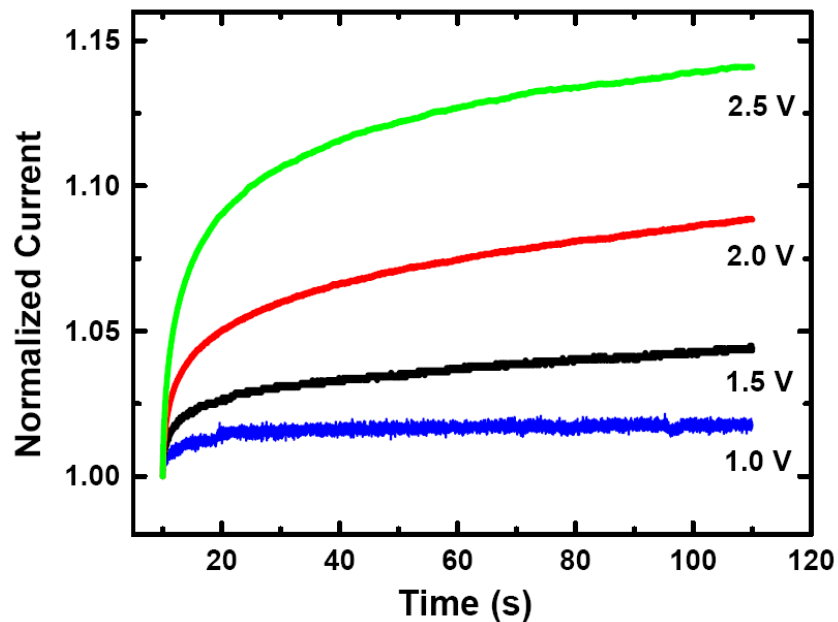


**Figure 4.5.** Current as a function of time following the application of voltages that span the SCLC and FGCC regions and normalized to the initial current.

#### 4.3.2. Application as Memory Device

The redistribution of cations with voltage and its time dependence offers new opportunities to produce electronic devices such as dynamic memory cells. For

example, the redistribution of cations that results in a junction with a reduced effective length remains for a period of time after the field is removed, since the cations do not instantaneously return to their equilibrium position. Indeed one would expect that upon reversing the applied potential, the internal configuration of charge and carriers remains largely unchanged. A reverse potential can be used to determine the magnitude of the previously applied potential. If the magnitude of the reversed potential is greater than the previous forward potential, the magnitude of the current will increase with time as the cations drift and reduce the effective length of the junction. If the magnitude of the reversed potential is smaller than the previous forward potential, the current will decrease with time as the cations drift to increase the effective junction width. This memory effect is analogous to an “echo” related to the potential applied prior to the potential reversal. This echo effect increases with increasing initial potentials as is observed in Figure 4.6.

Since the distribution of cations that results in the echo is detectable for periods over 60 s (Figure 4.6), this phenomenon can form the basis of a dynamic memory cell. In such a cell, the two states of the memory would be: 1) a junction to which a write voltage has been applied and 2) a junction to which no write voltage has been applied. The cell can be read with a voltage of magnitude lower than the voltage used to set the state. When a read voltage is applied to a junction where no write voltage was applied the current will start off low and rise to a higher steady-state current as the cations move (see Figure 4.7, inset). If a voltage is applied to a junction where a write voltage was applied, the current will start off higher and settle to a lower steady-state current as the cations reach a new equilibrium set by the read voltage (Figure 4.7, inset).

Using this principle, a simple memory circuit was constructed (Figure 4.8) for capturing memory data given by two distinctive states of current vs. time. Clock 1 controls whether a read voltage or a write voltage is applied to the device. In the

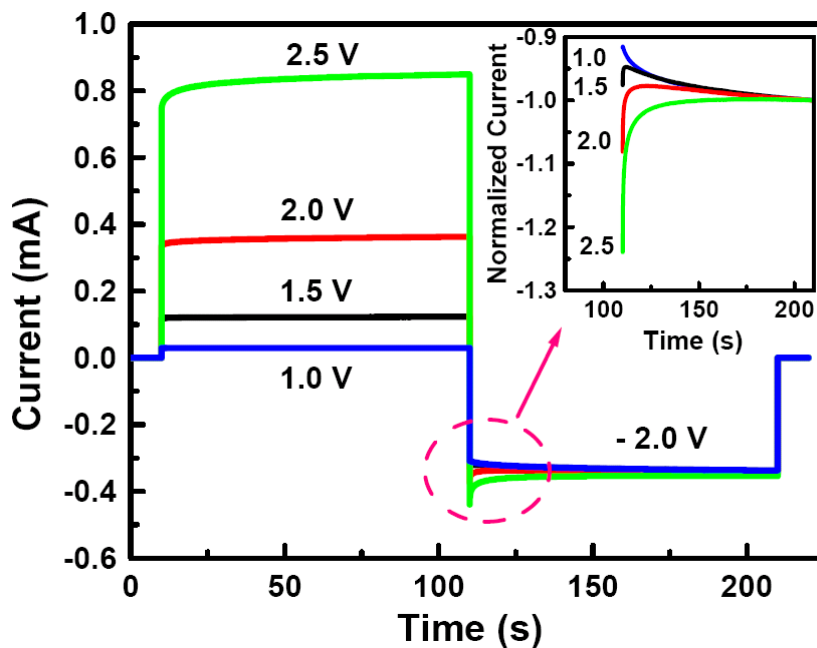


**Figure 4.6.** Current-time plot of  $\text{PPy}^0\text{Li}^+\text{DBS}^-$  device at different forward potentials

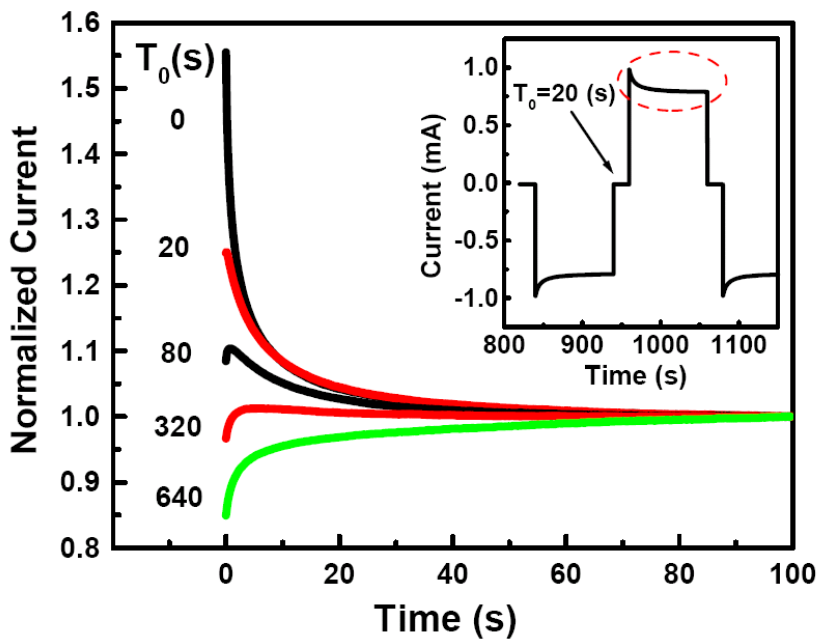


**Figure 4.7.** Current-time plot for  $\text{PPy}^0\text{DBS}^-\text{Li}^+$  device at different delay time ( $T_0$ ) values.

write state  $V_W = 0$  is applied for the low state and  $V_W = 2$  V is applied for the high state. In the read state  $V = -1.5$  V is applied and the current sensed through the resistor. This signal is amplified and the sample and hold amplifier 1 captures the signal shortly after the application of the read voltage. Sample and hold amplifier 2 captures the signal several seconds later. Clock 4 loads the memory state into a flip/flop several seconds after sample and hold 2 is triggered. This storage mechanism is interesting in that the information is extracted from a self referenced signal. The information is written into the cell using a write voltage as described above; the state of the cell is read out by comparing the current immediately after the application of the read voltage with the steady-state current (see Figure 4.8). If the current starts out higher than the steady-state value, a logic level high will be read out and if the current starts out lower, a logic level low will be read out (see Figure 4.9). The read function also acts to erase the state of the cell. No sequence of 1's and 0's were found that produced an error. This circuit is similar to conventional dynamic random access memory (DRAM) circuits where a reference capacitive line is charged and then differentially compared using an amplifier to a second capacitive line.<sup>20</sup>

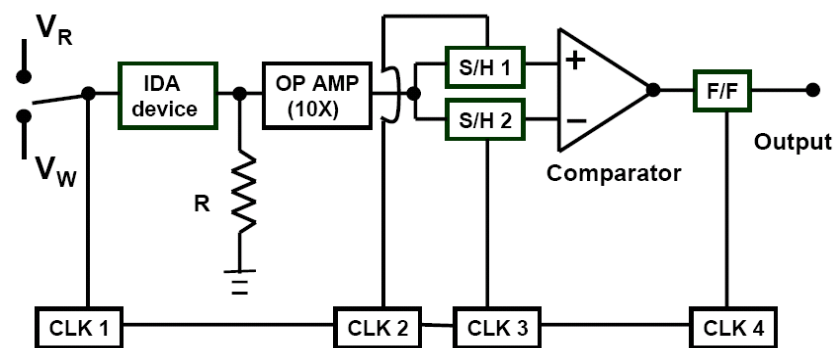


**Figure 4.8.** The schematic of a memory circuit, designed to capture two distinct current transit behaviors that correspond to the cation distribution in the device.

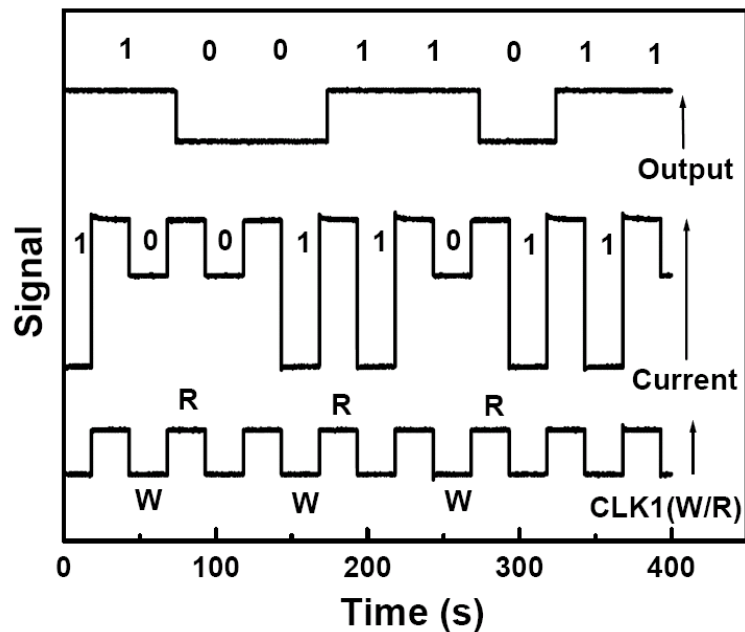


**Figure 4.9.** The wave forms for the read–write clock (CLK), the current passing through the PPy composite, and the output of the memory circuit during the storing and reading back the bit sequence 10011011.

The material system described in this work has significant advantages for application in nanometer-scale electronics, since the junctions are electrochemically grown and they can be fabricated after all conductor layers have been deposited and patterned. For example, in a cross-bar memory architecture, these junctions can be grown after the formation of the crossbars rather than between the metal layers.<sup>21</sup> The bulk dominated conductance of this system should result in better scaling with device size. If the dimensions of the device were all scaled by a factor of  $1/s$  then the space charge limited current would scale as  $s^3$  with the device length and  $1/s^2$  with device area resulting in an overall scaling of  $s^3/s^2=s$ . In interface-dominated devices, such as diodes, the current would scale as  $s^{-2}$  resulting in currents for nanometer-scale devices being very small.<sup>22</sup>

### 4.3.3 Fabrication of Smaller Polypyrrole Composite Device

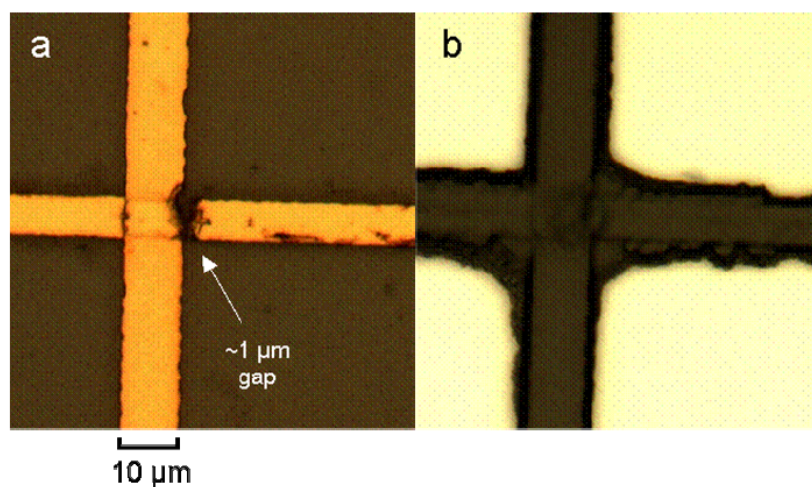


**Figure 4.10.** Optical micrograph of gold electrodes with an approximately 1  $\mu\text{m}$  gap before (a) and after (b) the deposition of a PPy composite.

Preliminary experiments demonstrate the scalability of polypyrrole hybrid device to smaller dimensions. The PPy composite material ( $\text{PPy}^0\text{Li}^+\text{DBS}^-$ ) was electrochemically deposited between two gold electrodes separated by approximately 1  $\mu\text{m}$  gap (Figure 4.10). The I-V behaviour (scan rate of 0.01 V/s) of the polypyrrole composite device in the reduced state with  $\text{Li}^+$  incorporated into the film exhibits nonlinear behaviour (Figure 4.11a) similar to that exhibited in Figure 4.4. The time-dependant behaviour of the current through these devices is shown in Figure 4.11b. Current as a function of time following the application of voltages spanning the SCLC and FGCC regions and normalized to the initial current as in Figure 4.5. At lower voltages steady-state current is achieved rapidly; however at larger

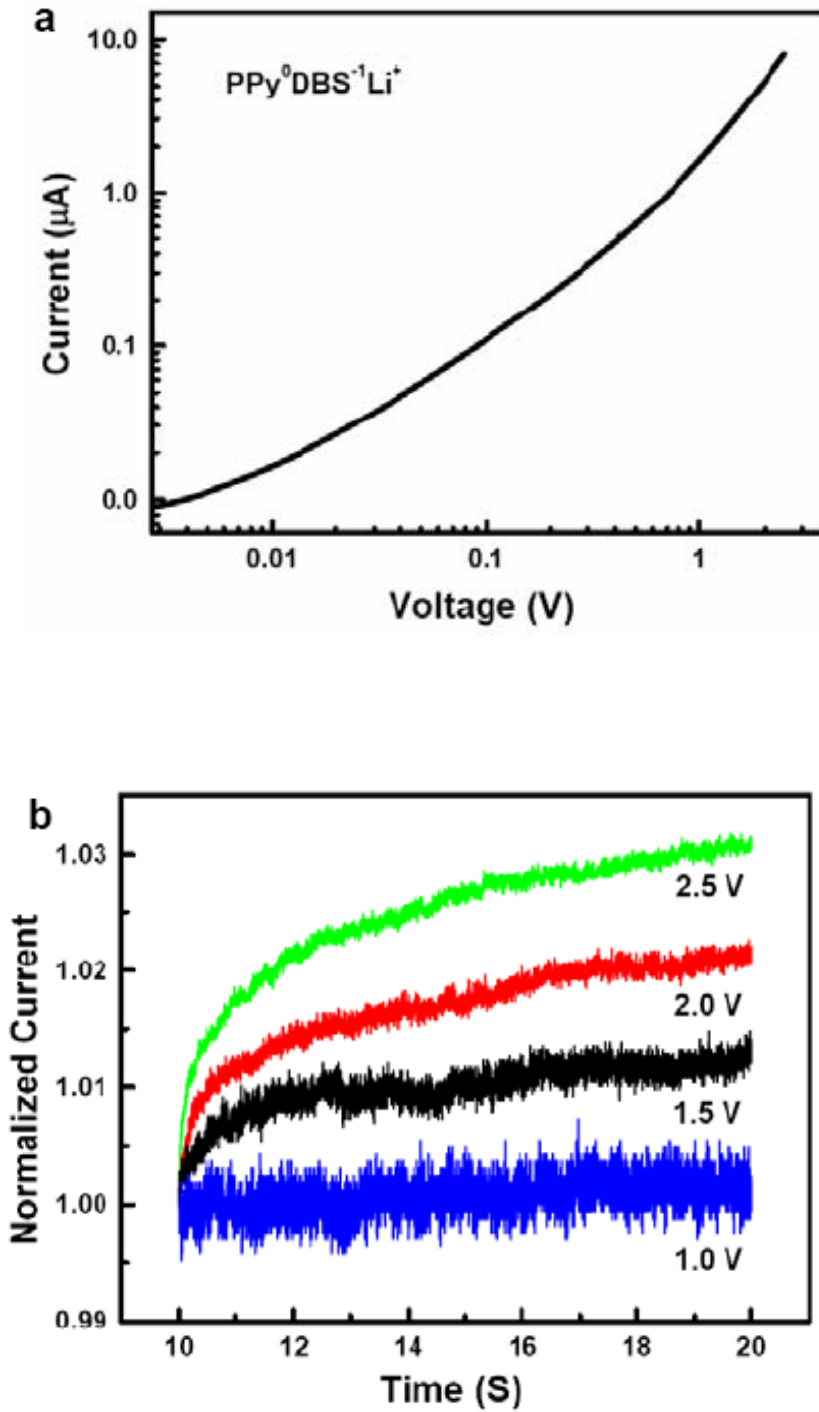


**Figure 4.11.** a) Current - voltage and b) Current – time behaviors of polypyrrole composite device, with smaller electrode spacing. In (b), the temporal current values are normalized to their initial values.

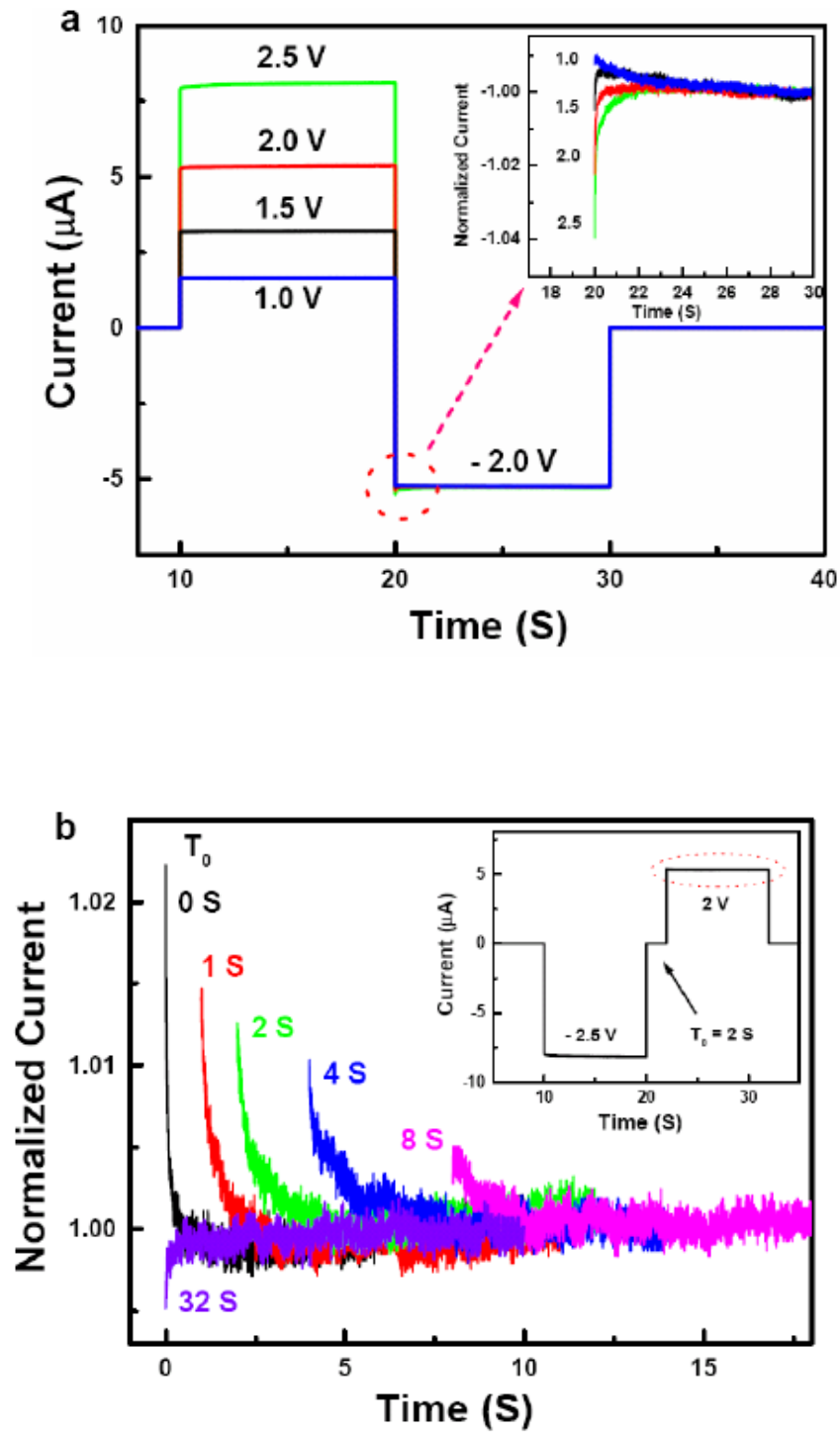


**Figure 4.12.** Current versus time behaviour of polypyrrole composite device with smaller electrode spacing.

voltages, ion drift resulting in FGCC is observed requiring significantly more time to approach steady state, although significantly less time in comparison to the device in Figure 4.1 with larger electrode spacing (20  $\mu\text{m}$ ).

Current versus time behaviour of polypyrrole composite device with smaller electrode spacing is shown in Figure 4.12. The device's behaviour is similar to that observed for the device containing larger electrode spacing (Figure 4.6) with the exception of the time scale of the behaviour related to ion drift. As expected, for the smaller spacing, these time scales are approximately an order of magnitude shorter. When a delay time ( $T_0$ ) is introduced between the forward and reverse potential the effects of the cation redistribution can be observed for time periods less than 8seconds (Figure 4.12b). The time scale of this "memory" remains significantly longer than required for standard DRAM applications where refresh rates are typically on the order of 100 ms. These results suggest that even in this unoptimized form, there is room for at least another order of magnitude reduction in size. It is reasonable to expect even further reduction in size by pursuing strategies for decreasing drift rates.

#### **4.4. Conclusions**

A new approach for the design of conjugated conducting polymer composites that exhibit dynamic asymmetric electronic behavior based on the movement of charge in response to the application of a field has been demonstrated. This work is expected to open up new avenues for device design and fabrication. Devices utilizing this material offer several potential advantages including ease of fabrication, simple structures and more favorable scalability factors.

## Acknowledgements

Financial support is gratefully acknowledged from the Natural Sciences and Engineering Research Council (NSERC) of Canada, the Canada Foundation for Innovation (CFI), the Manitoba Research and Innovation Fund, and the University of Manitoba. Also acknowledge the Manitoba Regional Materials and Surface Characterization Facility for access to XPS and Dr. Sergei Rudenja for performing XPS analysis. Support for contributions from RGP and MSF was provided in part from the Canada Research Chairs Program.

## References

1. Gustafsson, G.; Cao, Y.; Treacy, G. M.; Klavetter, F.; Colaneri, N.; Heeger, A. J., Flexible Light-Emitting-Diodes Made from Soluble Conducting Polymers. *Nature* **1992**, 357, (6378), 477-479.
2. Jager, E. W. H.; Inganas, O.; Lundstrom, I., Microrobots for Micrometer-Size Objects in Aqueous Media: Potential Tools for Single-Cell Manipulation. *Science* **2000**, 288, (5475), 2335-2338.
3. Eckhardt, H.; Shacklette, L. W.; Jen, K. Y.; Elsenbaumer, R. L., The Electronic and Electrochemical Properties of Poly(Phenylene Vinylenes) and Poly(Thienylene Vinylenes) - an Experimental and Theoretical-Study. *Journal of Chemical Physics* **1989**, 91, (2), 1303-1315.
4. Cheng, C. H. W.; Lonergan, M. C., A Conjugated Polymer p-n Junction. *Journal of the American Chemical Society* **2004**, 126, (34), 10536-10537.
5. Chiang, C. K.; Fincher, C. R.; Park, Y. W.; Heeger, A. J.; Shirakawa, H.; Louis, E. J.; Gau, S. C.; Macdiarmid, A. G., Electrical-Conductivity in Doped Polyacetylene. *Physical Review Letters* **1977**, 39, (17), 1098-1101.
6. Angelopoulos, M., Conducting Polymers in Microelectronics. *IBM Journal of Research and Development* **2001**, 45, (1), 57-75.
7. Faid, K.; Leclerc, M.; Nguyen, M.; Diaz, A., Localization Effects in Asymmetrically Substituted Polythiophenes - Controlled Generation of Polarons, Dimerized Polarons, and Bipolarons. *Macromolecules* **1995**, 28, (1), 284-287.

8. Macinnes, D.; Druy, M. A.; Nigrey, P. J.; Nairns, D. P.; Macdiarmid, A. G.; Heeger, A. J., Organic Batteries - Reversible N-Type and P-Type Electrochemical Doping of Polyacetylene, (CH)<sub>x</sub>. *Journal of the Chemical Society-Chemical Communications* **1981**, (7), 317-319.
9. Bredas, J. L.; Street, G. B., Polarons, Bipolarons, and Solitons in Conducting Polymers. *Accounts of Chemical Research* **1985**, 18, (10), 309-315.
10. Burroughes, J. H.; Jones, C. A.; Friend, R. H., New Semiconductor-Device Physics in Polymer Diodes and Transistors. *Nature* **1988**, 335, (6186), 137-141.
11. Cheng, C. H. W.; Boettcher, S. W.; Johnston, D. H.; Lonergan, M. C., Unidirectional Current in a Polyacetylene Hetero-ionic Junction. *Journal of the American Chemical Society* **2004**, 126, (28), 8666-8667.
12. Burroughes, J. H.; Bradley, D. D. C.; Brown, A. R.; Marks, R. N.; Mackay, K.; Friend, R. H.; Burns, P. L.; Holmes, A. B., Light-Emitting-Diodes Based on Conjugated Polymers. *Nature* **1990**, 347, (6293), 539-541.
13. Gurunathan, K.; Murugan, A. V.; Marimuthu, R.; Mulik, U. P.; Amalnerkar, D. P., Electrochemically Synthesised Conducting Polymeric Materials for Applications Towards Technology in Electronics, Optoelectronics and Energy Storage Devices. *Materials Chemistry and Physics* **1999**, 61, (3), 173-191.
14. Patil, A. O.; Ikenoue, Y.; Wudl, F.; Heeger, A. J., Water-Soluble Conducting Polymers. *Journal of the American Chemical Society* **1987**, 109, (6), 1858-1859.
15. Bidan, G.; Ehui, B.; Lapkowski, M., Conductive Polymers with Immobilized Dopants - Ionomer Composites and Auto-Doped Polymers - a Review and Recent Advances. *Journal of Physics D-Applied Physics* **1988**, 21, (7), 1043-1054.
16. Blom, P. W. M.; deJong, M. J. M.; vanMunster, M. G., Electric-field and temperature dependence of the hole mobility in poly(p-phenylene vinylene). *Physical Review B* **1997**, 55, (2), R656-R659.
17. Pai, D. M., Transient Photoconductivity in Poly(N-Vinylcarbazole). *Journal of Chemical Physics* **1970**, 52, (5), 2285-&.
18. Smela, E., Microfabrication of PPy Microactuators and Other Conjugated Polymer Devices. *Journal of Micromechanics and Microengineering* **1999**, 9, (1), 1-18.
19. deMello, J. C.; Tessler, N.; Graham, S. C.; Friend, R. H., Ionic space-charge effects in polymer light-emitting diodes. *Physical Review B* **1998**, 57, (20), 12951-12963.

20. Lu, N. C. C.; Chao, H. H., Half-Vdd Bit-Line Sensing Scheme in CMOS DRAMs. *Ieee Journal of Solid-State Circuits* **1984**, 19, (4), 451-454.
21. Green, J. E.; Choi, J. W.; Boukai, A.; Bunimovich, Y.; Johnston-Halperin, E.; Delonno, E.; Luo, Y.; Sheriff, B. A.; Xu, K.; Shin, Y. S.; Tseng, H. R.; Stoddart, J. F.; Heath, J. R., A 160-Kilobit Molecular Electronic Memory Patterned at  $10^{11}$  Bits Per Square Centimetre. *Nature* **2007**, 445, (7126), 414-417.
22. Cerofolini, G. F.; Mascolo, D., A Hybrid Micro-Nano-Molecular Route for Nonvolatile Memories. *Semiconductor Science and Technology* **2006**, 21, (9), 1315-1325.

## Chapter 5:

### Dynamic Resistive Crossbar Memories Based on Conjugated Polymer Composites

### **Authors' Contributions**

All electrochemical experiments mentioned in this chapter were designed and conducted by R. G. Pillai. J. H. Zhao, supervised by Dr. D.J. Thomson, fabricated the gold crossbars and performed the testing of the memory device. The electrical characterization experiments were conceptualized by Dr. D.J. Thomson and Dr. M.S Freund; designed and performed by J. H. Zhao and R. G. Pillai. Dr. D. J. Thomson wrote the first draft of the paper. The figures were prepared by J.H. Zhao and R. G. Pillai. All the authors contributed equally for revisions and final editing of the manuscript before its acceptance for publication in the AIP journal '*Applied Physics Letters*'.

# Dynamic Resistive Crossbar Memories Based on Conjugated Polymer Composites

Jun Hui Zhao,<sup>1</sup> Douglas J. Thomson,<sup>1</sup> Rajesh G. Pillai<sup>2</sup> and Michael S. Freund<sup>1,2</sup>

<sup>1</sup>Department of Electrical & Computer Engineering and <sup>2</sup>Department of Chemistry  
University of Manitoba, Winnipeg, Manitoba R3T 2N2, Canada

Reproduced with permission from *Applied Physics Letters* **2009**, 94, 092113

Copyright © 2009 American Institute of Physics

**Abstract**

A semiconducting polypyrrole composite was designed to exhibit electric field dependent charge carrier distributions. Junctions were grown electrochemically on gold crossbars. Application of fields results in the drift of mobile cations, creating regions with higher conductivity and increased current. The field induced carrier redistribution results in a field and time-dependent current with good junction-to-junction repeatability. The electrical transport dominated by space charge limited current will have better scaling behavior than surface dominated and Ohmic devices as the dimensions are reduced to the nanometer scale.

## 5.1 Introduction

Conventional Si-based semiconductor information storage technology continues to result in higher speed and higher density memory devices. However, scaling to smaller dimensions is difficult, resulting in the exploration of new device concepts.<sup>1</sup> A wide variety of novel memory schemes have emerged as alternatives to the current complementary metal-oxide-semiconductor (CMOS) technology.<sup>2, 3</sup> One promising approach pursued over the past decade is organic-based conductance switching memories,<sup>4-6</sup> in particular molecular electronics<sup>7</sup> that promise better scaling properties.

Conjugated semiconducting polymers are of interest since their electronic properties can be altered by electrochemically modifying their structures.<sup>8</sup> For example, their electrical conductivity can be altered by “doping” via oxidation or reduction and insertion of anions or cations into the polymer to create *p*-type or *n*-type semiconductor, respectively.<sup>9</sup> While these materials exhibit properties analogous to inorganic semiconductors, there are significant differences including reversible doping, mobile dopants, and high doping levels. These differences provide opportunities for creating electronic devices that operate under new paradigms. One characteristic that has been successfully exploited is the alternation of charge carrier density electrochemically and controlling the ions incorporated in the polymer. For example, the conductance state can be modified with an electric field driving the mobile ions<sup>10</sup> into and out of the polymer. This electrochemical approach of producing conductance switches has been explored as a means for creating electronic devices<sup>11-13</sup> by

introducing ionic conductors (solid electrolytes) as a “dopant” source for solid-state electrochemical switches.<sup>12-14</sup>

Taking advantage of this mechanism, we developed a new approach to design a material consisting of a single, solid-state, conjugated polymer composite, which contains both large immobile anions, acting as counter ions for the oxidized state of the polymer, and highly mobile cations that can balance the charges of the immobile anions under conditions where the polymer is reduced. The high mobility of the cations in this system results in a field- and time dependent electrical conductance. The polymer composite can be electrochemically integrated into a pre-fabricated crossbar array, forming a functional dynamic memory, which promises better scalability and reproducibility for construction of dense memory arrays.<sup>15</sup>

## 5.2 Experimental

The polymer composite used in this work consisted of polypyrrole (PPy) generated electrochemically in the presence of a bulky dopant anion (dodecylbenzenesulfonates, DBS<sup>-</sup>) and reduced in the presence of small mobile cation (lithium, Li<sup>+</sup>), which inserts to balance the charge of the immobile anions. The crossbar arrays were fabricated by making two layers of perpendicularly crossed gold electrodes with a sputtered dielectric SiO<sub>2</sub> spacer. Figure 5.1 shows the schematic diagram of the Au/SiO<sub>2</sub>/Au crossbar polymer junction and the 10x10 crossbar junctions. An atomic force microscopy (AFM) image of the crossbar junction with an electrode separation of about 400 nm and a width of 20 μm is shown in the inset of Figure 5.2. The Au/PPy/Au

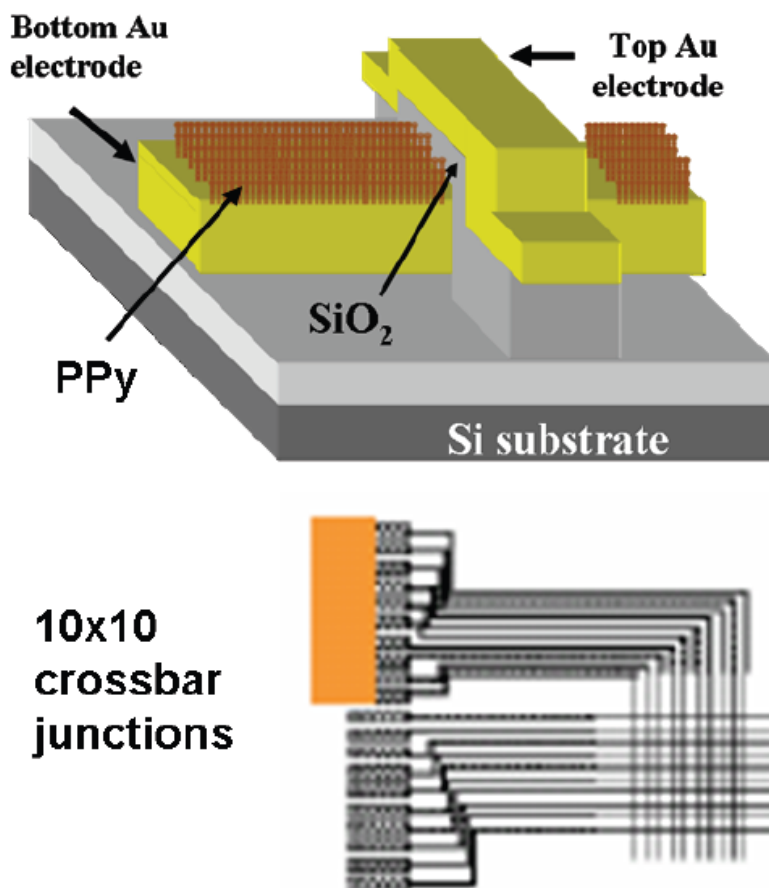


**Figure 5.1.** The schematic diagram of the Au/SiO<sub>2</sub>/Au crossbar polymer junction (top) and the 10x10 crossbar junctions (bottom).

junctions were formed by electrochemically growing the PPy polymer from the bottom Au electrodes to the top Au electrodes.<sup>15</sup> The initially synthesized thin film (PPy<sup>+</sup>DBS<sup>-</sup>) is in the *p*-doped oxidized state and was subsequently reduced in LiClO<sub>4</sub> electrolyte resulting in the incorporation of lithium cations into the polymer, creating the final composite polymer PPy<sup>0</sup>(DBS<sup>-</sup>Li<sup>+</sup>) in a semiconducting/insulating state.

## 5.3 Results and Discussion

### 5.3.1 Electrical Characterization of PPy Crossbar Devices

Most polymer-based electronic devices are designed based on the electrode-limited conductance where the potential barrier at the interface dominates (similar to the Si-based semiconductor). However, for most PPy polymer systems with Au electrodes, the conduction is bulk limited due to the low potential barrier at the interface.<sup>16</sup> In such devices, a linear (Ohmic) relationship of the current-voltage is observed at low potentials. With increasing applied potential across the junction, a nonlinear behavior associated with space charge limited current (SCLC) conditions can become dominant. These behaviors are demonstrated in our  $\text{PPy}^0(\text{DBS}^-\text{Li}^+)$  composite junctions as indicated in Figure 5.2.

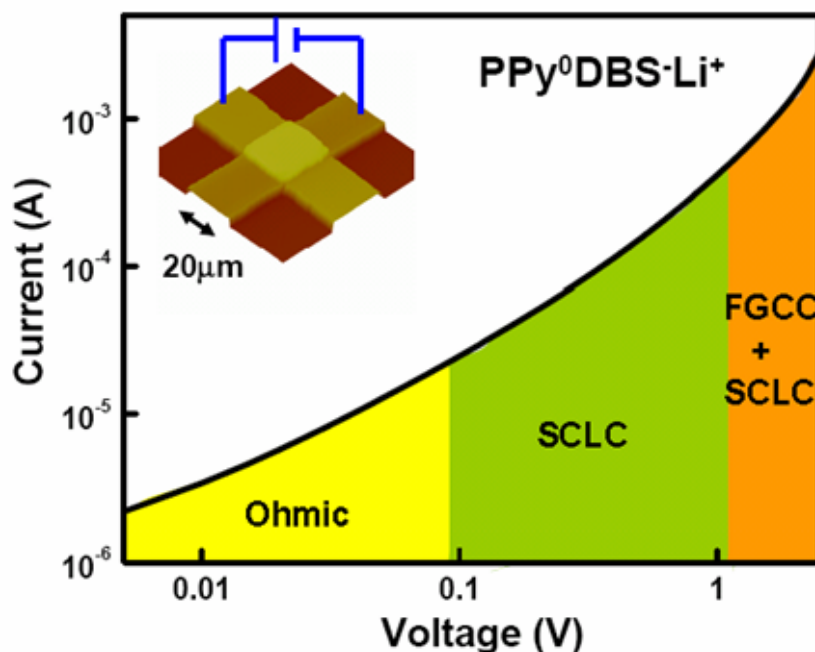


**Figure 5.2.** The polymer junction (AFM image in inset) shows three types of  $I$ - $V$  characteristics under an applied voltage.

The particularly interesting transport behavior in the  $\text{PPy}^0(\text{DBS}^-\text{Li}^+)$  composite is the conductance at higher potential. When the potential is sufficiently high to induce drifting of the mobile cations (lithium ions) in the composite, the configuration of internal ion species will change. This allows the formation of a  $p$ -doped conducting region ( $\text{PPy}^+\text{DBS}^-$ ) by depleting the cations, leading to an overall shorter effective path length. Since the SCLC current is proportional to the  $V^2$  and  $1/L^3$  (i.e.,  $J = (8/9)\epsilon\mu V^2(L)^{-3}$ , where  $V$  is the applied voltage and  $L$  is the distance between the electrodes)<sup>16</sup> in the absence of trapping effect, current will increase with a decrease in  $L$ . This additional current is referred to as field generated carrier current (FGCC) and current is assumed to be due to the drift of mobile  $\text{Li}^+$  ions under the electric field resulting in a higher conducting region, stabilized by the immobile anions ( $\text{DBS}^-$ ). This process is schematically described in Figure 5.3. It shows the configuration of charge carriers in the polymer junction (lower part) and the corresponding internal electric field distribution (upper part) where the electric field ( $E$ ) in space charged region shows spatial dependence as  $E$  proportional to  $x^{1/2}$ . The anion stabilized region behaves much more conductively due to the electrochemically oxidizing process induced by cation drift, which reduced the overall distance that free charges (holes) pass through, thus contributing additional current named FGCC.

Evidence of FGCC is observed in the time dependence of current flow through the junctions (Figure 5.4), where the current increases with time, approaching a new

equilibrium at higher applied potentials. The time dependent conductance related to the relaxation of the ions back to an equilibrium distribution was characterized by

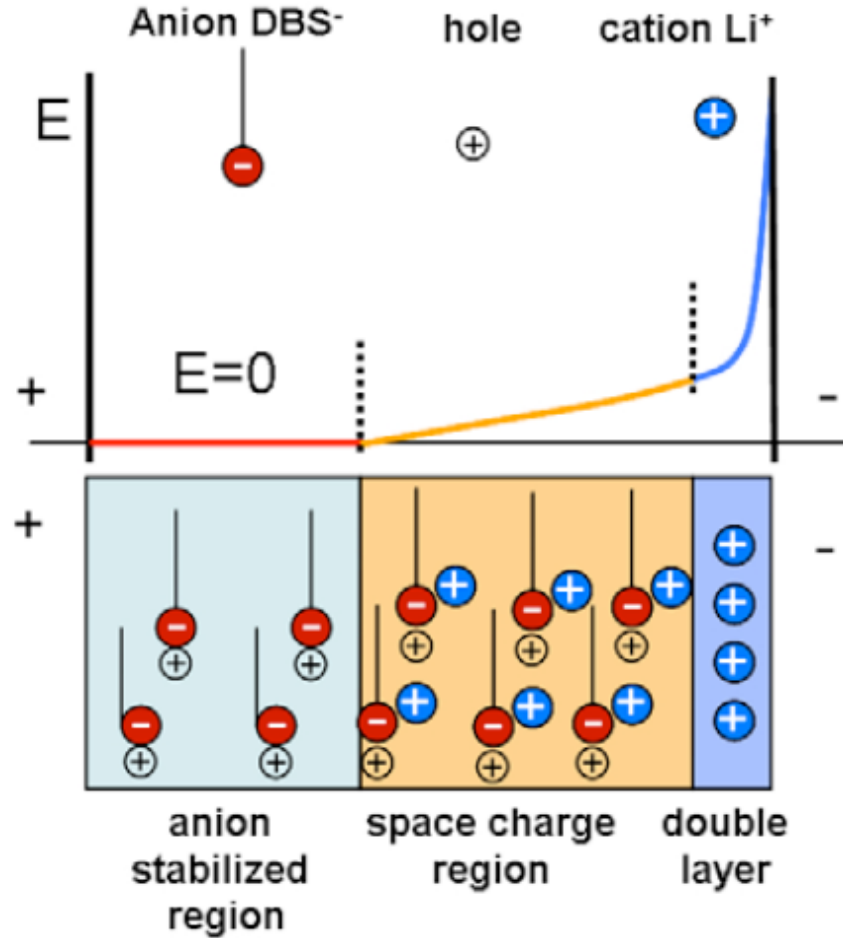


**Figure 5.3.** Schematic configuration of charge carriers in the polymer junction (bottom) and the corresponding internal electric field distribution (top).

measurements shown in Figure 5.5. The time dependent currents were normalized to the value under the steady state for different delay times ( $T_0$ ) introduced between forward and reversed fields, signaling the effect of the field driven ion redistribution. The effect of the ion redistribution was observed for time periods of about 1 second. For short field-free time before reversing the applied field, the cations do not

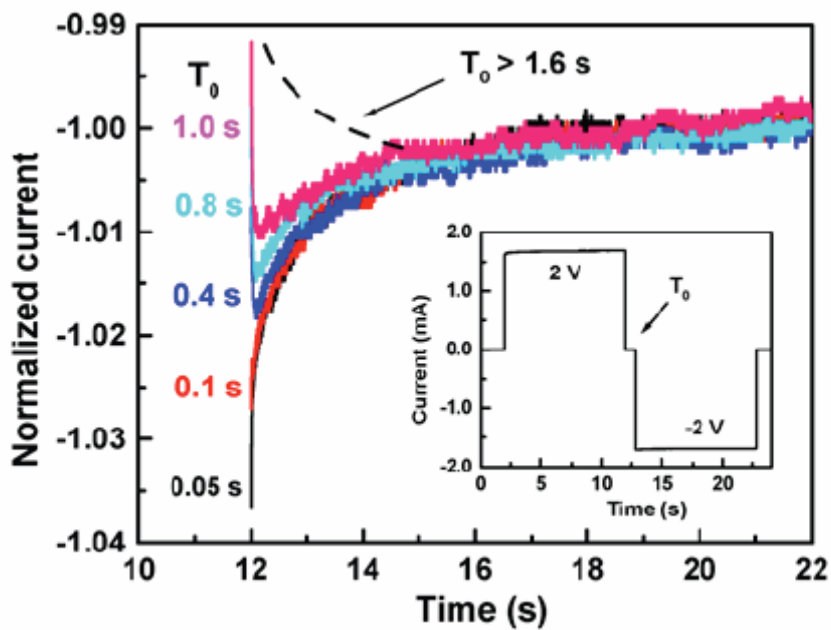


**Figure 5.4.** Normalized time dependent currents under the steady state for different delay times ( $T_0$ ) introduced between forward and reversed fields (see text).

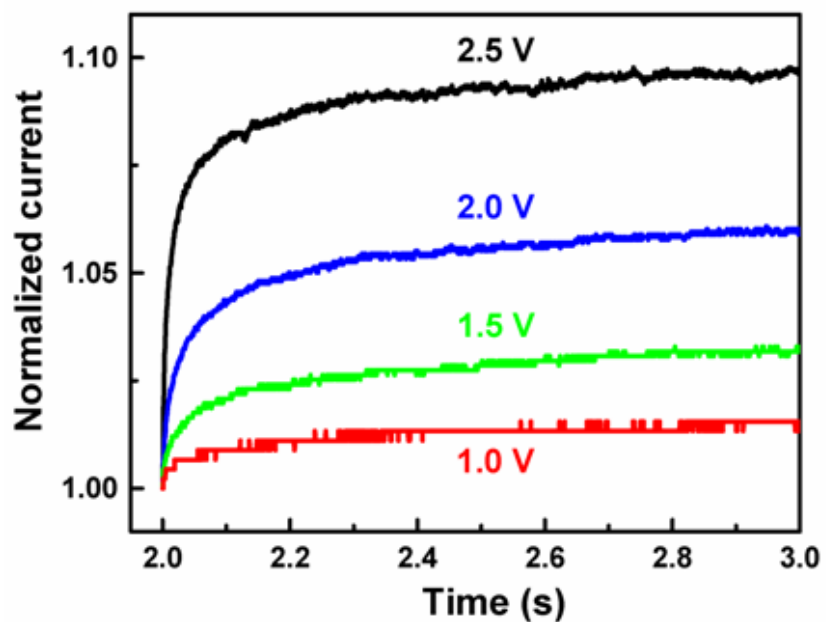


**Figure 5.5.** The temporal behavior of currents normalized to their initial values under applied step voltages.

return to their original equilibrium position and the time dependence is close to that of the zero time delay trace. With longer delays the distribution moves closer to the equilibrium position and the current versus time behavior changes closer to that observed in samples before any field has been applied. After the forward field was removed for more than about 1.6 second, the ion distribution, established under the forward field, returned to its initial equilibrium state and the current under the reversed field behaves as same as that when the forward field was applied at the first time. The time response of the junction was measured versus a resting time at 0 V. As this resting time  $T_0$  is increased, the current versus time plots approach those of junctions with undisturbed ion distributions ( $>1.6$  s). These experiments demonstrate that the conductance of the polymer junctions can be controlled by the electric field induced internal reconfiguration of charges and that they remain in this state for some time after the removal of the field. These effects are consistent with those in Figure 5.6. By application of a potential step, -2 V in this example, the conducting state of the junction can be determined. State "0" of the junction is produced by applying 1 V to the junction and state "1" is produced by applying a forward bias sufficient to induce the drift of ions in the junction, 2.5 V in this example. When the "read" voltage of -2 V is applied the junction in state "0" produces a current that will increase with time because the effective distance  $L$  of the junction becomes shorter due to the increased ion drift by the read voltage. When the read voltage is applied to the junction in state "1" the current will decrease with time as the cations relax under the weaker applied field and the

effective junction width  $L$  increases to a new equilibrium. This behavior provides a way to construct a dynamic memory cell by employing the two transient conductance states.

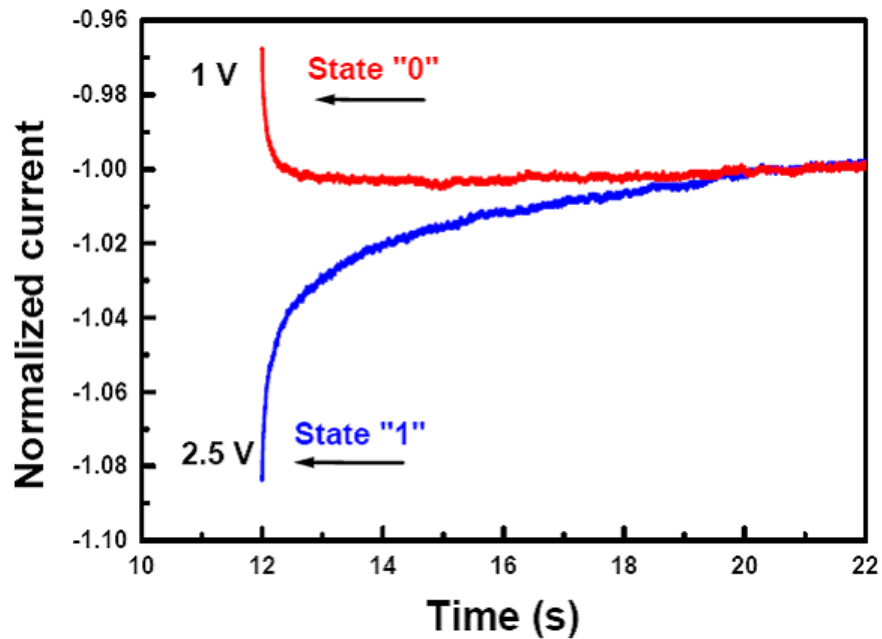


**Figure 5.6.** Two opposite transient states representing when reading potential (2 V) was applied, 1 was written high at 2.5 V and 0 was written low at 1.0 V.

### 5.3.2 Application as Memory Device

Figure 5.7 shows the schematic electronic memory circuit used to capture two opposite transient current states that represent two digitized states “0” and “1” written ( $W$ ) by first applying potential on the junction and then read ( $R$ ) by reversing potential. The current through the junction is detected and amplified by a transimpedance amplifier. Sample/hold amplifier 1 (S/H1) captures the current signal shortly after the application of the read voltage (0.02 s) and (S/H 2) captures the signal 0.2 seconds later. Then two signals are sent to a comparator that outputs signal either high or low corresponding to

the transient current behaviors. Finally a Flip/Flop stores the digitized signal of level high “1” or low “0”.

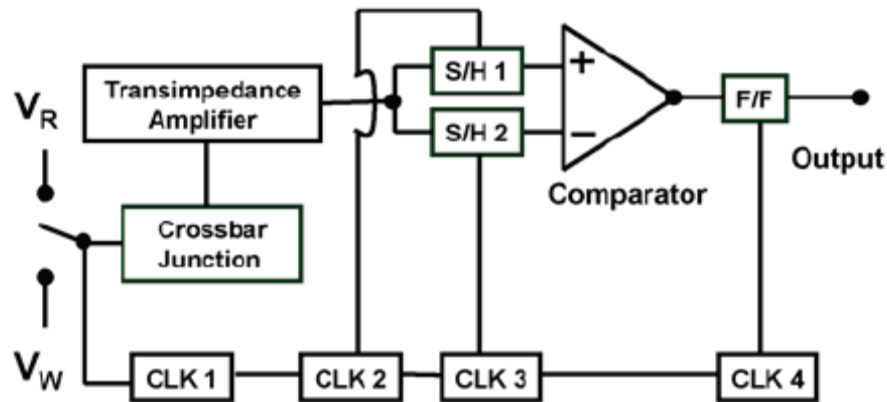


**Figure 5.7.** Schematic electronic memory circuit used to capture two transient conductance behaviors and their digitized states.

This memory mechanism is interesting in that the stored state is extracted from a self referenced signal and the read function also acts to erase the previous state of the device, which is analogous to conventional dynamic random access memory circuits where a reference capacitive line is charged and then differentially compared using an amplifier to a second capacitive line that is either pulled up or pulled down by the charge from a memory cell.<sup>17</sup> Figure 5.8 shows the waveforms captured with the read-write clock (CLK1), the current signal passing through the polymer junction, and the output of the memory cell corresponding to the writing and reading back the bit sequence 11100011100.

### 5.3.3 Scalability and Reproducibility of 10x10 Crossbar Junctions

An important advantage of this system that the demonstrated resistive memory

in the crossbar architecture promises significant advantages in nanometer-scale electronics since the conductance characterized with the space charge limited current should result in a better scaling, i.e., the current passing through the junction will scale as  $s$  rather than  $s^{-2}$  ( $s$  is a scaling factor)<sup>18</sup> as the SCLC equation suggests. Another

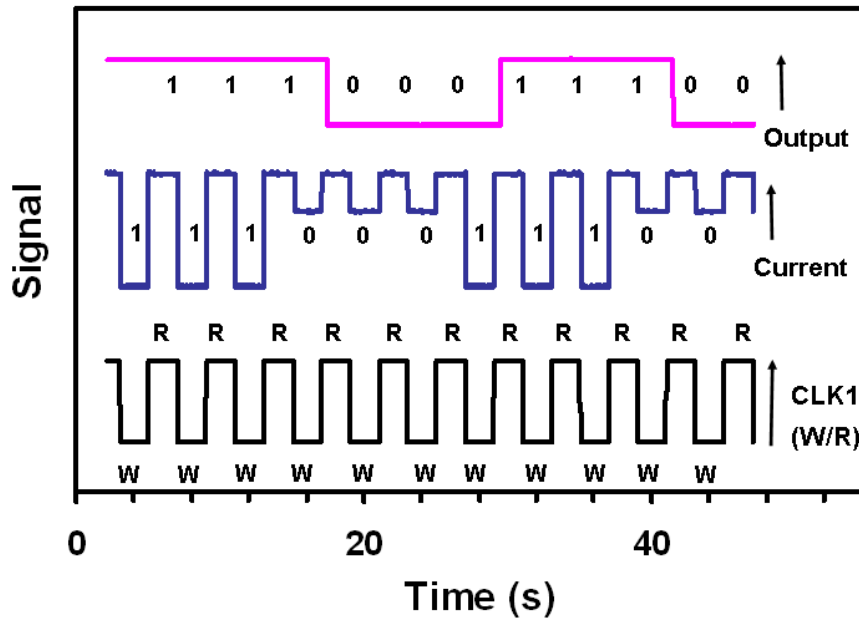


**Figure 5.8.** The waveforms of W/R clock (CLK1), current signal and memory data of 11100011100 bits were captured using an electrical memory circuit for W/R process. Clock and output are 0 to 5 V signals and current signal has a maximum magnitude of  $\sim 1$  mA.

advantage is that they can be made reproducibly by a controllable electrochemical deposition of the polymer, as shown in Figure 5.9, where  $10 \times 10$  polymer crossbar junctions were created by controlling the charge passed during the electrochemical deposition. The current clearly indicates that the polymer first started growing on the bottom Au electrodes then made connection with the upper Au electrodes, doubling the

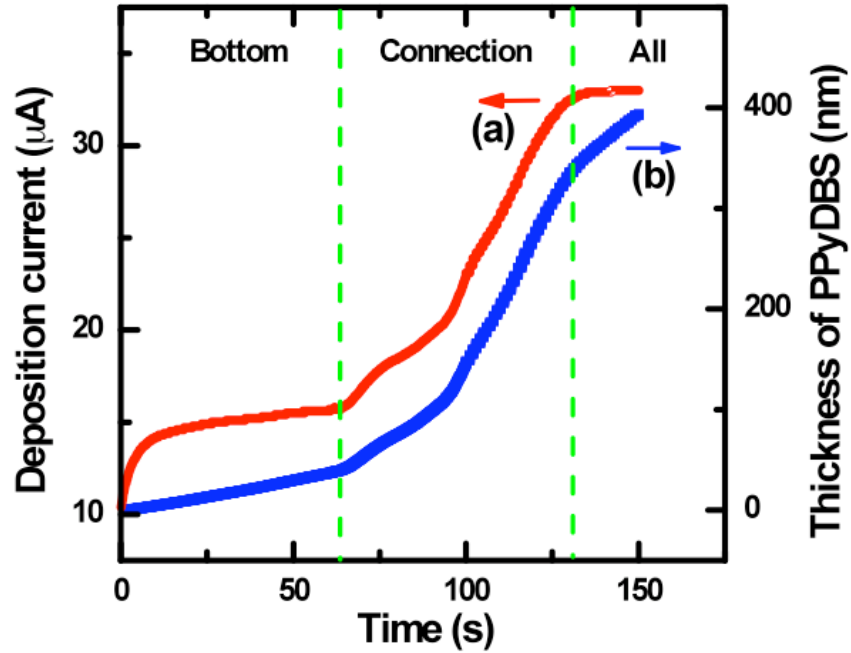


**Figure 5.9.** The current of electrochemical deposition indicates three stages of polymer's growth that can be utilized for controlling the thickness of the polymer.

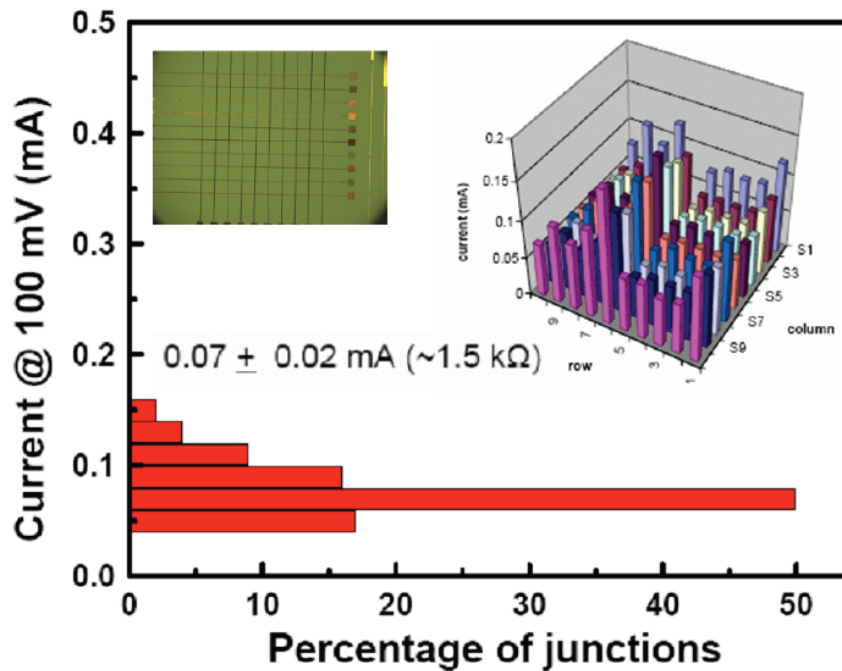


**Figure 5.10.** The histogram of the currents measured at 100 mV for the 100 crossbar polymer junctions shows the relative narrow distribution. On the left of top part is the optical image of the polymer crossbars and on the right of top part is the diagram of the current distribution with the 100 junctions.

current. Thickness of the polymer can be controlled (here around 400 nm) by calculating charge passed during deposition.<sup>19</sup>

Measurement of currents at 100 mV for all 100 junctions (Figure 5.10) indicates that they are fairly uniform and exhibit consistent electronic properties. Figure 5.11 shows the histograms of the normalized current differences representing the signals “1” and “0” for the 100 crossbar junctions, demonstrating good reproducibility and reliability of two well-defined memory states.

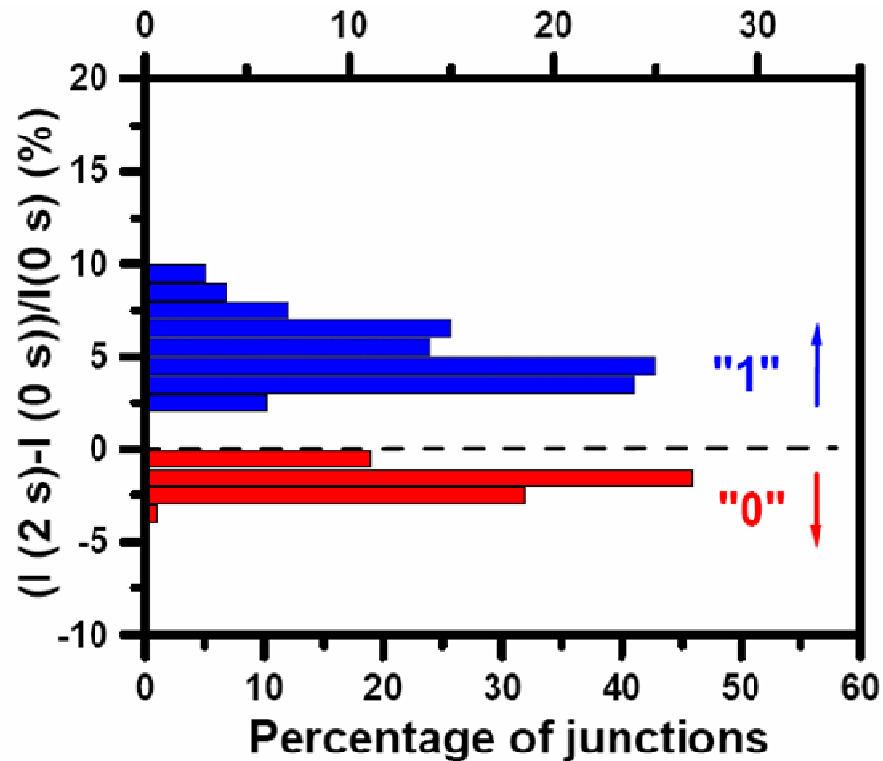


**Figure 5.11.** The histograms of the normalized differential currents measured at zero and 2 s for reading the signals 1 and 0, respectively, on the 10x10 polymer crossbar junctions show two highly polarized conducting states with fairly narrow distributions of the transient signals.

## 5.4 Conclusions

A polymer based resistive memory has been explored through designing a conjugated semiconducting polymer composite with the ability of tuning the conductance by the field driven ions reconfiguration. Also, the fabrication is compatible with standard CMOS circuits and memory cells can be electrochemically synthesized after all conductor layers have been built without considering the interface problems introduced by the postprocess of the contact electrodes where the polymer is sandwiched between the conductors.

## Acknowledgements

Financial support is gratefully acknowledged from the Natural Sciences and Engineering Research Council of Canada, the Canadian Institute for Advanced Research, the Canada Foundation for Innovation, the Manitoba Research and Innovation Fund, and the University of Manitoba. Support for contributions from RGP and MSF was provided in part from the Canada Research Chairs Program. J.H.Z. and R.G.P. contributed equally to this work.

## References

1. Lee, M. T.; Hsueh, C. C.; Freund, M. S.; Ferguson, G. S., Electrochemical Self-Assembly of Monolayers from Alkylthiosulfates on Gold. *Langmuir* **2003**, *19*, (13), 5246-5253.
2. Galatsis, K.; Wang, K.; Botros, Y.; Yang, Y.; Xie, Y. H.; Stoddart, J. F.; Kaner, R. B.; Ozkan, C.; Liu, J. L.; Ozkan, M.; Zhou, C. W.; Kim, K. W., Emerging Memory Devices -Nontraditional Possibilities Pased on Nanomaterials and Nanostructures. *IEEE Circuits & Devices* **2006**, *22*, (3), 12-21.

3. Ziegler, M. M.; Stan, M. R., CMOS/Nano Co-Design for Crossbar-Based Molecular Electronic Systems. *IEEE Transactions on Nanotechnology* **2003**, 2, (4), 217-230.
4. Scott, J. C.; Bozano, L. D., Nonvolatile Memory Elements Based on Organic Materials. *Advanced Materials* **2007**, 19, (11), 1452-1463.
5. Ling, Q. D.; Liaw, D. J.; Teo, E. Y. H.; Zhu, C. X.; Chan, D. S. H.; Kang, E. T.; Neoh, K. G., Polymer Memories: Bistable Electrical Switching and Device Performance. *Polymer* **2007**, 48, (18), 5182-5201.
6. Ouyang, J. Y.; Chu, C. W.; Szmanda, C. R.; Ma, L. P.; Yang, Y., Programmable Polymer Thin Film and Non-Volatile Memory Device. *Nature Materials* **2004**, 3, (12), 918-922.
7. Green, J. E.; Choi, J. W.; Boukai, A.; Bunimovich, Y.; Johnston-Halperin, E.; Delonno, E.; Luo, Y.; Sheriff, B. A.; Xu, K.; Shin, Y. S.; Tseng, H. R.; Stoddart, J. F.; Heath, J. R., A 160-kilobit Molecular Electronic Memory Patterned at  $10^{11}$  Bits per Square Centimeter. *Nature* **2007**, 445, (7126), 414-417.
8. Eckhardt, H.; Shacklette, L. W.; Jen, K. Y.; Elsenbaumer, R. L., The Electronic and Electrochemical Properties of Poly(Phenylene Vinylenes) and Poly(Thienylene Vinylenes) - an Experimental and Theoretical-Study. *Journal of Chemical Physics* **1989**, 91, (2), 1303-1315.
9. Cheng, C. H. W.; Loneragan, M. C., A Conjugated Polymer pn Junction. *Journal of the American Chemical Society* **2004**, 126, (34), 10536-10537.
10. Gadjourova, Z.; Andreev, Y. G.; Tunstall, D. P.; Bruce, P. G., Ionic Conductivity in Crystalline Polymer Electrolytes. *Nature* **2001**, 412, (6846), 520-523.
11. deMello, J. C.; Tessler, N.; Graham, S. C.; Friend, R. H., Ionic Space-Charge Effects in polymer light-emitting diodes. *Physical Review B* **1998**, 57, (20), 12951-12963.
12. Edman, L.; Swensen, J.; Moses, D.; Heeger, A. J., Toward Improved and Tunable Polymer Field-Effect Transistors. *Applied Physics Letters* **2004**, 84, (19), 3744-3746.
13. Bernardis, D. A.; Flores-Torres, S.; Abruna, H. D.; Malliaras, G. G., Observation of Electroluminescence and Photovoltaic Response in Ionic Junctions. *Science* **2006**, 313, (5792), 1416-1419.
14. Lai, Q. X.; Zhu, Z. H.; Chen, Y.; Patil, S.; Wudl, F., Organic Nonvolatile Memory by Dopant-Configurable Polymer. *Applied Physics Letters* **2006**, 88, (13), 133515
15. Pillai, R. G.; Zhao, J. H.; Freund, M. S.; Thomson, D. J., Field-Induced Carrier Generation in Conjugated Polymer Semiconductors for Dynamic, Asymmetric

Junctions. *Advanced Materials* **2008**, 20, (1), 49-53.

16. Blom, P. W. M.; Vissenberg, M., Charge Transport in Poly(p-phenylene vinylene) Light-Emitting Diodes. *Materials Science & Engineering R-Reports* **2000**, 27, (3-4), 53-94.
17. Lu, N. C. C.; Chao, H. H., Half-Vdd Bit-Line Sensing Scheme in CMOS Drams. *IEEE Journal of Solid-State Circuits* **1984**, 19, (4), 451-454.
18. Cerofolini, G. F.; Mascolo, D., A Hybrid Micro-Nano-Molecular Route for Nonvolatile Memories. *Semiconductor Science and Technology* **2006**, 21, (9), 1315-1325.
19. Smela, E., Microfabrication of PPy Microactuators and Other Conjugated Polymer Devices. *Journal of Micromechanics and Microengineering* **1999**, 9, (1), 1-18.

## Chapter 6:

### Preparation of Molecular Electronic Junctions on Gold Crossbar Arrays by Electrochemically Directed Self-Assembly

### **Authors' Contributions**

All experiments pertaining to this work were designed and performed by R. G. Pillai. All figures and manuscript drafts were prepared by R. G. Pillai. J. H. Zhao, supervised by Dr. D. J. Thomson, fabricated the gold crossbar array electrode used in this work. Dr. M. S. Freund and R. G. Pillai were responsible for revisions and final editing of the document.

Preparation of Molecular Electronic Junctions on Gold Crossbar Arrays by  
Electrochemically Directed Self-Assembly

Rajesh G. Pillai,<sup>1</sup> Jun Hui Zhao,<sup>2</sup> Michael S. Freund<sup>1,2</sup> and Douglas J. Thomson<sup>2</sup>

<sup>1</sup>Department of Chemistry and <sup>2</sup>Department of Electrical & Computer Engineering,  
University of Manitoba, Winnipeg, Manitoba R3T 2N2, Canada

## **Abstract**

This chapter discuss about the challenges that were identified in making a proof-of-concept molecular junction device using electrochemically directed self-assembly of alkylthiosulfates on gold crossbar arrays. Alkylthiosulfates with varying hydrocarbon chain lengths were electrochemically deposited on the top electrodes of a 10x10 gold crossbar array. A high-conducting polymer film was then spin coated or electrochemically deposited to act as a top contact for the SAMs. These molecular junctions were characterized using electrochemical methods and electron microscopy. Electrical measurements were performed across the top and bottom electrodes in the junction. Important design rules have been suggested for the creation of SAMs based molecular junctions in the future.

## 6.1 Introduction

The concept of molecular electronics is getting wide attention as a solution to the limitations imposed by silicon based electronic devices.<sup>1-3</sup> The ability to control and measure the electron transport through a molecular species is the basic requirement for building molecular electronic devices.<sup>4</sup> The major obstacles in the commercialization of molecular electronic devices are the fabrication of reliable metal/organic molecule/metal junctions and integration with conventional CMOS technologies.<sup>4-6</sup>

Molecular level control of the organic species is necessary to form stable and reproducible junctions between the metal contacts. The use of self-assembly technique has the advantage that the resulting structures form stable, covalent bonded monolayers on the metal surface.<sup>6</sup> The self assembled monolayers (SAMs) give additional advantages like tailoring the monolayer properties by changing the surface functional group and hydrocarbon chain length.<sup>6</sup> The incorporation of various aromatic systems can give some interesting properties like conductance switching due to the change of molecular conformation with an applied electric field.<sup>2</sup>

The basic electronic properties of the molecular junctions can be investigated from their current-voltage relationship.<sup>4, 7, 8</sup> The organic molecules should be kept in contact with at least two external electrodes for the measurement of their I-V properties.<sup>4, 8, 9</sup> The I-V behavior of insulating organic layers sandwiched between the two metal conductors under an applied electric field can be quite complex due to the probability of involving several possible mechanisms including thermal or Schottky

emission, tunneling, Poole-Frenkel effect, field emission and space charge limited conduction.<sup>2, 10</sup> The various factors that affect these mechanisms include the work function of the electrodes and the organic layer, applied electric field and structural defects in the organic films such as impurities and grain boundaries which can act as potential traps for the charge carriers.<sup>10</sup> The predominant conduction mechanism in alkanethiolate SAMs based molecular junctions are reported to be tunneling.<sup>2, 11</sup> The contact between the molecule and electrode must be robust, reproducible and able to provide sufficient electronic coupling between the molecule and the electrodes.<sup>4</sup>

Different experimental paradigms have been reported for the preparation and electrical characterization of SAMs based molecular electronic junctions. For example, STM and conducting probe AFM are used for the conductance measurements of single molecules and small ensembles ( $<10^3$  molecules).<sup>7, 12, 13</sup> A wide range of experimental testbeds have been reported for junctions with large ensemble of molecules ( $10^3$ - $10^{12}$ ) including nanopore junctions,<sup>14</sup> crossed wire junctions,<sup>15</sup> hanging mercury drop junctions,<sup>16</sup> and metal evaporated molecular junctions.<sup>17, 18</sup> All these experimental testbeds have their own merits and drawbacks, and none has been emerged as the dominant approach for the fabrication of molecular electronic junctions. Metal deposition on organic molecules, particularly SAMs, is highly undesirable due to possible damage of the organic layer that results in short-circuiting of the molecular junctions.<sup>11</sup> Therefore, considerable interest has been given to other alternative methods for making top contacts on SAMs based molecular junctions.<sup>19</sup>

Recently, SAM based large-area molecular junction has been reported where a conjugated conducting polymer film, PEDOT: PSS, is used as the top contact over alkanethiol or dithiol monolayers.<sup>5, 20</sup> These junctions demonstrate excellent long term stability at room temperature without any significant loss in their electrical properties.<sup>21</sup> However, the fabrication of these junctions involves complex lithographic processes including e-beam lithography and gold deposition over conducting polymer film.<sup>5</sup>

The work presented herein explores a simple and reliable method for making SAM based large-area molecular junctions on pre-fabricated gold electrodes. This process does not involve exposing the monolayers to complex lithographic steps or metal evaporation on the monolayers. Crossbar-configured electrodes have the potential for scalable, high density nanoelectronic devices.<sup>1</sup> Conducting polymer thin films are used as the soft top contact on SAMs for the fabrication of molecular junctions. Electrochemically directed self-assembly of alkylthiosulfates enables the selective SAM formation on desired areas of a gold electrode array, not possible with conventional self-assembly techniques. The present work discusses about the challenges identified in making a 'proof of concept' device by integrating distinct SAMs based molecular electronic junctions on the same substrate using electrochemically directed self-assembly. Here, selected electrodes of a gold array electrode (IDA or crossbar array) were selectively modified with alkylthiosulfate monolayers of varying hydrocarbon chain lengths. In order to make the top contacts of molecular junctions, a conjugated conducting polymer film was deposited, by spin coating or electrochemical methods, in such a way that it covers both bare and SAM modified gold electrodes. The electronic

characteristics of the resulting molecular junction, Au/SAM/Conducting Polymer/Au, were studied using a probe station and compared with the corresponding alkanethiol molecular junctions previously reported.<sup>5</sup>

## 6.2 Experimental

**6.2.1 Preparation of Alkylthiosulfates:** Alkylthiosulfates are synthesized and purified according to previous reports.<sup>22</sup> The details of the alkylthiosulfate synthesis and characterization are given in Chapter 2 (section 2.2.1).

**6.2.2 Fabrication of Au crossbars:** The gold crossbar electrodes were prepared on silicon nitride-coated silicon wafers. The insulating silicon nitride is 100 nm thick. Initially a very thin adhesion layer of titanium (10 nm) and gold (~200 nm) were plasma-sputtered onto the SiN surface. Then the Ti/Au thin films were lithographically patterned and etched, forming Au electrodes with a width of approximately 20 micrometers as a bottom layer of electrodes. A layer of dielectric SiO<sub>2</sub> of approximately 500 nm was plasma-sputtered onto these bottom electrodes, and subsequently a thin layer of Ti and Au were sputtered on the surface of the SiO<sub>2</sub>. The Ti/Au layer was lithographically patterned and etched, forming Au electrodes of approximately 20 micrometers wide which are perpendicular to the lithographically patterned bottom Au electrodes. The gold surface of the bottom electrodes were exposed by continuous etching of SiO<sub>2</sub> layer covering the bottom gold electrode

**6.2.3 Electrodeposition of Polypyrrole:** Polypyrrole (PPy) films were grown across the IDA electrodes (Chapter 4, Figure 4.1) using an aqueous solution of freshly distilled

pyrrole monomer (100 mM) and an electrolyte (100 mM, NaDBS or LiClO<sub>4</sub>) at a constant potential of +0.65 V vs. Ag/AgCl. The thickness of the polypyrrole films were controlled by passing specific amount of charge (200 mC/cm<sup>2</sup> for 1 μm thick film)<sup>23</sup> during the electrodeposition.

**6.2.4 Preparation of Au/PEDOT:PSS/SAMs/Au Molecular Junctions:** The Au crossbar junctions were first cleaned with solvents of different polarity (hexane, methanol, and water) and then treated with “piranha” solution (3:1 mixture of concentrated H<sub>2</sub>SO<sub>4</sub> and 30% H<sub>2</sub>O<sub>2</sub>; *CAUTION: Piranha solution reacts violently with most organic materials and should be handled with extreme care*) for two minutes. The electrodes are then washed with Millipore water and dried in a stream of dry nitrogen gas. The cleanliness of the electrode surfaces were checked with 3mM Fe(CN)<sub>6</sub><sup>2+/3+</sup> redox couple in 0.1 M KCl.

The monolayers were selectively deposited on the top electrodes of the gold crossbar using electrochemically directed self-assembly in THF. The top electrodes were selected for monolayer deposition since they were cleaner and more well-defined than the lithographically patterned bottom electrodes in the gold crossbar array. Alkylthiosulfates of three different chain lengths, C20, C18, and C16, were electrochemically deposited in that order on a pair of alternate sets of top electrodes. For example, eicosyl thiosulfate SAM was deposited on the first two electrodes on the top electrode. Then the crossbar electrodes were washed with pure THF and later with water to remove any sulfate salts formed during the electrochemically directed self assembly of alkylthiosulfates. Thereafter, octadecyl thiosulfate was deposited on 5th

and 6<sup>th</sup> electrodes. After rinsing with THF and water, electrode was dried in dry nitrogen. A conducting PEDOT: PSS (High conductivity grade, Aldrich) film was spin coated over the entire 10x10 crossbar junction area to act as the top electrode for SAMs based molecular junctions. Then these crossbar electrodes were kept for vacuum drying (at ~400 torr) for approximately five hours before the electrical characterization of the junctions.

**6.2.5 Scanning Electron Microscopy (SEM):** SEM analyses were performed using a Field Emission Scanning Auger Microprobe (JEOL, JAMP-9500F). The measurements were done at room temperature.

**6.2.6 Electrical Characterization:** The current-voltage data of the 10x10 crossbar junctions were obtained under nitrogen atmosphere using a Suss MicroTec probe station with Agilent 4155C Parameter Analyzer or CH Instrument electrochemical work station (CHI 760c).

### **6.3 Results and Discussion**

Previous attempts in the preparation of SAM based molecular junctions using polypyrrole as a soft top contact were not successful. For example, one of the electrode arrays in a gold IDA electrode was selectively modified with an alkyl thiosulfate monolayer using electrochemically directed self-assembly and the polypyrrole (PPy-DBS or PPy-ClO<sub>4</sub>) was electrochemically grown on the other electrode until it had grown over the electrode modified with the monolayer. The electrodes were then rinsed with water and dried. The I-V characterization of these Au/SAM/PPy(doped)Au junctions were

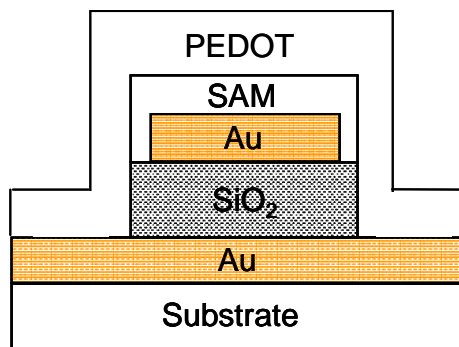
similar to the control junctions (No SAMs, Au/PPy(doped)/Au). The polymer film may physically disrupt SAM while growing or get connected to the already exposed areas/SAM defect sites on gold IDA electrode.

Spin coating of polypyrrole<sup>24</sup> (PPy-PMA) from THF over a monolayer modified gold IDA electrode has been tested as an alternative attempt to prepare SAM based molecular junctions with polymer top contacts. Here, one of the electrode arrays in the gold IDA electrodes were selectively modified with alkylthiosulfate SAMs and PPy films were spin coated over IDA electrodes to make Au/SAM/PPy(doped)Au junctions. However, the electrical characterization of these junctions did not give any promising results due to short-circuiting of the junctions. Efforts were made to use an aqueous based polymer dispersion (PEDOT: PSS) for spin coating that may avoid any possible solvation of SAMs, as in the case of non-aqueous solvents, and avoid short-circuit of the molecular junctions.<sup>5, 25</sup>

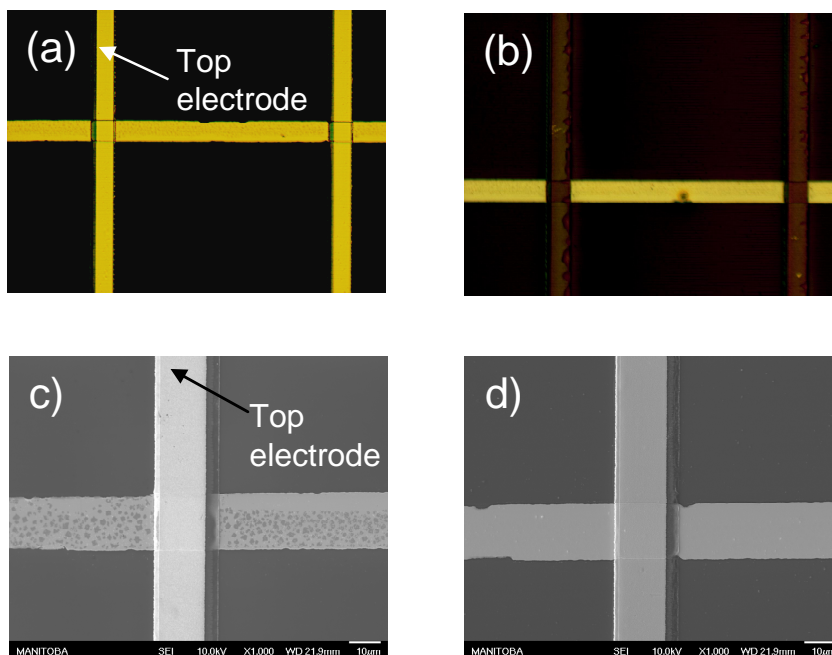
### **6.3.1 Characterization of Au/PEDOT: PSS/SAMs/Au Junctions**

Figure 6.1 shows the schematic representation of the proposed molecular junction, Au/PEDOT: PSS/SAM/Au. The crossbar electrode junctions were characterized by redox electron transfer blocking experiments, optical and electron microscopies. The spin coated PEDOT: PSS film was found to be fairly uniform across the gold crossbars and capable of making good contacts between the junctions (Figure 6.2). Blocking experiments using ferro/ferricyanide redox probe showed that monolayers made in this fashion are passivating and selectively formed on desired electrode areas. However, the faradaic process on the monolayer modified gold surface is not completely suppressed

and indicates the presence of bare electrode area, possibly due to the presence of monolayer defects at the gold substrate edges or pinholes.



**Figure 6.1.** Schematic representation of the cross-sectional view of an ideal molecular junction (Au/PEDOT: PSS/SAM/Au) on gold crossbar arrays.



**Figure 6.2.** Optical photographs (a&b) and SEM images (c&d) of gold crossbar junctions before (a, c) and after (b, d) monolayer deposition and spin coating of PEDOT.

Figure 6.3 shows the cyclic voltammograms of one of the top gold electrodes with ferro/ferricyanide redox probe, before and after hexadecylthiosulfate monolayer deposition. Comparison of the ratio of ferro/ferricyanide redox peak currents on the crossbar electrode with the reports of Majda et al.<sup>26</sup> regarding the blocking behavior of similar redox probe on C18SH/C18-OH monolayer modified gold electrodes with hydrogenated ubiquinone 'gate molecules' give an approximate surface defect density of about  $2 \times 10^{-16}$  mole/cm<sup>2</sup>. Based on the area of 'gate molecules' reported ( $81 \text{ \AA}^2$ /molecule), the total area of the surface defects can be estimated as approximately  $1 \times 10^{-6}$  cm<sup>2</sup> defects per cm<sup>2</sup> geometric area.

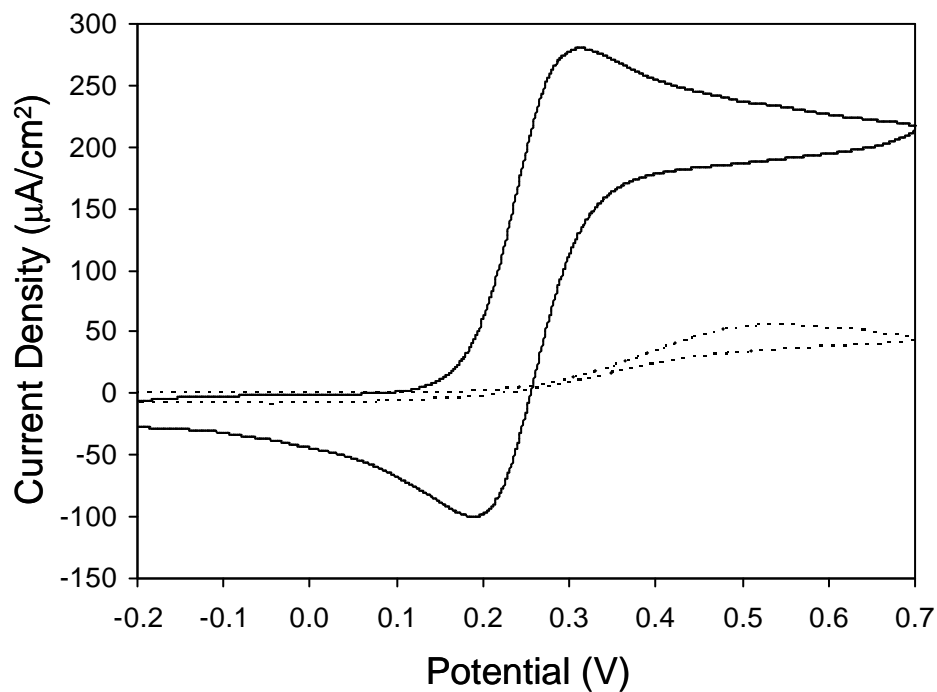


**Figure 6.3.** Cyclic voltammograms (3 mM  $\text{K}_3\text{Fe}(\text{CN})_6$ , 0.1 M KCl, scan rate  $100 \text{ mV s}^{-1}$ ; saturated Ag/AgCl reference electrode) of a top electrode in gold crossbar array, before ( — ) and after ( - - - - ) modification with 10 mM sodium hexadecylthiosulfate (in THF, 0.1 M TBATFB).

### 6.3.2 I-V Characterization of Gold Crossbar Junctions

The current-voltage characteristics of 10x10 Au/PEDOT: PSS/SAMs/Au Junctions were similar to that of control junctions without SAMs. Short-circuiting of these junctions can occur through pinholes or surface defects in the monolayers. The current estimated ( $\sim 0.1 \text{ A/cm}^2$ ) to through a short of surface defect area estimated as above is less than the current reported<sup>27</sup> for a good monolayer ( $\sim 10^1 \text{ A/cm}^2$ ).

The pinholes in SAMs result from poor adsorption or loss of organosulfur species. This may occur because due to impurities present in the solvent or adsorbent, surface contaminants and defects on the substrates.<sup>28, 29</sup> To date, no reliable procedures have been reported for the preparation of pinhole-free alkanethiolate SAMs on gold.<sup>30</sup> <sup>31</sup> Different methods have been adopted to reduce the density of pinholes in SAMs including rigorous substrate cleaning, etching to expose fresh metal surface and monolayer deposition on freshly prepared gold substrates.<sup>31</sup> Scanning electrochemical techniques show that the pinholes are less than  $0.5 \mu\text{m}$  in diameter (or  $< 0.2 \mu\text{m}^2$ ).<sup>31</sup> The large-area molecular junction previously reported with alkanethiols had junction areas ( $\sim 80\text{-}8000 \mu\text{m}^2$ ) larger than the area of the average pinhole ( $0.2 \mu\text{m}^2$ ) reported.<sup>5, 31</sup> The resistance per area of their control junctions (Au/PEDOT: PSS/ No SAM/Au) was  $10^{-2} \Omega/\mu\text{m}^2$  ( $10^{-4} \Omega/\mu\text{m}^2$ , after considering contact resistance).<sup>27</sup> When a pinhole of average area  $0.2 \mu\text{m}^2$  short-circuits the molecular junction, the expected current density at 1 V through this junction is  $10^{10} \text{ A/m}^2$  ( $10^8 \text{ A/m}^2$ , after considering contact resistance).<sup>27</sup> These values are approximately three orders larger than the current densities reported for the shorter alkanethiol (octanethiol) SAMs in large-area molecular junctions.<sup>5</sup> Since

these large-area molecular junctions show excellent reproducibility and long term stability, pinholes normally associated with a densely packed SAM may not be the reason for short-circuiting the junction. Since alkythiosulfate also forms monolayers of similar quality of the corresponding alkanethiols,<sup>5, 31</sup> they can still be considered for making the molecular electronic junctions.

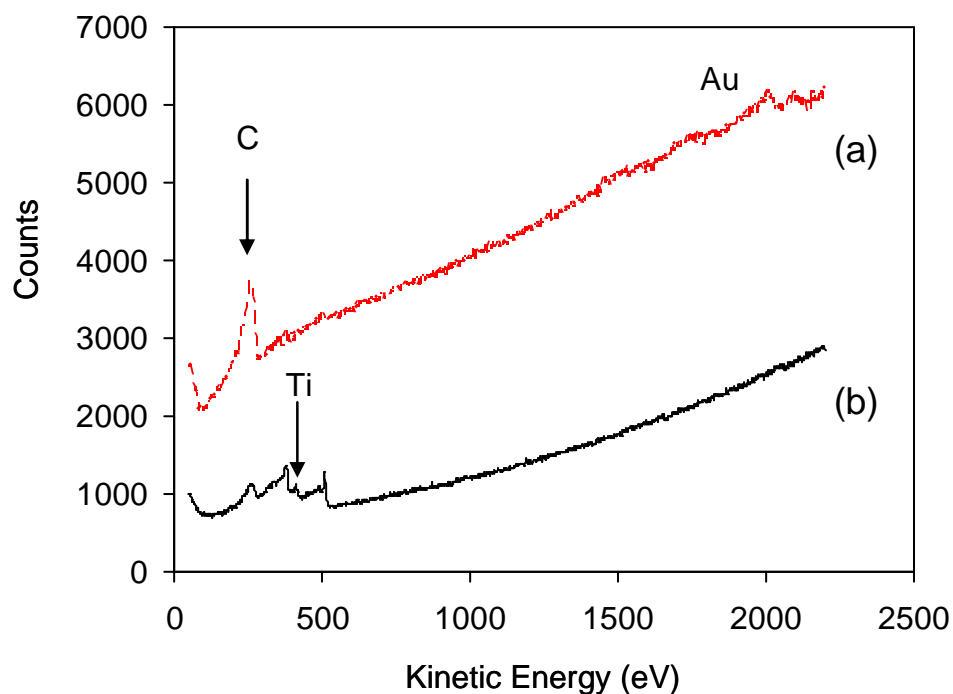


**Figure 6.4.** Auger spectra collected at different locations of a gold crossbar array electrode; a) at the centre and b) edges of the top gold electrode.

The configurations of the molecular junctions used in this work were very different than previously reported large-area alkanethiol junctions. For example, the proposed molecular junctions had larger dimensions ( $\sim 100,000 \mu\text{m}^2$ ) than the alkanethiol molecular junctions in the previous reports ( $\sim 80\text{-}8000 \mu\text{m}^2$ ).<sup>5</sup> Preparing a

uniform and defect free SAM for this larger area may be difficult due to defects in the monolayer predominantly at the edges of the crossbar. Furthermore, Auger analysis of the crossbar array electrode showed the presence of exposed titanium metal on the edges of the crossbar (Figure 6.4). The large area molecular junctions previously reported were absent from any sharp substrate edges.<sup>5, 11</sup> Here, the monolayers were formed on underlying gold substrate exposed in the holes of a lithographically patterned photoresist.<sup>5</sup>

## 6.4 Conclusions

Electrochemically directed self-assembly of alkylthiosulfates has been explored as a tool to prepare very large area molecular electronic junctions on gold crossbar structures. The preparations of these molecular junctions on gold crossbar electrodes using conducting polymer top contacts on SAMs were unsuccessful. The resulting molecular junctions show similar I-V characteristics as that of the control junctions without SAMs. The titanium metal exposed at the edges of the crossbar-array electrode and defects in the monolayers are possible reasons for the shorting of the molecular junctions. These results show that gold substrate with sharp edges should be avoided for the preparation of SAMs based molecular junctions.

## Acknowledgements

We acknowledge the Manitoba Regional Materials and Surface Characterization Facility for access to Scanning Auger Microprobe and Dr. Kevin McEleney for performing AES & SEM analysis.

## References

1. Lu, W.; Lieber, C. M., Nanoelectronics from the Bottom Up. *Nature Materials* **2007**, 6, (11), 841-850.
2. McCreery, R. L., Molecular Electronic Junctions. *Chemistry of Materials* **2004**, 16, (23), 4477-4496.
3. Carroll, R. L.; Gorman, C. B., The Genesis of Molecular Electronics. *Angewandte Chemie-International Edition* **2002**, 41, (23), 4379-4400.
4. Chen, F.; Hihath, J.; Huang, Z. F.; Li, X. L.; Tao, N. J., Measurement of single-molecule conductance. *Annual Review of Physical Chemistry* **2007**, 58, 535-564.
5. Akkerman, H. B.; Blom, P. W. M.; de Leeuw, D. M.; de Boer, B., Towards Molecular Electronics with Large-Area Molecular Junctions. *Nature* **2006**, 441, (7089), 69-72.
6. Love, J. C.; Estroff, L. A.; Kriebel, J. K.; Nuzzo, R. G.; Whitesides, G. M., Self-Assembled Monolayers of Thiolates on Metals as a Form of Nanotechnology. *Chemical Reviews* **2005**, 105, (4), 1103-1169.
7. McCreery, R. L.; Bergren, A. J., Progress with Molecular Electronic Junctions: Meeting Experimental Challenges in Design and Fabrication. *Advanced Materials* **2009**, 21, (43), 4303-4322.
8. James, D. K.; Tour, J. M., Electrical Measurements in Molecular Electronics. *Chemistry of Materials* **2004**, 16, (23), 4423-4435.
9. Mirkin, C. A.; Ratner, M. A., Molecular Electronics. *Annual Review of Physical Chemistry* **1992**, 43, 719-754.
10. Goswami, A., *Thin Film Fundamentals*. New Age International Ltd: New Delhi, **1996**.
11. Akkerman, H. B.; de Boer, B., Electrical conduction through single molecules and self-assembled monolayers. *Journal of Physics-Condensed Matter* **2008**, 20, (1).
12. Xu, B. Q.; Tao, N. J. J., Measurement of Single-Molecule Resistance by Repeated Formation of Molecular Junctions. *Science* **2003**, 301, 1221-1223.
13. Engelkes, V. B.; Beebe, J. M.; Frisbie, C. D., Length-Dependent Transport in Molecular Junctions Based on SAMs of Alkanethiols and Alkanedithiols: Effect of Metal Work Function and Applied Bias on Tunneling Efficiency and Contact Resistance. *Journal of the American Chemical Society* **2004**, 126, 14287-14296.

14. Zhou, C.; Deshpande, M. R.; Reed, M. A.; Jones, L.; Tour, J. M., Nanoscale metal self-assembled monolayer metal heterostructures. *Applied Physics Letters* **1997**, 71, (5), 611-613.
15. Kushmerick, J. G.; Holt, D. B.; Yang, J. C.; Naciri, J.; Moore, M. H.; Shashidhar, R., Metal-Molecule Contacts and Charge Transport Across Monomolecular Layers: Measurement and Theory. *Physical Review Letters* **2002**, 89, (8).
16. Slowinski, K.; Chamberlain, R. V.; Miller, C. J.; Majda, M., Through-Bond and Chain-to-Chain Coupling. Two Pathways in Electron Tunneling Through Liquid Alkanethiol Monolayers on Mercury Electrodes. *Journal of the American Chemical Society* **1997**, 119, (49), 11910-11919.
17. de Boer, B.; Frank, M. M.; Chabal, Y. J.; Jiang, W. R.; Garfunkel, E.; Bao, Z., Metallic Contact Formation for Molecular Electronics: Interactions Between Vapor-Deposited Metals and Self-Assembled Monolayers of Conjugated Mono- and Dithiols. *Langmuir* **2004**, 20, (5), 1539-1542.
18. Shimizu, K. T.; Fabbri, J. D.; Jelincic, J. J.; Melosh, N. A., Soft Deposition of Large-Area Metal Contacts for Molecular Electronics. *Advanced Materials* **2006**, 18, (12), 1499-1504.
19. Haick, H.; Cahen, D., Contacting Organic Molecules by Soft Methods: Towards Molecule-Based Electronic Devices. *Accounts of Chemical Research* **2008**, 41, (3), 359-366.
20. Akkerman, H. B.; Naber, R. C. G.; Jongbloed, B.; van Hal, P. A.; Blom, P. W. M.; de Leeuw, D. M.; de Boer, B., Electron Tunneling Through Alkanedithiol Self-assembled Monolayers in Large-Area Molecular Junctions. *Proceedings of the National Academy of Sciences of the United States of America* **2007**, 104, (27), 11161-11166.
21. Akkerman, H. B.; Kronemeijer, A. J.; Harkema, J.; van Hal, P. A.; Smits, E. C. P.; de Leeuw, D. M.; Blom, P. W. M., Stability of Large-Area Molecular Junctions. *Organic Electronics* **2010**, 11, (1), 146-149.
22. Lee, M. T.; Hsueh, C. C.; Freund, M. S.; Ferguson, G. S., Electrochemical Self-Assembly of Monolayers from Alkylthiosulfates on Gold. *Langmuir* **2003**, 19, (13), 5246-5253.
23. Smela, E., Microfabrication of PPy microactuators and other conjugated polymer devices. *Journal of Micromechanics and Microengineering* **1999**, 9, (1), 1-18.
24. Freund, M. S.; Karp, C.; Lewis, N. S., Growth of thin processable films of poly(pyrrole) using phosphomolybdate clusters. *Inorganica Chimica Acta* **1995**, 240, (1-2), 447-451.

25. Anderson, M. R.; Evaniak, M. N.; Zhang, M. H., Influence of Solvent on the Interfacial Structure of Self-Assembled Alkanethiol Monolayers. *Langmuir* **1996**, *12*, (10), 2327-2331.
26. Bilewicz, R.; Sawaguchi, T.; Chamberlain, R. V.; Majda, M., Monomolecular Langmuir-Blodgett-Films at Electrodes - Electrochemistry at Single-Molecule Gate Sites. *Langmuir* **1995**, *11*, (6), 2256-2266.
27. Van Hal, P. A.; Smits, E. C. P.; Geuns, T. C. T.; Akkerman, H. B.; De Brito, B. C.; Perissinotto, S.; Lanzani, G.; Kronemeijer, A. J.; Geskin, V.; Cornil, J.; Blom, P. W. M.; De Boer, B.; De Leeuw, D. M., Upscaling, Integration and Electrical Characterization of Molecular Junctions. *Nature Nanotechnology* **2008**, *3*, (12), 749-754.
28. Campuzano, S.; Pedrero, M.; Montemayor, C.; Fatas, E.; Pingarron, J. M., Characterization of Alkanethiol Self-Assembled Monolayers Modified Gold Electrodes by Electrochemical Impedance Spectroscopy. *Journal of Electroanalytical Chemistry* **2006**, *586*, (1), 112-121.
29. Finklea, H. O.; Snider, D. A.; Fedyk, J.; Sabatani, E.; Gafni, Y.; Rubinstein, I., Characterization of Octadecanethiol-Coated Gold Electrodes as Microarray Electrodes by Cyclic Voltammetry and Ac-Impedance Spectroscopy. *Langmuir* **1993**, *9*, (12), 3660-3667.
30. Lu, X. Q.; Yuan, H. Q.; Zuo, G. F.; Yang, J. D., Study of the size and separation of pinholes in the self-assembled thiol-porphyrin monolayers on gold electrodes. *Thin Solid Films* **2008**, *516*, (18), 6476-6482.
31. Finklea, H. O., Self-Assembled Monolayers on Electrodes. In *Encyclopedia of Analytical Chemistry : Applications, Theory, and Instrumentation*, Meyers, R. A., Ed. Wiley: New York, **2000**.

## Chapter 7: Summary and Future Outlook

## 7.1 Summary

The work described in this thesis focuses on the mechanistic details of alkylthiosulfate self-assembly and explores the use of conjugated conducting polymers for organic electronic applications. Throughout this work, prefabricated electrodes are used and any metal deposition or post-lithographic processes are avoided after the deposition of organic molecules.

The results presented herein demonstrate several substantial and original contributions to knowledge. These contributions include the following. (1) The determination that spontaneous self-assembly of alkylthiosulfates on gold surface is facilitated by trace amounts of water present in the solvent. (2) That the electrolyte, TBATFB, inhibits the spontaneous chemisorption of alkylthiosulfate by sequestering trace water present in the solvent. (3) Electrochemically assisted self-assembly of alkylthiosulfates involves gold surface oxidation, and that monolayer formation is accompanied by reduction of gold oxide and gold corrosion. (4) The corrosion of gold is limited by the surface oxide formation and that this mechanism may serve as a surface cleaning process and explain the previous report of monolayer formation on soiled gold substrate under electrochemically directed self-assembly conditions. (5) The demonstration of the dynamic nature of the monolayer under electrochemically assisted self-assembly conditions by monitoring rapid exchange of thiols in the monolayer with alkylthiosulfate molecules in solution using XPS. (6) The creation of a new conjugated polymer hybrid material capable of exhibiting field-induced generation of charge carriers. These materials exhibit unique dynamic asymmetric electronic

behavior which can be explained on the basis of movement of ions inside the bulk polymer in response to the applied electric field. (7) The design of prototypes of a dynamic polymer resistive memory devices based on our conjugated polymer hybrid materials. This approach has more favorable scaling of properties in comparison to interfacial phenomena observed with Si-based devices. (8) The design of memory arrays fabricated on a 10x10 gold crossbar structure illustrating good junction to junction reproducibility and promising scalability for nanoelectronics applications. (9) Important design rules to guide the creation of future of SAMs based molecular junctions in the future.

Self-assembly of alkylthiosulfates on gold forms monolayers identical to those formed from the corresponding alkanethiols.<sup>1, 2</sup> These self-assembly processes follow more complex mechanisms of monolayer formation than originally recognized.<sup>3</sup> Studies on the mechanism of alkylthiosulfate chemisorption on gold show that the self-assembly process is influenced by electrolyte and solvent. Plausible mechanisms have been proposed for the role of trace water in the solvent on conventional as well as electrochemically directed self-assembly of alkylthiosulfates on gold. These results are particularly important since they conclude that the solvent must be sufficiently dry to get good selectivity in monolayer formation by electrochemically directed self-assembly. The mechanistic studies on alkylthiosulfate and alkanethiol monolayer formation under electrochemical conditions show that the process does not involve an outer-sphere one-electron oxidation of the organosulfur compound. These studies further suggest that gold surface oxidation is the major source of the irreversible anodic peak in the

voltammograms, and not thiol or thiosulfate oxidation. Self-assembly involving alkylthiosulfates as well as alkanethiols in THF under oxidative conditions proceed through direct reaction with gold surface oxide and corrosion. In contrast to the results obtained in THF, EQCM measurements in methanol show no evidence of gold corrosion presumably due to solubility issues. However, the exact mechanism of the gold corrosion process and nature of the soluble gold species formed remains unclear. Amperometric experiments performed below the oxidation potential of gold exhibit transient anodic currents after alkanethiol addition, consistent with the previous reports indicating the oxidation of alkanethiol to form well ordered monolayers. At potentials above oxidation potential of gold, no oxidative current is observed with either alkanethiol or alkylthiosulfate addition suggesting that the redox reaction takes place between gold oxide and the organosulfur compound with no net electron flow through the external circuit.

Conjugated polypyrrole hybrid materials ( $\text{PPy}^0\text{DBS}^-\text{Li}^+$ ) were electrochemically prepared on prefabricated gold electrodes including IDAs and crossbar arrays. Electrical characterization of these materials shows nonlinear conductance behavior at higher electric fields. This behavior is attributed to the presence of  $\text{Li}^+$  ions, since pure ohmic behavior is observed with control experiments in the absence of lithium ( $\text{PPy}^+\text{DBS}^-$ ). The presence of  $\text{Li}^+$  ions affects the local conductance and the dynamic control of their concentration and spatial distribution can be used to manipulate the electronic conductance of the hybrid materials. The field generated carrier current (FGCC) associated with the non-linear current-voltage characteristics of these materials can be

related to the field-driven migration of  $\text{Li}^+$  ions. The presence of FGCC and ion redistribution generates distinct conductance states inside the polymer which can be used to construct digital memories. Based on this principle, functioning polymer resistive memory devices have been demonstrated which can be scalable to lower dimensions for nanoelectronics applications.

## 7.2 Future Outlook

Most of the work reported in the literature that discusses selective monolayer formation relies on the difference in the adsorption kinetics of molecules under various conditions; for example, in the presence and absence of an applied potential.<sup>4, 5</sup> This approach may be useful for bulky adsorbents with slower adsorption rates,<sup>4</sup> however, good selectivity in deposition may not be possible for small molecules that adsorb at faster rates. Under anhydrous solvent conditions, electrochemically directed self-assembly offers better selectivity even for the deposition of relatively small molecules. This method is expected to offer excellent selectivity in the deposition of large, bulky molecules with desired functional groups which can be used for various applications including molecular electronics that require precise and discrete placement of the molecules on patterned surfaces.

Functionalized alkylthiosulfates can be used for making SAMs with variable surface properties. For example, these monolayers can be selectively deposited on respective electrode of an electrode array for making electrochemical or surface plasmon resonance based chemical and biosensors responsive to a wide range of analytes.<sup>6, 7</sup> Mixed monolayers formed by the co-deposition of alkanethiols provide

chemical control over surface wettability.<sup>8</sup> Similarly, electrochemically assisted co-deposition of alkylthiosulfates with hydrophobic and hydrophilic functional groups can provide selective and rapid modification of surface properties than conventional self-assembly methods.

The dynamic nature of the monolayers, as observed with XPS, opens up new opportunities for selective exchange of monolayers under electrochemically directed self-assembly conditions. For example, it may be possible to replace a monolayer of long chain alkanethiolate SAMs with short chain alkylthiosulfate molecules in solution; otherwise not possible under spontaneous self-assembly conditions. Alkylthiosulfates with different functional groups can also be considered as candidates for these exchange studies. Similar electrochemical exchanges under oxidative conditions can be applied to alkanethiols where complete replacements of alkanethiol SAMs are possible. Selective exchange of a preformed alkanethiolate monolayer on desired electrode areas is significant for making diverse molecular arrays, especially with functionalized bulky alkanethiols, for electronic and sensing applications.

The polypyrrole hybrid devices exhibiting field dependent conductivity offer several potential advantages including ease of fabrication, simple structures and more favorable scalability factors. This approach can be extended for other conjugated polymer (e.g polythiophenes, PEDOT) hybrid materials with bulky dopant anions (e.g. dodecyl sulfate, poly(styrene sulfonate)) and mobile cations (e.g.  $\text{Na}^+$ ,  $\text{K}^+$ ). Since removal of ions in this class of polymers is also known to modify optical and mechanical properties, it may also

have application in fields such as tunable optical systems and micro-electromechanical systems.

The device performance can be improved by tuning the field-dependent mobility of cations. An increase in the applied electric field can considerably decrease the time required to 'write' the information on to these devices.<sup>9</sup> With further scaling of these devices, the write time is expected to decrease rapidly since the effective field responsible for the movement of ions increases with decreasing device size. Recently, experiments performed on devices with systematically varied electrode spacing show that writing time decreases with the device dimensions.<sup>10</sup>

The time scale of the conductivity changes of the polymer hybrid materials can be manipulated by combining them with materials that can intercalate or trap the mobile cations. For example, tuneable solid-state heterojunctions have been recently demonstrated by combining polypyrrole hybrid material [PPy<sup>0</sup>(DBS<sup>-</sup>Li<sup>+</sup>)] with WO<sub>3</sub>, an n-type semiconductor having Li<sup>+</sup> intercalation capabilities.<sup>11</sup> These heterojunctions exhibit field-driven conductivity changes and are capable of rectification as well as charge storage. Selection of appropriate intercalation methods and careful modification of the polymer may lead to the creation of long term (non-volatile) information storage systems.

## References

1. Lukkari, J.; Meretoja, M.; Kartio, I.; Laajalehto, K.; Rajamaki, M.; Lindstrom, M.; Kankare, J., Organic thiosulfates (Bunte salts): Novel Surface-Active Sulfur Compounds for the Preparation of Self-Assembled Monolayers on Gold. *Langmuir* **1999**, 15, (10), 3529-3537.

2. Hsueh, C. C.; Lee, M. T.; Freund, M. S.; Ferguson, G. S., Electrochemically Directed Self-Assembly on Gold. *Angewandte Chemie-International Edition* **2000**, 39, (7), 1228-1230.
3. Lee, M. T.; Hsueh, C. C.; Freund, M. S.; Ferguson, G. S., Electrochemical Self-Assembly of Monolayers from Alkylthiosulfates on Gold. *Langmuir* **2003**, 19, (13), 5246-5253.
4. Cheng, L.; Yang, J. P.; Yao, Y. X.; Price, D. W.; Dirk, S. M.; Tour, J. M., Comparative Study of Electrochemically Directed Assembly Versus Conventional Self-Assembly of Thioacetyl-Terminated Oligo(Phenylene Ethynylene)S on Gold and Platinum Surface. *Langmuir* **2004**, 20, (4), 1335-1341.
5. Wang, J.; Jiang, M.; Kawde, A. M.; Polsky, R., Electrochemically Induced Deposition of Thiol-Based Monolayers onto Closely Spaced Microelectrodes. *Langmuir* **2000**, 16, (25), 9687-9689.
6. Wink, T.; vanZuilen, S. J.; Bult, A.; vanBennekom, W. P., Self-Assembled Monolayers for Biosensors. *Analyst* **1997**, 122, (4), R43-R50.
7. Flink, S.; van Veggel, F.; Reinhoudt, D. N., Sensor Functionalities in Self-Assembled Monolayers. *Advanced Materials* **2000**, 12, (18), 1315-1328.
8. Bain, C. D.; Whitesides, G. M., Correlations between Wettability and Structure in Monolayers of Alkanethiols Adsorbed on Gold. *Journal of the American Chemical Society* **1988**, 110, (11), 3665-3666.
9. Zhao, J. H.; Thomson, D. J.; Pilapil, M.; Pillai, R. G.; Rahman, G. M. A.; Freund, M. S., Field Enhanced Charge Carrier Reconfiguration in Electronic and Ionic Coupled Dynamic Polymer Resistive Memory. *Nanotechnology* **2010**, 21, 134003.
10. Pilapil, M., Systematic Development and Characterization of a Polypyrrole Hybrid for Dynamic Random Access Memory. *MS Thesis, University of Manitoba* **2009**.
11. Rahman, G. M. A.; Zhao, J. H.; Thomson, D. J.; Freund, M. S., Compensation Doping in Conjugated Polymers: Engineering Dopable Heterojunctions for Modulating Conductivity in the Solid State. *Journal of the American Chemical Society* **2009**, 131, (43), 15600-156001.